



# Biofuel production, hydrogen production and water remediation by photocatalysis, biocatalysis and electrocatalysis

Ahmed I. Osman<sup>1</sup> · Ahmed M. Elgarahy<sup>2,3</sup> · Abdelazeem S. Eltaweil<sup>4</sup> · Eman M. Abd El-Monaem<sup>4</sup> · Hisham G. El-Aqapa<sup>4</sup> · Yuri Park<sup>5</sup> · Yuhoon Hwang<sup>5</sup> · Ali Ayati<sup>6,7</sup> · Mohamed Farghali<sup>8,9</sup> · Ikko Ihara<sup>8</sup> · Ala'a H. Al-Muhtaseb<sup>10</sup> · David W. Rooney<sup>1</sup> · Pow-Seng Yap<sup>11</sup> · Mika Sillanpää<sup>12,13,14,15</sup>

Received: 1 February 2023 / Accepted: 13 February 2023 / Published online: 10 March 2023  
© The Author(s) 2023

## Abstract

The energy crisis and environmental pollution have recently fostered research on efficient methods such as environmental catalysis to produce biofuel and to clean water. Environmental catalysis refers to green catalysts used to breakdown pollutants or produce chemicals without generating undesirable by-products. For example, catalysts derived from waste or inexpensive materials are promising for the circular economy. Here we review environmental photocatalysis, biocatalysis, and electrocatalysis, with focus on catalyst synthesis, structure, and applications. Common catalysts include biomass-derived materials, metal–organic frameworks, non-noble metals nanoparticles, nanocomposites and enzymes. Structure characterization is done by Brunauer–Emmett–Teller isotherm, thermogravimetry, X-ray diffraction and photoelectron spectroscopy. We found that water pollutants can be degraded with an efficiency ranging from 71.7 to 100%, notably by heterogeneous Fenton catalysis. Photocatalysis produced dihydrogen (H<sub>2</sub>) with generation rate higher than 100 μmol h<sup>-1</sup>. Dihydrogen yields ranged from 27 to 88% by methane cracking. Biodiesel production reached 48.6 to 99%.

**Keywords** Environmental catalysis · Biocatalysis · Photocatalysis · Carbon-based catalyst · Biofuel

## Abbreviations

CMC-Co	Carboxymethyl cellulose-stabilized cobalt nanoparticles
Co/NHC@mCs	Co/N-heterocyclic carbene-supported magnetic chitosan composite
TEMPO	2,2,6,6-Tetramethylpiperidinyloxy
TOCNF	2,2,6,6-Tetramethylpiperidinyloxy (TEMPO)-oxidized cellulose nanofibril

## Introduction

Industrialization and urbanization have resulted in a significant increase in the consumption of finite fossil fuel reserves, leading to a cascade of environmental issues that

pose a considerable threat to human health, environmental preservation, and energy demand. Recent years have seen a growing emphasis on utilizing environmentally friendly, efficient, and cost-effective technology to eliminate pollutants, produce clean energy, and synthesize valuable compounds. Among many methods, catalysis plays a major role in reducing production costs and boosting reaction efficiency, which will significantly advance the development of human society. Sustainability, on the other hand, is the development that meets the needs of the current generation without compromising the ability of future generations to meet their own needs. Environmental catalysis involves developing catalysts to degrade undesirable substances or enable alternative catalytic synthesis of essential molecules without generating environmentally unacceptable by-products, and their role in achieving sustainability is crucial. Environmental catalysts have made remarkable strides in pollutant elimination as well as energy and material production over the past decades. Novel environmental catalysts derived from waste or cost-effective materials reduce waste and promote a circular economy while improving catalytic performance.

Homogeneous catalysts have high catalytic performance and well-defined structures, but their stability and

✉ Ahmed I. Osman  
aosmanahmed01@qub.ac.uk

✉ Pow-Seng Yap  
PowSeng.Yap@xjtlu.edu.cn

✉ Mika Sillanpää  
mikaesillanpaa@gmail.com

Extended author information available on the last page of the article

recyclability are low. Due to the significant potential for separation, reusability, and stability, heterogeneous catalysts are subsequently considered efficient for environmental applications. Although much progress has been achieved in heterogeneous catalysts, producing catalysts with high catalytic selectivity, high atom utilization efficiency, low cost, easy preparation, and well-defined active sites remains a significant challenge. For instance, designing catalytic systems such as single-atom catalysts enhance atom utilization efficiency to reduce catalytic costs and inherit the benefits of heterogeneous and homogeneous catalysts for several environmental applications (Xu et al. 2022). Another example is biochar; due to its porous and functional structure along with superior performance, it has been widely employed in agriculture, composting, gas storage, animal feed, energy storage, construction, and environmental remediation, with the potential to eliminate environmental contaminants, improve soil fertility, and reduce greenhouse gas emissions (Osman et al. 2022a). Adsorption is the most efficient method for decontaminating the environment; however, unsatisfied adsorption capacity, sluggish equilibrium rate, unstable adsorption conditions, and others continue to be obstacles to biochar adsorption applications (Song et al. 2022a).

Herein, we review the advances in photocatalysis, biocatalysis, and electrocatalysis as environmental catalysts and identify their promising and challenging issues. The main commonly used environmental catalysts discussed are biomass- and carbon-based, metal–organic frameworks, nanocomposites, non-noble metal nanoparticles, and enzymes. The advances and challenges in preparation methods for environmental catalysis are also highlighted. In addition, linking the chemical structure of environmental catalysis with their catalytic performance is exhaustively analyzed and discussed. In addition, the applications of environmental catalysis in three major fields, namely recent progress in water and soil remediation, biomass valorization, product upgrading, and biofuel and hydrogen production, are summarized and evaluated, as shown in Fig. 1.

## Environmental catalysis

### Photocatalysis

Photocatalysis has emerged as the most promising solution for the world's current energy crisis, environmental pollution, and global warming (Byrne et al. 2018). Since 1972, when Fujishima and Honda discovered the photoelectrochemical properties of titanium oxide (Fujishima and Honda 1972; Byrne et al. 2018; Yap and Lim 2011, 2012), significant effort has been made to develop photocatalysts for efficient photocatalytic processes. Other semiconducting materials, including zinc oxide and cadmium sulfide,

have also been proposed as potential photocatalysts due to their similar band gap to titanium oxide. In contrast, their chemical stability and environmental toxicity limit their application in environmental remediation. As a result, titanium oxide remains one of the most researched semiconductor photocatalysts in academia and industry, and its photocatalytic properties have been commercialized in air-purifying (nitrogen oxide and volatile organic compounds conversion) and self-cleaning window film systems (Cha et al. 2019; Lyulyukin et al. 2018). Although their practical application in water and wastewater treatment is still limited, titanium oxide-based photocatalysts have been widely used in persistent pollution-burdened environments, implying that titanium oxide systems may be a viable solution for the removal of widespread emerging pollutants from aquatic environments.

A photocatalytic reaction, in general, consists of three steps. First, photocatalysis is initiated by bombarding a photocatalyst with ultraviolet light photons. Second, suppose the photon energy is greater than the band gap. In that case, these photons cause the generation of electrons ( $e^-$ ) on the surface of the photocatalyst to become 'excited' in the valence band (VB), causing them to move to the conduction band (CB). Simultaneously, a positive hole ( $h^+_{VB}$ ) is formed on the valence band. Electrons and holes are excited and migrate to the surface of photocatalysts, where they react with adsorbed electron acceptors and donors, respectively (Fig. 2).

In the preceding decades, bare titanium oxide nanomaterials have attracted considerable interest due to their potential applications in environmental pollution removal and photocatalytic hydrogen production (Osman et al. 2020a). Nevertheless, due to its relatively large band gap energy (3.2 eV and 3.0 V for anatase and rutile phases, respectively) (Fig. 3), it can only absorb approximately 6% of the solar energy that reaches the earth at any given time. Thus, significant effort has been devoted to enhancing titanium oxide's absorption properties in the visible spectrum and developing new photocatalytic materials that can capture a broad range, from ultraviolet to visible light and even the near-infrared region. This strategy will lead to the efficient use of solar energy as a clean, abundant, and renewable energy source. The photocatalysts' surface modification, alteration, and structure design can be optimized to increase and broaden light absorption.

Doping titanium oxide with non-metal dopants (such as carbon, nitrogen, sulfur, and fluorine) or metal dopants (such as iron, silver, chromium, and manganese) can narrow the band gap between the valence and conduction bands, thereby enhancing photocatalytic properties (Akpan and Hameed 2011; Elbanna et al. 2016; Luo et al. 2019). There has been a growing interest in the development of novel photocatalysts, such as zinc oxide (Lee et al. 2016; Ani et al. 2018), zinc

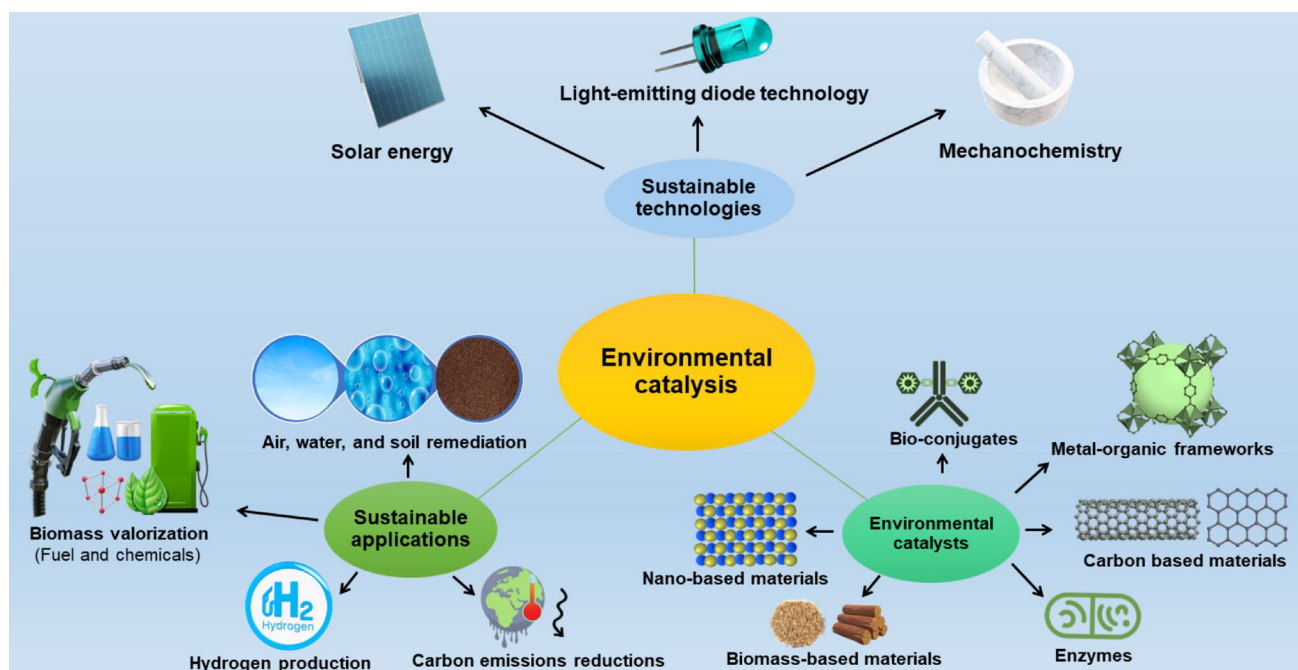


**Fig. 1** Applications of environmental catalysis, ranging from sustainable applications and technologies to sustainable catalysis approaches. Using catalysts, such as biomass- and carbon-based catalysts, metal–organic frameworks, nanocomposites, non-noble metal nanoparticles, and enzymes for environmental catalysis is a promising area of research. Notably, while some nano-based materials are

sustainable, others are not and may be toxic or environmentally damaging. Applying environmental catalysis in three main areas: water and soil remediation, biomass valorization, product upgrading, and biofuel and hydrogen production can provide valuable insights for achieving global environmental protection

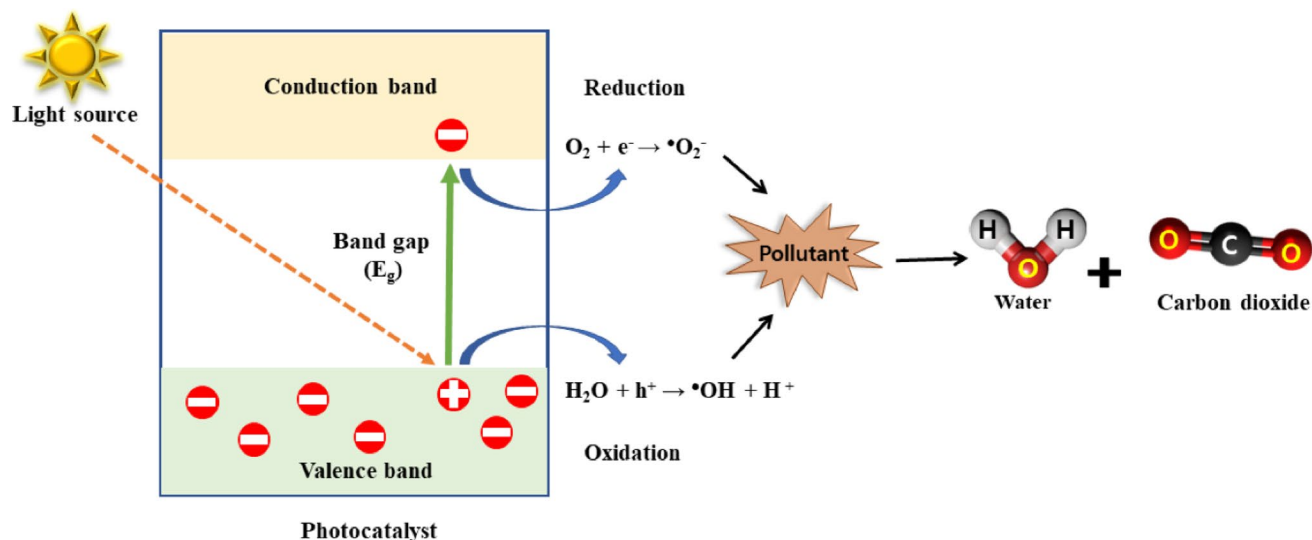


**Fig. 2** Photocatalytic redox reaction for the degradation of pollutants. Photocatalysis is initiated by bombarding a photocatalyst with ultraviolet light. When the photon energy is greater than the band gap energy, electrons can be generated on the surface of the photocatalyst, where becoming excited in the valence band, which moves to

the conduction band. Simultaneously a positive hole is formed on the valence band. Generated electrons and holes further developed superoxide anions and hydroxyl radicals used to remove pollutants.  $\text{H}_2\text{O}$ ,  $\text{O}_2$ ,  $\text{OH}$ ,  $\text{H}^+$ , and  $\text{H}_2$  refer to water, oxygen, hydroxyl, hydrogen ion, and hydrogen, respectively

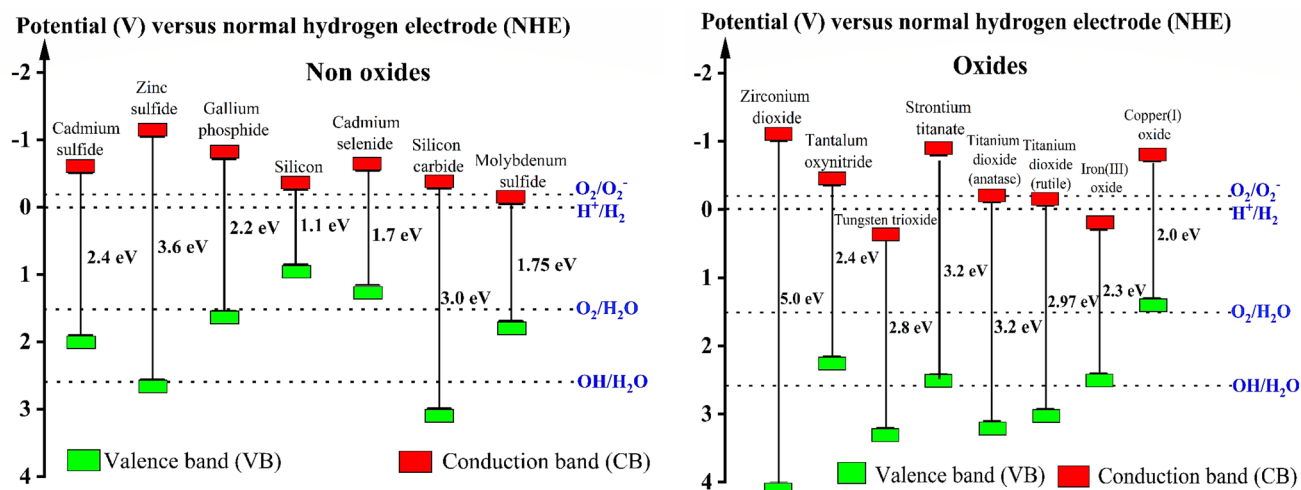


**Fig. 3** Band gaps of non-metal oxide and metal oxide photocatalysts at a pH of 7. Other non-metals and metals have various band gap energies than titanium dioxide. Solar energy can be more effectively adapted to prepare visible-light-driven photocatalysts using their properties, which require narrow band gap energy. Additionally, doping with other non-metal dopants can narrow the band gap energy

sulfide (Antoniadou et al. 2011; Hojamberdiev et al. 2020; Zhang et al. 2011), zirconium dioxide (Basahel et al. 2015; Tian et al. 2019; Pirzada et al. 2015), perovskites (Wei et al. 2021a; Bresolin et al. 2020), molybdenum disulfide (Yuan et al. 2019; Li et al. 2018a; Chang et al. 2014), tungsten trioxide (Wang et al. 2012a; Yu et al. 2017; Dutta et al. 2021), cadmium sulfide (Cheng et al. 2018a; Jing and Guo 2006; Zhu et al. 2019), and iron oxide (Hitam and Jalil 2020; Shi et al. 2012; Palanisamy et al. 2013) due to their potential to improve photocatalytic performance and efficiency.

In recent years, lightweight and abundant elements such as carbon, phosphorus, binary carbon nitride, hexagonal boron nitride, and boron carbide have given rise to a new class of metal-free materials opens up new photochemical possibilities. In photocatalytic fields, graphene has been extensively studied as an efficient electron acceptor capable of enhancing charge transfer and decreasing electron–hole pair recombination. Polymer graphite carbon nitride (g-C<sub>3</sub>N<sub>4</sub>), an analog of graphene, has become a hot material in photocatalysis due to its unique electronic band structure, low cost, and ease of preparation (Cao et al. 2015). The visible light can excite the graphite carbon nitride with a narrow bandgap of 2.7 eV, indicating its potential use in photocatalytic degradation, photocatalytic sterilization, hydrogen generation, and carbon dioxide reduction (Li et al. 2016a; Zheng et al. 2012).

However, a narrower band gap restricts the reduction and oxidation of photogenerated electrons/holes. In addition, the rapid recombination of photogenerated electron–hole pairs in semiconductors with a narrow bandgap diminishes their

between the valence and conduction bands. The unit used herein is eV (electron volt), which is a unit of energy commonly used in photocatalysis research to express the energy of photons or electron excitations. It measures the amount of energy gained or lost by an electron when it moves between energy levels in a material. H<sub>2</sub>O, O<sub>2</sub>, OH, and H<sub>2</sub> refer to water, oxygen, hydroxyl, and hydrogen

photocatalytic activity. Thus, significant effort is being put into developing an efficient photocatalyst that uses doping, coupling with other nanomaterials, precipitation with metal particles, crystal growth designs, and heterojunctions. Compared to single-phase semiconductor photocatalysts, hybrids of two or more semiconductor systems, such as heterojunction, appear to be one of the most promising methods for optimizing solar light utilization efficiency. In addition, the design of heterojunctions prevents photogenerated electron–hole pair recombination and permits rapid charge transport. Based on their adjacent band structures, heterojunctions can be classified as conventional type-I and type-II heterojunctions, Z-scheme heterojunctions, p-n heterojunctions, and homojunction band alignments (Wang et al. 2012a; Wang et al. 2012b; Su et al. 2011; Liu et al. 2011). Recent advances in heterojunction-based photocatalysts indicate a promising strategy for boosting photocatalytic activity in environmental pollution degradation, hydrogen production, and carbon dioxide reduction (De Wolf et al. 2012). While significant progress has been made in photocatalysis over the past few decades, its practical application is currently limited due to insufficient activity, poor stability, and high cost. There is still a great deal of work to improve photocatalyst systems.

## Electrocatalysis

In recent years, there has been a growing interest in electrochemical processes for treating polluted waters. The ability of electrochemical systems to operate at ambient

temperature and pressure, as well as their robust performance and adaptability to changes in the influent composition and flow rate, are a few advantages over alternative methods (Chen 2004). In addition, they typically do not require additional chemicals and produce no waste. Besides, electrochemical processes can be easily integrated with other technologies, such as electrochemical advanced oxidation processes (e.g., anodic oxidation, electro-Fenton, and electrocoagulation) (Sirés et al. 2014). Furthermore, the coupling efficiency with biological technologies (e.g., aerobic, anaerobic, membrane bioreactors, and microbial fuel cells) is also evaluated (Mousset et al. 2021).

In the 1920s, Bowden and Rideal developed electrocatalysis to measure hydrogen evolution reactions (Wu and Hu 2021; Popovski 2004; Boudjemaa 2020). Since then, electrochemistry has been extensively studied for energy conversion devices (such as batteries, fuel cells, and solar cells), electroanalytical sensors, organic synthesis, corrosion science, and wastewater treatment applications (Carlesi Jara et al. 2007; Zhang et al. 2019a; Comninellis 1994). Using palladium dioxide anodes, the degradation of phenolic compounds was studied, creating new opportunities for electrochemical applications in wastewater treatment (Wu and Hu 2021; Nilsson et al. 1973). The ability of electrocatalysis to remove various organic and inorganic contaminants, including dyes, phenols, pesticides, herbicides, and antibiotics, was then investigated (Comninellis 1994; Quiroz et al. 2014; Ansari and Nematollahi 2020; Xing et al. 2018).

Electrocatalysis is responsible for initiating or accelerating redox reactions in the presence of electrodes by supplying an external potential, which an electric field can provide. As depicted in Fig. 4, micropollutant degradation in an electrocatalysis system is primarily accomplished by direct and indirect oxidation processes. Electrocatalytic degradation processes consider several variables, including electrode materials, electrolytes, water matrices' physical and chemical properties (e.g., pH, coexisting ions, and ionic strength), and operating conditions. An electrode conducts electricity, initiates reactions, accelerates electron transfer, and selectively promotes electrochemical reactions. Moreover, catalysts are essential components of the electrodes used in the electrocatalytic degradation of environmental contaminants.

The choice of electrode material affects the efficiency of electrochemical treatment and the possibility of byproduct formation. Electrocatalysts are categorized as either metal oxides such as ruthenium dioxide, iridium dioxide, lead dioxide, or tin dioxide, or carbon, e.g., boron-doped diamonds. Metal-oxide electrodes are categorized as either active anodes, such as iridium dioxide and ruthenium dioxide, or inactive anodes, e.g., ruthenium dioxide, lead dioxide, and tin dioxide. Titanium/lead dioxide is an excellent electrode, for instance, due to its high oxygen evolution

potential, excellent electrical conductivity, chemical stability, and low cost. However, the widespread use of titanium/lead dioxide electrodes is limited due to their distinct disadvantages, including relatively high interface resistance, toxic lead ion leaching, film instability, and low current efficiency. To overcome this disadvantage, either a three-dimensional ordered microporous lead dioxide film based on a porous titanium substrate (Liu et al. 2017) or an aluminum-doped lead dioxide electrode via doping was synthesized (Chen et al. 2015). Tin dioxide-based electrodes are commonly used, but their wide band gap (3.6 eV) restricts their applications. Due to its high oxygen evolution potential, stability, and excellent electrocatalytic properties, antimony is the most used dopant. A tin dioxide-antimony/titanium electrode was synthesized using the sol-gel method for the electrochemical oxidation of antibiotics (e.g., ciprofloxacin) (Wang et al. 2016a). Recently, a titanium/carbon nanotube/tin dioxide-antimony-erbium electrode was prepared as the anode, with the carbon nanotube exhibiting a high specific surface area and high oxygen evolution potential in increased hydroxyl radical production at the anode (Lei et al. 2020).

In addition, carbon-based electrodes such as boron-doped diamond, graphite, and carbon nanotubes are commonly used due to their low resistance and high chemical stability. Still, there is a high cost associated with boron-doped diamond electrodes. Boron-doped diamond is the most frequently used carbon-based electrode due to its high oxygen evolution potential, high corrosion resistance, wide electrochemical potential window, excellent electrochemical stability, and low background current, which produces more reactive radicals to achieve a higher mineralization rate of antibiotics (such as sulfamethoxazole and trimethoprim) than other carbon-based electrodes (de Amorim et al. 2013). However, the reported catalysts for electrochemical have been evaluated for environmental remediation applications; limited efforts have been made for the toxic assessment of pollutants that are not efficiently mineralized via electrochemical and electrode materials, which should be considered in future research.

## Biocatalysis

Biocatalysis is an integral component of the 'green chemistry' concept pioneered in the 1990s, and its impact on sustainability is now established beyond dispute, as shown in Fig. 5 (Alcalde et al. 2006). Compared to conventional physical and chemical methods, which have several significant drawbacks, such as insufficient purification, low efficiency, high costs, the production of hazardous byproducts, and application to a narrow concentration range for mineralizing organic compounds from wastewater, this method has several significant advantages (Bilal et al. 2019a; Wong et al. 2019). To overcome these obstacles, environmental

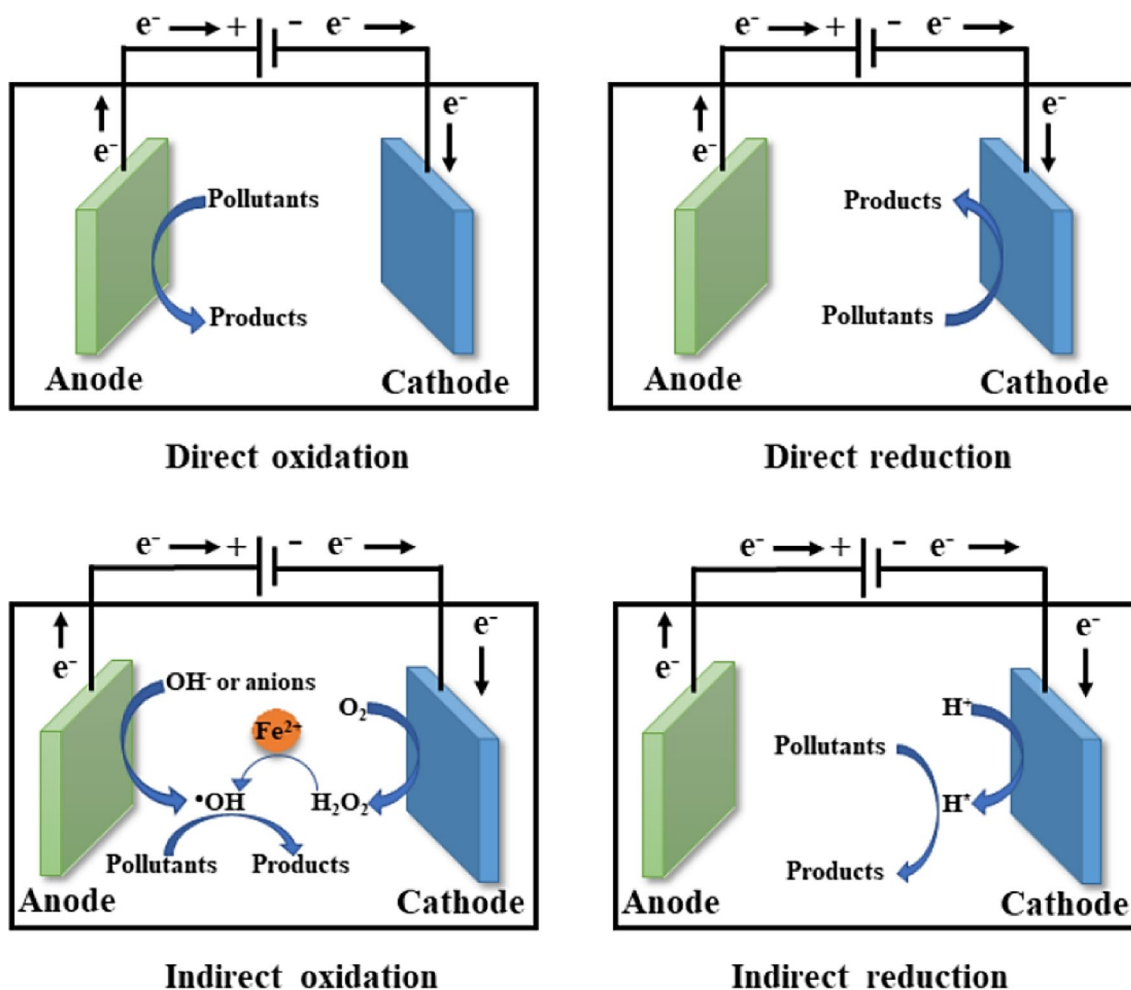


**Fig. 4** Electrochemical system's direct and indirect oxidation mechanisms. The anode surface and the target contaminants undergo direct oxidation, whereas the anions or  $OH^-$  generated on the anode surface

interact with the contaminants via indirect oxidation.  $e^-$ ,  $OH^-$ ,  $H^+$ ,  $Fe^{2+}$ , and  $H_2O_2$  refer to electrons, hydroxide ions, ferrous ions, hydrogen ions, and hydrogen peroxide, respectively

engineers and biotechnologists are developing an innovative bioremediation technique that is efficient, cost-effective, and environmentally safe. Enzymes provide new options for treating effluent streams containing organic contaminants resistant to treatment (Bilal et al. 2019a). Enzymes are preferred environmental candidates over whole organisms because isolated enzymes are more specific and easier to handle, and their activity can be tailored to the reaction conditions more precisely (Sutherland et al. 2004; Pieper et al. 2004). Numerous biocatalysts, including hydrolases, oxidoreductases, laccases, and peroxidases, are actively involved in biological treatment (Kadri et al. 2017).

In addition, it was determined that other microorganisms, such as fungi, algae, and bacteria, could use a catabolic process to degrade pollutants. Recent interest has centered on microbial lipolytic enzymes because of their

ability to catalyze biotransformation reactions involving compounds with ester bonds (e.g., converting waste into biofuel or other value-added products such as fatty acid esters, mono- and diacylglycerols, and others), as listed in Table 1 (Kumar et al. 2020a, b). Since enzyme catalysts are typically water-soluble and difficult to recover from aqueous solutions, using modified and immobilized enzymes is one of the emerging strategies for treating target wastes and lipids today. Enzymes were immobilized using various techniques (Bilal et al. 2017a, b, c, 2018; Zhang et al. 2015) to reuse expensive biocatalysts. It was found that enzyme attachment on solid carriers, either through physical adsorption or covalent bonds, is one of the most practical techniques (Bilal et al. 2018). Therefore, lipolytic enzymes can reduce the massive amount of

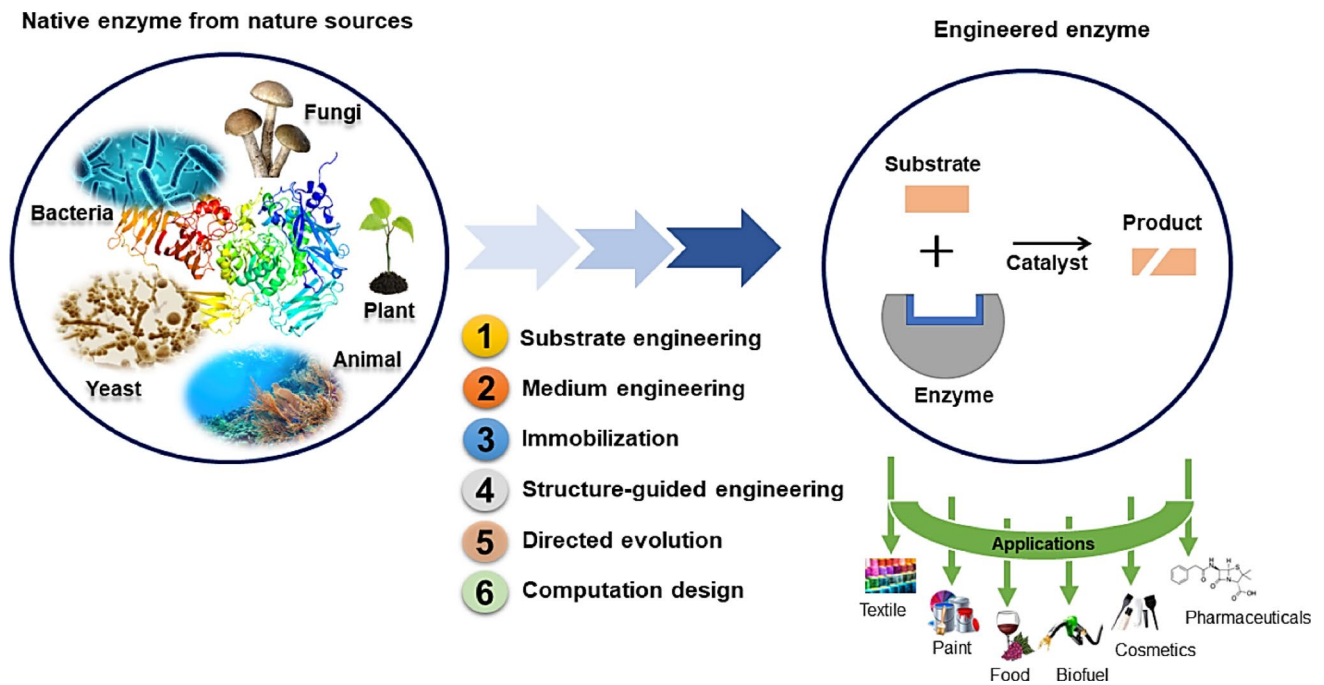


**Fig. 5** Biocatalytic evaluation and improvement strategies. Biocatalysis involves the application of microbes and biocatalysts (or enzymes). Many biocatalysts have been engineered by rational and directed evolution, contributing to the catalytic activity, enantioselectivity, and stability that are essential for biocatalytic applications.

This evolution allows using of biocatalysts for the biosynthesis of value-added pharmaceuticals and fine chemicals. Investigation of the modification of biocatalysts in a short time and recovery of water-soluble enzymes by enzyme immobilization or assistance with solid support attachment greatly enhances the catalytic features of enzymes

**Table 1** Waste as a source of lipolytic enzymes and high-value products produced using microbial lipases (Kumar et al. 2020a). Several microbes produces high-economic-value products using lipases as biocatalysts

Waste source	Microorganism	High economic value	Reference
Coconut oil mill waste	<i>Staphylococcus pasteurii</i>	Lipase and other important extra-cellular hydrolytic enzymes	Kanmani et al. (2015)
Agro-industrial hydrocarbons and oily substances	Two yeast isolates of <i>Yarrowia lipolytica</i>	Lipase and citric acid	Mafakher et al. (2010)
Grease waste	<i>Penicillium chrysogenum</i>	Lipase	Kumar et al. (2011)
Olive mill wastewater and olive oil cake	<i>Yarrowia lipolytica</i>	Lipase production	Moftah et al. (2013)
Polluted waters by fat materials from the Mascara region	<i>Pseudomonas</i> sp. <i>Streptococcus</i> sp.	Lipase production	Hachemi et al. (2017)
Agro-industrial wastes	Engineering <i>Yarrowia lipolytica</i>	Lipase and single-cell protein production	Yan et al. (2018a)
Waste grease	<i>Penicillium chrysogenum</i>	Fatty acid	Kumar et al. (2011), Pilusa et al. (2013), Kumar and Negi (2015), Kumari et al. (2017)
Dairy wastewater	<i>Penicillium</i> sp.	Biogas	Rosa et al. (2009)
Slaughterhouses and meat processing wastes	Lipase from <i>Candida rugosa</i>	Biogas	Cavaleiro et al. (2013)
Poultry slaughterhouse lipid-rich waste	<i>Staphylococcus xylosus</i> strain exhibiting lipolytic activity	Biogas	Affes et al. (2017)

lipid waste environmentally friendly and address energy security concerns.

Furthermore, various soil-derived enzymes, such as lipases, dehydrogenases, ureases, and catalases, have been proposed as bioindicators for pollution assessments (Margesin et al. 2000). Lipase@ZIF-8 nanoparticle-based biosensor was used to directly detect methyl parathions and organophosphorus pesticides with higher sensitivity and lower cost than laboratory-based methods (Herranz et al. 2018). However, lipase-based biosensors for bioremediation are not yet suitable for commercial use, and additional research is necessary for implementation.

## Common environmental catalysts

Fields associated with the environment and energy have adopted the fostered approaches that use benign solvents and mild reaction conditions and produce limited amounts of waste using cost-effective techniques (Chen et al. 2017a). The utilization of environmental catalyst materials contributes to numerous aspects of the United Nations' seventeen Sustainability Development Goals, particularly Goal 12 (enabling responsible production) and Goal 13 (climate action). Short preparation time, ambient temperature, less hazardous solvents, solvent-free conditions, simple methods, low energy consumption, and fewer by-products are generally considered to be among the most essential characteristics of a green synthesis route (Guesh et al. 2017). Remarkably, environmental catalyst materials have been utilized in various applications, such as electrocatalysis, organic synthesis, biocatalysis, desulfurization, water and soil remediation, biomass valorization, biofuel, and hydrogen production, among others. To reduce environmental pollution and achieve sustainability objectives, numerous materials have been engineered to serve as environmental catalysts instead of traditional catalysts. Metal–organic frameworks, biomass- and carbon-based materials, non-noble metal nanoparticles, nanocomposites, and enzymes are frequently used as environmental catalysts among these materials. A diagrammatic illustration of commonly used environmental catalysts is shown in Fig. 6.

### Biomass-derived carbon materials

To scale up the technology, scientists must prioritize several essential criteria, such as production cost, efficiency, durability, and environmental impact. Recently, biomass-derived carbon-based materials have been heavily utilized in many applications, including energy storage and conversion, sensing, catalysis, and environmental applications (Park et al.

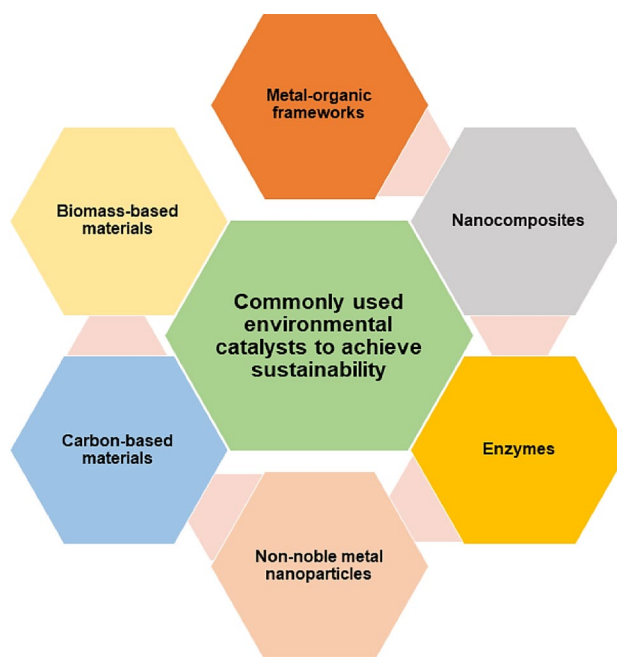


**Fig. 6** Common environmental catalysts. Metal–organic frameworks are synthesized via metal-linker coordination, forming a uniform porous structure. Carbon-based catalysts are widely used as environmental catalysts in environmental applications. Non-noble metal nanoparticles are considered environmental catalysts under green conditions. Nanocomposites have exhibited remarkable performance in many environmental applications, and enzymes are biological catalysts consisting of protein and active metal sites

2022). This was attributed to the outstanding properties of carbonaceous materials in terms of good mechanical stability, unique electronic properties of carbon atoms, electrical conductivity, and structural tenability (Xiao et al. 2022). Notably, researchers have introduced many fabrication strategies to scale carbonaceous materials, such as arc discharge, laser ablation, chemical vapor deposition, pyrolysis, and electrochemical methods, depending on non-renewable petroleum carbon sources such as methane, ethylene, and other petrochemicals (Wang et al. 2021a). However, these strategies unveiled some negative aspects, such as high energy consumption, emission of a large amount of greenhouse gas carbon dioxide, and environmental pollution. For instance, the production of activated carbon consumes large amounts of energy (97 MJ/Kg) with an emission of 6.6 kg/Kg of carbon dioxide. Similarly, graphene production's energy demand was 1100–1640 MJ/Kg with a high carbon dioxide emission (80 kg/Kg) (Boyjoo et al. 2021). On this basis, researchers have attempted to produce novel next generations of carbon materials with desirable characteristics such as affordable cost, facile and sustainable fabrication strategies, low energy consumption, and eco-friendly merit. From an economical and sustainable point of view, researchers have considered biomass an excellent



alternative, renewable organic feedstock to crude oil and natural gas (Osman et al. 2022b; Farghali et al. 2022). This is ascribed to the abundance of enormous biomass resources, including plant and animal-derived materials.

The worldwide annual disposal of food waste was found to be equivalent to a third of food production (1300 million tons) (Matharu et al. 2016); also, agricultural practices generate 570 million tons of waste annually (Morrison and Golden 2015). For instance, plant-derived biomass comprises three components: (1) inedible portions (lignin, cellulose, and hemicellulose); (2) edible portions (starch, free sugars, protein, and vegetable oils (triglycerides)); and (3) essential oils and other secondary metabolites of high value (Sherwood 2020). Accordingly, the exclusion of unnecessary wastes and the rational upcycling of those wastes guarantee viable, high-quality products, minimize the environmental problems related to unwise waste disposal, i.e., waste management, and achieve the circular economy aspects (Sherwood 2020; Clark et al. 2016; Peng et al. 2023).

Recently, biomass-derived carbon materials were established as the most sustainable and scalable strategy due to the enormous annual production of biomass from agriculture and forestry (104.9 billion tons/year) (Field et al. 1998). Interestingly, there are numerous macrostructures with tunable porosity in biomass-derived carbon materials, including spherical (Xia et al. 2012), reticular (Ubeyitogullari and Ciftci 2016), fibrous (Hu et al. 2016), ribbon-like (Ai et al. 2018), bubble-like (Xie et al. 2018), and plate-like materials (Ling et al. 2015), expanding their applications. Besides, the remarkable characteristics of such materials outperform the noble metals in many aspects, including (1) cost-effectiveness, i.e., carbon price is 0.03\$ per gram while gold price is 60\$ per gram, silver price is 25\$ per gram, and platinum price is 34\$ per gram; (2) ease of fabrication due to the abundance of raw materials; (3) tailorable structure due to the presence of heteroatoms, for example nitrogen, oxygen, and sulfur, that facilitate the functionalization and enhance the catalytic activity (Li et al. 2020; Wu and Zhang 2020). However, the synthesis strategy played a crucial role in carbon materials' porosity and surface chemistry. Therefore, a challenging issue is fabricating a uniform porous structure with a well-defined shape of sustainable biomass-derived carbon materials.

The world demand for energy has become a quintessential priority for better and sustainable life for humanity. The massive emissions of carbon dioxide into the atmosphere, which amount to about 30 billion tons annually, have severely threatened the environment with issues like global warming and air pollution as a result of the overuse of fossil fuels as a major source of energy (about 80%) to support the industrial revolution and satisfy population growth (Seh et al. 2017; Zhang et al. 2020; Panwar et al. 2011). According to the international energy agency, atmospheric

carbon dioxide concentration increased from 280 to 480 ppm in 2019 (Chu et al. 2017; Swann et al. 2016). As a result, this dangerous environmental crisis has drawn considerable public concern. Therefore, many researchers have devoted their efforts to creating innovative technologies and strategies and generating an alternative, green, and renewable energy source.

The exploitation of hydrogen gas as a clean energy source has become a promising approach owing to its non-toxic combustion by-product and the higher caloric value (142 MJ/kg) comparable to fossil and hydrocarbon fuels (Muradov and Veziroğlu 2008; Schlapbach and Züttel 2011). Therefore, great efforts have been exerted to foster an alternative strategy instead of the conventional methods like steam reforming fossil fuel and water electrolysis, which consume a large amount of energy and money (Karayilan et al. 2019; Hosseini and Wahid 2016). Subsequently, photocatalytic water splitting has gained significant interest as a sustainable and green strategy to produce hydrogen (Gopinath and Nalajala 2021). Especially, photocatalytic water splitting has demonstrated an excellent efficiency of solar energy conversion into hydrogen, reaching 5–10%, indicating its proficiency and possible application on a large scale (Arunachalam et al. 2021; Wang et al. 2019a).

Three-dimensional biomass-derived carbon materials revealed an excellent performance in different catalytic applications due to their large specific surface area, high porosity, good conductivity, and propitious thermal and chemical stability, as shown in Table 2. In this perspective, a sustainable and cost-effective three-dimensional carbon aerogel support from seaweed biomass (carrageenan) was prepared to boost the efficiency and photostability of cadmium sulfide photocatalyst (CdS@CAs) (Quan et al. 2018). Carrageenan provided a non-toxic sulfur source, i.e., sulfated galactons, that extended across the double helix structure of carrageenan and was integrated by cadmium cations, resulting in photocatalysts with interconnected macropores and mesopores that accelerated the mass transfer of reactants. The results exhibited an excellent hydrogen evolution rate of 113.5  $\mu\text{mol h}^{-1}$  with a photocurrent density of 100  $\mu\text{A cm}^{-2}$ . This finding may be attributed to the good electrical conductivity of the photocatalyst that accelerated the photogenerated charge separation and the photocorrosion resistance of cadmium sulfide. A certain carbon coating thickness for cadmium sulfide inhibited the self-oxidation of cadmium-sulfur bonds by the photogenerated holes. Therefore, cadmium sulfide photocatalyst achieved excellent photostability after 4000 s under light illumination.

Further, a sustainable strategy for the catalytic hydrolysis of ammonia borane (ammonia, borane trihydridoboron, ammonia borane) was proposed using magnetically recoverable ruthenium and cobalt (Ru and Co) bimetallic nanoparticles supported on costless cotton-derived carbon fibers (Ru@

**Table 2** Carbon-based and biochar-based catalysts: carbon source, preparation conditions, surface area, catalytic applications, and efficiency. Biomass-derived carbon materials with large specific surface areas served as catalytic species hosts, enhancing stability and inhibiting agglomeration

Catalyst	Carbon source	Preparation condition	Surface area (m <sup>2</sup> g <sup>-1</sup> )	Catalytic application	Efficiency	Reference
Wood flour biochar/bismuth oxybromide (BiOBr)	Industrial wood flour waste	Pyrolysis of wood flour at different temperatures (200–800 °C) under nitrogen conditions with a constant raising rate (5 °C min <sup>-1</sup> )	222.3	Photocatalytic removal of chromium (IV) and rhodamine B	100%	Geng et al. (2020)
Silver-loaded activated carbon (Ag-AC)	Bio-waste jute stick	Carbonization of jute stick at ≈ 500 °C under inert conditions	620	Photocatalytic degradation of malachite green oxalate and clofibrac acid	98% (malachite green oxalate) 97% (clofibrac acid)	Devi et al. (2019)
Biomass-derived carbon dots	Raw palm veneers	Hydrothermal treatment of palm powder mixed with thionyl chloride(co-dopant) at 200 °C for 7 h, followed by vacuum freeze-drying step	–	Photocatalytic degradation of Rhodamine B and methylene blue	71.7% (Rhodamine B) 94.2% (methylene blue)	Zhu et al. (2020)
Nitrogen-doped mesoporous carbon	Wheat flour	Carbonization of wheat flour and silica mixture at 850 °C for 3 h under nitrogen flow, followed by hydrofluoric acid etching to remove silica template	672	Catalytic hydrochlorination of acetylene	73.3%	Lan et al. (2018)
Nitrogen and sulfur co-doped biochar	Rice straw	Pyrolysis of rice straw and nitrogen, sulfur doping precursors at 1000 °C for 4 h under nitrogen flow condition	109.2	Catalytic degradation of metolachlor	–	Ding et al. (2020)
Nitrogen-doped porous carbon	Waste air-laid paper	Calcination of the carbon precursor under 10% ammonia/argon for 5 h	1143	Catalytic oxidation of hydrogen sulfide	496.6 g <sub>sulfur</sub> kg <sub>catalyst</sub> <sup>-1</sup> h <sup>-1</sup>	Xu et al. (2021)
Nitrogen-doped porous carbon	Cellulose	Pyrolysis of specific mass ratios of cellulose, polyamide (nylon waste), and zinc chloride (activator) at different temperatures (700 °C, 800 °C, 900 °C) under argon flow for 2 at a heating rate of 10 °C min <sup>-1</sup>	1327.3	Electrochemical oxygen reduction	–	Xu et al. (2019)

Table 2 (continued)

Catalyst	Carbon source	Preparation condition	Surface area (m <sup>2</sup> g <sup>-1</sup> )	Catalytic application	Efficiency	Reference
Nitrogen-doped honeycomb-like carbon tube	Dandelion seed	Carbonization of dandelion seed at a given temperature (700, 800, 900, and 1000 °C) at a heating rate of 5 °C min <sup>-1</sup> for 1 h in a nitrogen atmosphere	1324.1	Electrochemical oxygen reduction	–	Tang et al. (2019)
Ruthenium and cobalt/cotton-derived carbon fiber)	Cotton	Carbonization of cotton at 400 °C under inert conditions	–	Catalytic hydrolysis of ammonia borane	139.59 mol <sub>H<sub>2</sub></sub> mol <sub>metal</sub> <sup>-1</sup> min <sup>-1</sup>	Yang et al. (2018a)
Carbon–silica supported nickel	Rice husk	Pyrolysis process of dried rice husk (473–873 K) under an inert atmosphere	174	Catalytic hydrogenation of furfural and levulinic acid	1.119 K <sub>g<sub>furfuryl alcohol</sub></sub> h <sup>-1</sup> K <sub>g<sub>catalyst</sub></sub> <sup>-1</sup> 0.964 kg <sup>-1</sup> h <sup>-1</sup> K <sub>g<sub>γ-valerolactone</sub></sub> <sup>-1</sup>	Madduluri et al. (2020)
Cobalt-anchored nitrogen-doped porous carbon nanobelt (Co-ISA/CNB)	Chitosan	Pyrolysis of chitosan and cobalt precursor, zinc chloride (activator for efficient graphitization) mixture at 900 °C for 1 h in a nitrogen atmosphere	2513	Catalytic oxidation of ethylbenzene	98%	Zhu et al. (2018)
Single zinc atoms supported on microporous nitrogen-doped carbon (SA-Zn/MNC)	Anhydrous glucose	Carbonization of the precursors at 800 °C for 4 h under an argon protection atmosphere	525	Electrochemical reduction of carbon dioxide to methane	85%	Han et al. (2020)
Cadmium sulfide photocatalyst (CdS@CAs)	Carrageenan	Cadmium-carrageenan hydrogel was formed by adding cadmium acetate/ethanol solution to carrageenan solution via a freeze-drying process, then carbonized for 1 h under a nitrogen atmosphere (500–800 °C) to obtain cadmium sulfide photocatalyst (CdS@CAs)	132.83	Photocatalytic hydrogen production	113.5 μmol h <sup>-1</sup>	Quan et al. (2018)

“–” means not reported

BET: Brunauer–Emmett–Teller

Co/CCF) (Yang et al. 2018a). Transmission electron microscope and elemental mapping images revealed the uniform dispersion of ruthenium and cobalt bimetallic nanoparticles with an average diameter of 5–15 nm onto helical-shaped carbon fiber support. This was related to the large number of –OH functional groups on the surface of the carbon fibers that uniformly adsorbed  $\text{Co}^{2+}$ . Interestingly, ruthenium and cobalt on cotton-derived carbon fibers showed a satisfactory turnover frequency ( $139.59 \text{ mol}_{\text{H}_2} \text{ mol}_{\text{Ru}}^{-1} \text{ min}^{-1}$ ) at 30 °C. Due to the cobalt nanoparticles' ferromagnetic properties, ruthenium and cobalt on cotton-derived carbon fibers were involved in several catalytic cycles with good catalytic activity and facile recovery by an external magnet. The chemical storage of hydrogen could be a promising strategy rather than the traditional storage methods such as compression, liquefaction, and adsorption due to its high volumetric and gravimetric hydrogen content (i.e., ammonia borane trihydridoboron has a molecular weight of 30 g mol<sup>-1</sup> with a hydrogen content of 19.6 wt%) (Sadhasivam et al. 2017).

### Metal–organic frameworks

Metal–organic frameworks are a dominant category of catalysis owing to their unparalleled characteristics that are not wholly exploited, including flexibility, superb reusability, immense surface area, unique physicochemical properties, and intrinsic structures. In addition, metal–organic frameworks are synthesized via metal-linker coordination bonds in three directions, forming a uniform porous structure (Vasanthakumar et al. 2020). Solvothermal is generally the most common method to fabricate metal–organic frameworks; however, it involves dissolving metals and ligands in organic solvents such as dimethyl formamide (Omer et al. 2021; Abd El-Monaem et al. 2022). Notably, dimethyl formamide is a quite detrimental solvent that decomposes to dimethylamine at high temperatures, causing environmental and handling problems (Chen et al. 2017a). Hence, for applying the concept of sustainability and avoiding environmental issues, the preparation of metal–organic frameworks via solvent-free approaches has become a research hotspot. The alternative green synthesis methods of metal–organic frameworks are sorted into two categories according to solvent amount and energy consumption; the first one includes aging (Cliffe et al. 2012; Mottillo et al. 2013), mechanochemical (Užarević et al. 2016; Do and Friščić 2017), and thermochemical (Lanchas et al. 2012). In comparison, the second category contains microwave-assisted (Liang et al. 2013; Klinowski et al. 2011), sonochemical (Song et al. 2016; Yuan et al. 2016), and electrochemical (Liang et al. 2013; Klinowski et al. 2011). Overall, to fabricate metal–organic frameworks in a sustainable and green approach, Julien et al. (2017) summarized the main aspects that should be considered (Fig. 7); (1) utilizing biocompatible building blocks, (2) eschewing

bulk solvents, (3) utilizing supercritical liquids or water as a solvent, and (4) rationalizing the energy inputs.

Indeed, metal–organic frameworks' heterogeneous character and porous nature render them outstanding catalysts compared to other catalysts, such as aluminosilicates, zeolites, and others. (Table 3). In addition, the synergistic effect between the Brønsted acid (linker) and Lewis acid (metal node) greatly promotes the strength of catalytic reactions (Jiang et al. 2014). More importantly, the functionality of metal–organic frameworks endows them one more merit than conventional catalysis since it facilitates the modification of metal–organic frameworks with active species, enhancing their catalytic performance (Chen et al. 2017b). The introduction of active species to metal–organic frameworks typically takes place via three strategies: post-synthetic approach, encapsulation of active species into metal–organic frameworks, and functionalization via the unsaturated metal sites or the organic ligand (Dhakshinamoorthy and Garcia 2014; Liu et al. 2014a).

Despite the merits mentioned above of metal–organic framework-based catalysts, they suffer a critical shortcoming: the poor stability of their structure, particularly in organic solvents and water, limiting their applications in water treatment (Tan et al. 2015). The robustness study of metal–organic frameworks in water, acidic and basic media, and water vapor found that the weak coordination

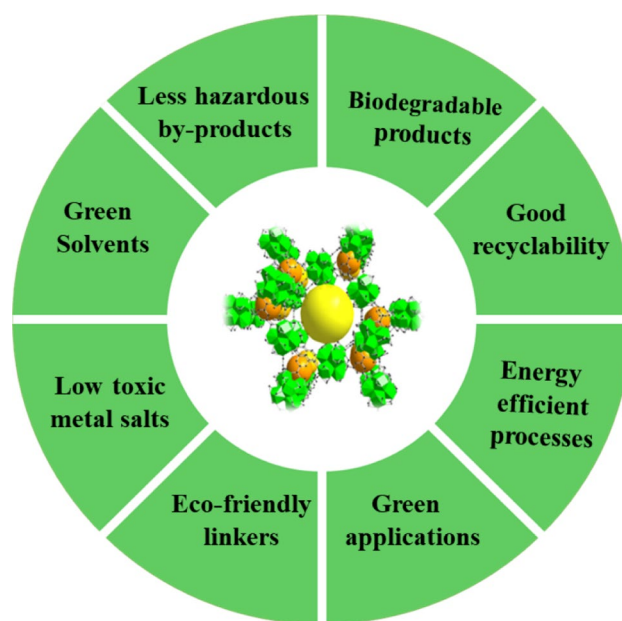


**Fig. 7** Environmental criteria for metal–organic framework-based catalysts. Green metal–organic can be obtained using green solvents and less toxic metal salts. The linker should be eco-friendly and produces biodegradable products with less hazardous by-products. The process should be energy efficient, and the metal–organic framework-based catalysts should have good recyclability and be applied in green applications

**Table 3** Synthesis conditions and applications of metal–organic frameworks (MOF)-based, non-noble metal-based, and nanocomposite-based catalysts

Catalyst group	Catalyst name	Synthesis conditions			Application	Reference
		Solvent	Temperature	Time		
<b>Metal–organic framework-based catalysts</b>	NiFe-BTC-G nanoparticles	Water/dimethyl formamide/ethanol	85 °C	24 h	Water electrolysis	Thangavel et al. (2020)
	magnetic metal–organic framework (Fe <sub>3</sub> O <sub>4</sub> @GlcA@Ni-MOF)	Water/dimethyl formamide	160 °C	15 h	Organic synthesis	Ghorbani-Choghmarani et al. (2021)
	PDA@GOx/ZIF-8	Water	Room temperature	30 min	Enzymatic catalysis	Wu et al. (2015)
	Fe-BTC	Water	Room temperature	10 min	Fenton oxidation	Martínez et al. (2018)
	Metal–organic framework (MIL-100(Fe))	Water	Room temperature	24 h	Fenton oxidation	Martínez et al. (2018)
	Platinum /UiO-66 (Univer-sitetet I Oslo) metal–organic framework (Pt/UiO-66)	Water	120 °C	24 h	Olefin hydrogenation	Zhang et al. (2014)
	Metal–organic framework (MIL-101(HPW))	Water	210 °C	40 min	Alcoholysis of styrene oxide	Wee et al. (2014)
	Hybrid material (Fe <sub>3</sub> O <sub>4</sub> @GO@MIL-100(Fe))	Water	70 °C	24 h	Photo-Fenton process	Gong et al. (2019)
	Iron oxide (magnetite, Fe <sub>3</sub> O <sub>4</sub> )/zeolitic imidazolate frame-work-67) (ZIF-67) metal–organic framework material (Fe <sub>3</sub> O <sub>4</sub> /ZIF-67)	Methanol	Room temperature	24 h	Peroxy monosulfate activation	Alamgholilo et al. (2021)
	Multi-component hybrid material (Pd@Fe <sub>3</sub> O <sub>4</sub> -NH <sub>2</sub> @MIL-101(Cr)-NH <sub>2</sub> )	Water	218 °C	18 h	Mizoroki–Heck Cross-coupling	Nuri et al. (2020)
	Tin dioxide-ZIF-8 composite	Methanol	Room temperature	24 h	Photodegradation of methylene blue	Chandra et al. (2019)
	Ni-hyperbranched poly-aromatic polymer	Toluene	120–180 °C	2 h	Catalytic transfer hydrogenation	Basaveni et al. (2019)
	Silver nanoparticles@rGO/MIL-88B(Fe)	Water	Room temperature	4 h	Oxygen evolution	Islam et al. (2017)
	A metal–organic framework (NU-1000)/ polyethyl-encimine (PEI) (NU-1000/PEI)	Water	–	–	Dimethyl methylphosphonate hydrolyzes	Moon et al. (2016)
	Metal–organic framework (Cu <sub>3</sub> (BTC) <sub>2</sub> )	Supercritical carbon dioxide	60 °C	24 h	Aerobic oxidation of benzylic alcohols	Peng et al. (2014)

Table 3 (continued)

Catalyst group	Catalyst name	Synthesis conditions			Application	Reference
		Solvent	Temperature	Time		
	Platinum/ metal–organic framework (MIL-101(Cr)) (Pt@MIL-101(Cr))	Supercritical carbon dioxide	220 °C	10 h	Catalytic ammonia borane hydrolysis	Matsuyama et al. (2016)
	Gold-X@nickel-metal organic framework (Au-X@NMOF-Ni)	Water	–	–	Reduction of nitro-aromatics	Yan et al. (2018b)
	Iron oxide@metal–organic framework (Fe <sub>3</sub> O <sub>4</sub> @MIL-100)	Water	70 °C	30 min	Photocatalytic degradation	Zhao et al. (2015)
	Titanium dioxide@university of Oslo-68-covalent organic framework (TiO <sub>2</sub> @UiO-68-CIL)	Methanol	Room temperature	24 h	Morita–Baylis–Hillman	Hu et al. (2018)
	Magnetic metal–organic framework (amidase@F <sub>3</sub> O <sub>4</sub> @UiO-66-NH <sub>2</sub> )	Water	–	–	Enzymatic activity	Lin et al. (2019b)
	Metal–organic framework (mHKUST-1@ZIF-8)	Water	Room temperature	12 h	Electrocatalysis	Yang et al. (2016a)
	Cobalt–metal–organic framework 74@N,N'-dihydroxypyromellitimide (NDHPI) (Co-MOF-74@NDHPI)	Dimethyl formamide-ethanol–water	100 °C	1 h	Aerobic oxidation	Pliekhov et al. (2018)
	Platinum and copper/Hong Kong University of Science and Technology-1 (HKUST-1) (Pt–Cu frame@HKUST-1)	Deionized water	200 °C	7 h	Hydrogenation of olefins	Jiang et al. (2017)
	Copper Oxide/ Hong Kong University of Science and Technology-1 (HKUST-1) (CuO/HKUST-1)	Solvent-free	180 °C	96 h	Photocatalytic Hydrogen evolution	Jin et al. (2019)
	Ulathrin MOF nanosheets (UMOFNs@ reduced graphene oxide- fluorine (UMOFNs@rGO-F)	Methanol/water	Room temperature	30 s	Oxygen evolution	Liu et al. (2020)
	Metal–organic framework (NENU-5)	Ethanol	–	12 h	Biomass transformation	Wang and Chen (2016)

Table 3 (continued)

Catalyst group	Catalyst name	Synthesis conditions		Application	Reference
		Solvent	Temperature		
<b>Non-noble metal-based catalysts</b>	Copper nanoparticles	–	–	Synthesis of S-aryl- and S-vinyl dithiocarbamates	Bhadra et al. (2008)
	Copper nanoparticles	Water	35–45 °C	Degradation of methyl red	Sinha and Ahmaruzzaman (2015)
	Copper nanoparticle-supported nanocrystalline cellulose	Water	110 °C	Catalytic reduction of methylene blue	Musa et al. (2017)
	Iron-palladium nanoparticles	Water	Room temperature	Dehalogenation	He and Zhao (2008)
	Platinum-coated cobalt nanoparticles	Dichlorobenzene	120–180 °C	Oxygen reduction reaction	Wang et al. (2017a)
	Nickel@ platinum (Ni@Pt) nanoparticles	Benzyl ether	200 °C	Oxygen reduction reaction	Park et al. (2016)
	Copper-2,2,6,6-tetramethylpiperidinyloxy (TEMPO)-oxidized cellulose nanofibril (Cu-TOCNF film)	Hydrochloric acid	Room temperature	Catalytic reduction of 4-nitrophenol	Bendi and Imae (2013)
	Iron nanoparticles	Water	Room temperature	Fenton oxidation of monochlorobenzene	Kuang et al. (2013)
	Silica and copper (SiO <sub>2</sub> @Cu)	Water	Room temperature	Aza-Michael reaction	Sreedhar et al. (2008)
	GT-nZVI	Water	–	Catalysis of hydrogen peroxide for the degradation of bromothymol blue	Hoag et al. (2009)

Table 3 (continued)

Catalyst group	Catalyst name	Synthesis conditions			Application	Reference
		Solvent	Temperature	Time		
<b>Nanocomposite-based catalysts</b>	Copper oxide/zinc oxide (CuO/ZnO) nanocomposite	Water	75 °C	2 h	Reduction of 4-nitrophenol and Rhodamine B	Bordbar et al. (2018)
	Zinc oxide/magnesium oxide (ZnO/MgO) nanocomposite	Water	Room temperature	4 h	Degradation of methyl orange, methylene blue, and 2-nitrophenol	Maruthai et al. (2018)
	Metal–organic framework (ZIF-8/PI) film	Methanol	Room temperature	24 h	Knoevenagel	Jin et al. (2013)
	Iron and zinc oxide (Fe-ZnO) nanoparticles	–	37 ± 1 °C	–	Photodegradation of naphthalene	Muthukumar et al. (2017)
	Cu/Fe <sub>3</sub> O <sub>4</sub> /eggshell nanocomposite	Water	70 °C	3 h	Reduction of methyl orange, 4-nitrophenol, Congo red, Rhodamine B, and methylene blue	Nasrollahzadeh et al. (2016)
	Nanocomposite material made of palladium (Pd) nanoparticles, UiO-66 metal–organic framework (MOF), and polydimethylsiloxane-coated thermoplastic (PDMS-T) (Pd/UiO-66@PDMS-T)	–	200 °C	–	Hydrogenation	Huang et al. (2016)
	Cobalt(II) supported on ethylenediamine functionalized nanostructured cellulose (EDANC) complex (Co(II)-EDANC)	Water	Room temperature	24 h	Oxidation of benzyl alcohols	Shaabani et al. (2014)
	Copper-doped zinc oxide nanoparticles	Water	200 °C	2–3 min	Degradation of Acid Black 234 dye	Khan et al. (2018a)
	Cobalt–metal–organic framework 74@N,N,N'-dihydroxypyromellitimide (NDHPI) (Co-MOF-NDHPI)	Methanol/acetone/nitrile	200 °C	5 h	Aerobic oxidation	Plietkhov et al. (2018)
	Chitosan-iron beads–chromium (CT-Fe beads-Cr)	Sodium hydroxide aqueous solution	Room temperature	–	Fenton oxidation for degradation of methylene blue	Chagas et al. (2019)

Several synthesis conditions are applied to optimize the uses of catalysts in water electrolysis, chemical synthesis, processes, and others. “–” not reported. BTC refers to 1,3,5-benzene tricarboxylic acid. G refers to graphene. Fe<sub>3</sub>O<sub>4</sub> and MOF refer to magnetite and metal–organic frameworks, respectively. ZIF-8, PDA, and GOx refer to zeolitic imidazolate framework-8, polydopamine, and glucose oxidase, respectively. GO refers to graphene oxide. NH<sub>2</sub> and rGO refer to amine and reduced graphene oxide, respectively. UMOFNs refer to ultrathin MOF nanosheets



bond between metal and linker is the leading cause of oxidative leaching of metal nodes. Thus, the metal-linker coordination bonds' strength has controlled the metal–organic frameworks' stability (Rashid et al. 2020). Nevertheless, few metal–organic frameworks possess high stability in water, especially MIL-family, such as MIL-101 (chromium, iron, aluminum), MIL-100 (chromium, iron), and MIL-53 (chromium, aluminum), as well as zirconium-based metal–organic frameworks (Schoenecker et al. 2012; Lan et al. 2016). Furthermore, porous coordination network-222 and porous coordination network-224 showed relatively high stability in both acidic and basic conditions, while the linker protonation of aluminum- metal–organic frameworks endows excellent stability in the acidic medium (Feng et al. 2013; Feng et al. 2012). The stability of zeolitic imidazolate frameworks was examined in boiling water, sodium hydroxide, and benzene at different temperatures for seven days. The results revealed the superb structural stability of ZIF-8 in boiling benzene and water for seven days and only 24 h in sodium hydroxide solution (Panda et al. 2019). Several studies have focused on enhancing the metal–organic framework's stability, suggesting that the linker's basicity is the key parameter in the robustness of the metal–organic framework since it controls the bond strength between metal and linker (Ali et al. 2021). Owing to these unparalleled advantages, metal–organic frameworks are intensively utilized in diversified applications as follows:

Pascanu et al. (2013) fabricated palladium-loaded MIL-101(Cr)-NH<sub>2</sub> composite (Pd@ MIL-101(Cr)-NH<sub>2</sub>) with different loading ratios of Pd (4, 8, 12, and 16 wt%). It was observed a diminution in the specific surface area ( $S_{\text{BET}}$ ) of MIL-101(Cr)-NH<sub>2</sub> from 2869 to 1321 m<sup>2</sup>/g and pore volume from 1.403 to 0.625 m<sup>3</sup>/g with the increase in the Pd loading ratios from 4 to 16 wt%, respectively. This finding may be attributed to the particle aggregation of the extra amount of Pd. Furthermore, the catalytic activity of the as-fabricated Pd@ MIL-101(Cr)-NH<sub>2</sub> composite was examined in the Suzuki–Miyaura cross-coupling reaction. It was found that the optimal Pd-loading ratio was 8 wt% since aryl and heteroaryl bromides and chlorides were coupled in eco-friendly solvents (H<sub>2</sub>O and ethanol) within a quite short reaction time and at an ambient temperature of 80 °C. More importantly, the recyclability study depicted the promising catalytic activity of 8 wt% for Pd@MIL-101Cr-NH<sub>2</sub> even after the 10th cycle.

In that context, Nuri et al. (2020) investigated the catalytic activity of Pd-supported amino magnetic MIL-101(Cr) composite (Pd@Fe<sub>3</sub>O<sub>4</sub>-NH<sub>2</sub>@MIL-101(Cr)-NH<sub>2</sub>) toward Mizoroki–Heck Cross-Coupling reaction of iodobenzene and methyl acrylate. They recorded a decline in the saturation magnetization (Ms) of iron oxide (Fe<sub>3</sub>O<sub>4</sub>) after binding with Pd and MIL-101(Cr). However, the Ms of Pd@Fe<sub>3</sub>O<sub>4</sub>-NH<sub>2</sub>@MIL-101(Cr)-NH<sub>2</sub> was still sufficient for the

separation by an external magnet instead of the conventional techniques that consumes a long time. Such perfect and easy separation is the prominent role of iron oxide since it does not possess catalytic activity toward Heck cross-coupling reaction. The reusability study displayed the ability of Pd@Fe<sub>3</sub>O<sub>4</sub>-NH<sub>2</sub>@MIL-101(Cr)-NH<sub>2</sub> to reuse for seven cycles with no significant decrease in its activity. Furthermore, it was suggested that the reduction of the catalytic activity of the as-fabricated magnetic composite is most likely due to the Pd leaching. Notably, Pd@Fe<sub>3</sub>O<sub>4</sub>-NH<sub>2</sub>@MIL-101(Cr)-NH<sub>2</sub> revealed a high catalytic activity and stability toward cross-coupling iodobenzene and methyl acrylate since the turnover frequency reached 2438 h<sup>-1</sup> within 30 min at 120 °C.

In one investigation, Alamgholilo et al. (2021) inspected the catalytic activity of magnetic ZIF-67 composite (Fe<sub>3</sub>O<sub>4</sub>/ZIF-67) toward the degradation of ciprofloxacin through peroxymonosulfate activation. The rhombic dodecahedron ZIF-67 was greenly synthesized in a benign solvent (methanol). However, ZIF-67 was successfully synthesized via a green approach in an eco-friendly solvent, and the yield was low (about 57%). Consequently, the green strategies for metal–organic framework preparation need further developments to be applicable in industrial applications.

Notably, Fe<sub>3</sub>O<sub>4</sub>/ZIF-67 composite showed high efficiency in degrading ciprofloxacin since the degradation rate reached 98% during 48 h using 0.4 g/L Fe<sub>3</sub>O<sub>4</sub>/ZIF-67 and 0.5 g/L peroxymonosulfate. Furthermore, the pure Fe<sub>3</sub>O<sub>4</sub> and ZIF-67 revealed a lower ciprofloxacin degradation efficiency compared to the Fe<sub>3</sub>O<sub>4</sub>/ZIF-67 composite, reflecting the synergistic effect between the pristine components. To determine the predominant radical species in the degradation of ciprofloxacin, the scavenger effect was studied in the presence of isopropyl alcohol, benzoquinone, and ethanol. The result clarified that both SO<sub>4</sub><sup>•-</sup> and ·OH are the controlled radicals. Besides, Electron spin resonance confirmed the same result since only the characteristic signals of SO<sub>4</sub><sup>•-</sup> and ·OH appeared in the Fe<sub>3</sub>O<sub>4</sub>/ZIF-67/peroxymonosulfate system. These findings indicated that the degradation mechanism of ciprofloxacin most probably occurs via the radical pathway.

In another investigation, Chandra et al. (2019) adopted the green synthesis approach to fabricate another ZIF MOF to photodegrade methylene blue from an aqueous solution. The core–shell tin dioxide (SnO<sub>2</sub>)-ZIF-8 composite was fabricated with various ratios of tin dioxide, revealing a decrease in the degradation efficiency of methylene blue with the increase in the ratios of tin dioxide due to particle aggregation. It was reported that the photocatalytic degradation mechanism of methylene blue using tin dioxide-ZIF-8 composite occurred as follows: the movement of the generated e<sup>-</sup> and h<sup>+</sup> in the conduction and valance bands of tin dioxide to ZIF-8, reducing the recombination of e<sup>-</sup> and h<sup>+</sup> pair. Then, this e<sup>-</sup> and h<sup>+</sup> pair could form ·OH via the

oxygenation of H<sub>2</sub>O. Thus, ·OH is the responsible radical for the photocatalytic degradation of methylene blue, agreeing with several previous studies (Chandra and Nath 2017; Jing et al. 2014; Kim et al. 2016).

Further, Gong et al. (2019) successfully prepared a magnetic core–shell Fe<sub>3</sub>O<sub>4</sub>@GO@MIL-100(Fe) microsphere catalyst using water as a solvent instead of dimethyl formamide in a green and sustainable route. The scanning electron microscope and transmission electron microscope images of the synthesized materials demonstrated that Fe<sub>3</sub>O<sub>4</sub> particles have rough surface spheres with particle sizes ranging from 300 to 350 nm. However, a crinkled surface texture was obtained after being wrapped with graphene oxide (GO) with a 4.5 nm thickness of the GO layer. Upon coating with MIL-100(Fe), the MOF layer was 61 nm thick, confirming the formation of magnetic core–shell Fe<sub>3</sub>O<sub>4</sub>@GO@MIL-100(Fe) microspheres. The fabricated catalyst was used for 2,4-dichlorophenol (2,4-DCP) degradation via the photo-Fenton process with almost 100% efficiency in 40 min. The reusability tests revealed that the magnetic core–shell Fe<sub>3</sub>O<sub>4</sub>@GO@MIL-100(Fe) catalyst has good stability and recycling ability.

### Non-noble metals nanoparticles

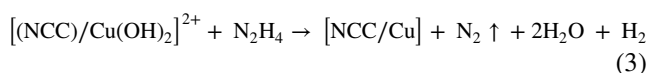
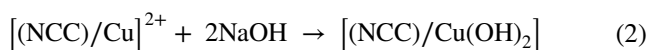
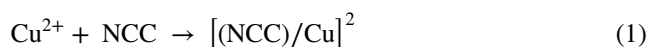
Undoubtedly, metal nanoparticles have received immense interest in the last few years in the catalysis field owing to their unique physical and chemical properties (Song et al. 2015). Interestingly, it was deduced that the metal catalysts in a nano-size possess advanced catalytic performances compared to their bulk equivalents since the size and shape play significant roles in the chemical activity of the catalyst (Table 3). The catalyst shape impacts its activity and selectivity toward the catalytic reactions, while the catalyst size controls its specific surface area (Mandić et al. 2017). Nonetheless, the fabrication of shape-controlled metal nanoparticles is still a big challenge and a complicated process. For this purpose, several strategies have been developed to synthesize stable metal nanoparticles with a defined shape, such as the addition of inorganic capping agents, organic ligands, colloids, polymers, or the fabrication of core–shell materials (Campelo et al. 2009).

Among the metals nanoparticles, noble metals have revealed exceptional catalytic performance in various potential applications (Wang and Astruc 2017). However, they could not be classified as sustainable catalysts due to their high price, rare abundance on earth, and detrimental impacts on the biological system. Contrariwise, the availability, premium activity, and selectivity of non-noble metals have acquired considerable fame among the diverse as more favorable catalyst types (Ilies et al. 2020). Therefore, extensive studies have been implemented focusing on preparing

non-noble metal nanoparticle-based catalysts under green conditions, considering using nontoxic solvents and consuming low energy. In addition, the utilization of bio-reducing agents such as algal, sugars, glutathione, and mainly plant extract (Fig. 8) instead of the toxic reducing agents such as sodium borohydride or lithium borohydride. For instance, Lohrasbi et al. (2019) fabricated an iron nanocatalyst using *Plantago* as a bio-reducing agent. The transmission electron microscope image revealed that the particles are uniform spherical with a size range between 4.6 and 30.6 nm.

Furthermore, Din et al. (2018) utilized the wild plant *Calotropis gigantea* as a bio-reducing and stabilizing agent to fabricate nickel nanocatalysts. The various characterization tools inferred the successful fabrication of nickel in a nano-size of 20–40 nm. Thus, such bio-reducing agents could fabricate non-noble metal nanoparticles with controlled particle size and shape in some cases (Murphy 2008).

Unfortunately, there are some flaws in non-noble metal nanoparticles as catalysts, including their rapid deactivation, poor recyclability, and difficult separation. Several previous studies have reported that using supported nanoparticles is the most effective method among the other approaches to overcome these demerits of non-noble metals (Wang et al. 2021b). However, supported metal nanoparticles provoke researchers' anxiety about whether the quite active and dispersed supported metal nanoparticles are harmful to human tissues or not. On the other hand, no cytotoxicity or cellular oxidative stress was inferred for the unsupported metals, although they were retained in human tissues (Campelo et al. 2009). In this perspective, Musa et al. (2017) fabricated copper nanoparticle-supported nanocrystalline cellulose (Cu@NCC) for the catalytic reduction of methylene blue in the presence of sodium borohydride (NaBH<sub>4</sub>) as a reducing agent. The following equations represent the proposed preparation mechanism of copper nanoparticle-supported nanocrystalline cellulose;



To infer the successful preparation of copper nanoparticle-supported nanocrystalline cellulose, the elemental composition was examined by X-ray fluorescence, clarifying the presence of Cu in nanocrystalline cellulose (NCC). Moreover, the thermogravimetric analysis elucidated an improvement in the thermal behavior of NCC after binding with Cu nanoparticles, proving the interaction between NCC and Cu nanoparticles. At the same time, a noticeable

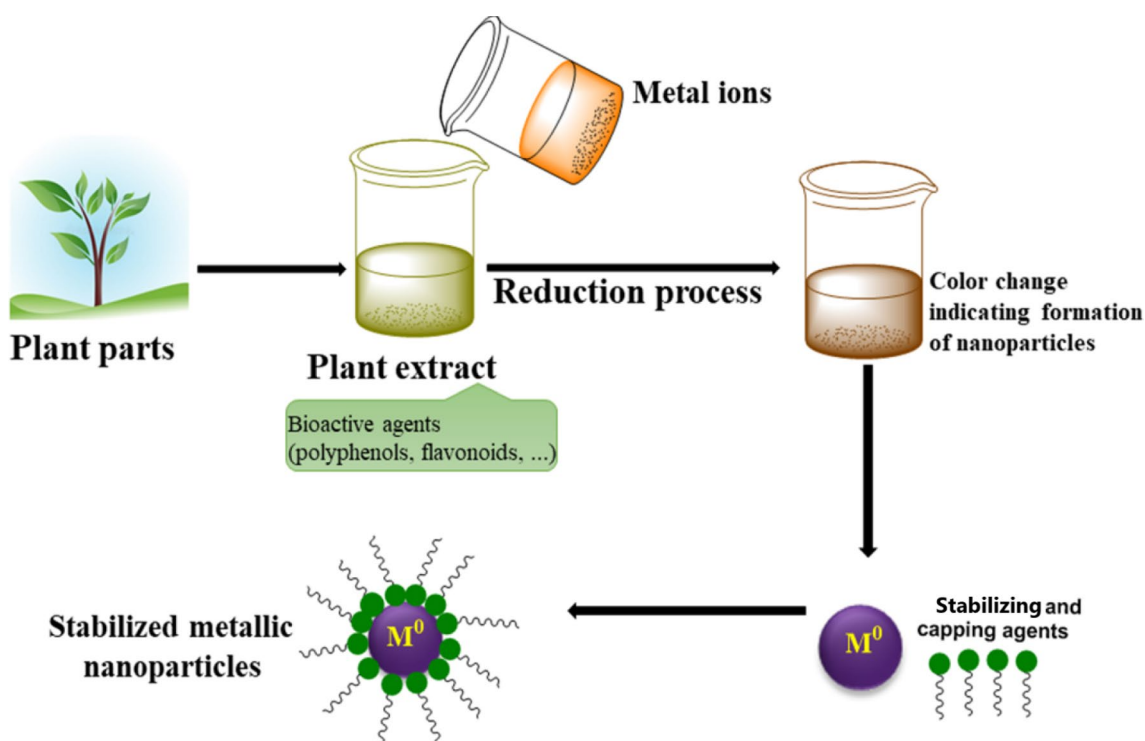


**Fig. 8** Synthesis of non-noble metal nanoparticles from plant materials, such as leaves, seeds, flowers, stems, roots, or fruits. The plant extract contains a variety of bioactive agents, such as polyphenols and flavonoids. These bioactive agents can reduce the metal ions to pro-

duce metallic nanoparticles. The capping agents in the plant extract act as capping agents for the metallic nanoparticles. These non-noble metal nanoparticles are suitable more preferably-type catalysts.  $M^0$  refers to metal nanoparticles

decline in the surface area of copper nanoparticle-supported nanocrystalline cellulose was recorded compared to that of NCC, most likely due to the dispersion of Cu nanoparticles onto the NCC surface and its pores (Ghosh et al. 2015). Results confirmed the auspicious catalytic activity of copper nanoparticle-supported nanocrystalline cellulose toward reducing methylene blue since the reaction completely terminated within merely 12 min. In comparison, the unsupported Cu nanoparticles reduced methylene blue within 44 min. This finding revealed that the supported nanoparticles possessed higher catalytic activity than the unsupported ones. Contrariwise, Kamal et al. (2019) pointed out that the unsupported carboxymethyl cellulose-stabilized cobalt nanoparticles (CMC-Co) contained higher catalytic activity toward reducing methylene blue than the supported carboxymethyl cellulose-stabilized cobalt bacterial-cellulose nanofibers (CMC-Co-bacterial cellulose nanofibers). This behavior may be explained by the availability of the whole surface area of cobalt nanoparticles of carboxymethyl cellulose-stabilized cobalt nanoparticles to adsorb the methylene blue molecules. In contrast, in carboxymethyl cellulose-stabilized cobalt-bacterial cellulose nanofibers, the cobalt nanoparticles are partly available.

In another attempt, Wang et al. (2017) adopted an innovative technique to prepare an electrocatalyst for the oxygen reduction reaction. The platinum-coated cobalt nanoparticles (Co@Pt) were fabricated via in situ seed growth approach. Such a preparation method enables self-nucleation and growth by adjusting the Pt deposition rate to be slower than its diffusion rate on the surface (Park et al. 2016). Besides the generated CO during the Co growth from cobalt carbonyl facilities, the coating of Pt on the Co. Transmission electron microscope image inferred the core-shell-like structure of platinum-coated cobalt with an average diameter of 10 nm, whereas the diameter of the platinum shell was 1 nm. It was found that the catalytic activity of platinum-coated cobalt for oxygen reduction reaction was enhanced 10 times compared to pure platinum.

Furthermore, platinum-coated cobalt exhibited a high stability potential cycling since the non-noble Co nanoparticles were conserved from leaching out by the noble platinum nanoparticles shell. This result was consistent with Park et al. (2016), which enhanced the durability of nickel-platinum (Ni-Pt) electrocatalyst for oxygen reduction reaction by coating it with a thin layer of platinum. It was deduced that Ni-Pt@Pt protected Ni nanoparticles from leaching; however, 11% of Ni was leaching from Ni-Pt. In addition, the activity of Ni-Pt dwindles by about 75% after 10,000

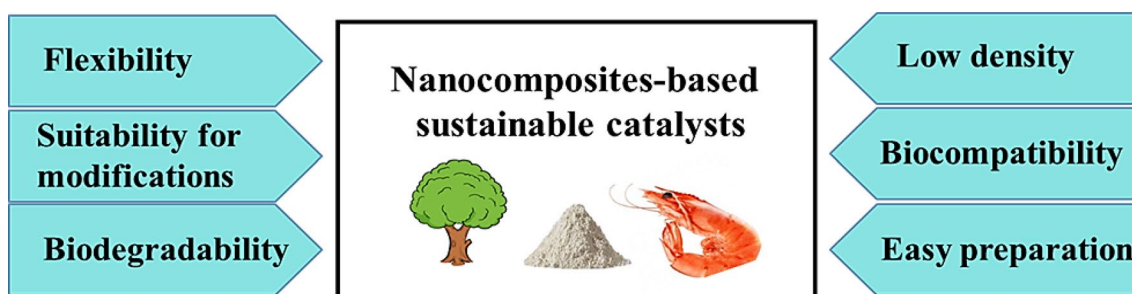


**Fig. 9** Characteristics of the nanocomposite-based sustainable catalysts fabricated from renewable resources. Bio-renewable resources such as lignin, starch, and chitin are widely used in nanocomposite-based sustainable catalysts preparation. Nanocomposite-based catalysts should be flexible and suitable for modifications. Biodegradability

is the primary condition for nanocomposites to be considered sustainable catalysts. Low density, biocompatibility, and ease of preparation are among the main criteria of nanocomposite-based sustainable catalysts

cycles of the oxygen reduction reaction, while the activity of Ni–Pt@Pt decreased by only 25%.

### Nanocomposites

Using any pure substance as a catalyst has advantages and disadvantages, so combining two or more to form composites is a superior avenue in modern technology. Such an approach enables the exploitation of the best merits of each substance by overcoming some of its demerits (Ates et al. 2017). Composites are classified into three groups based on their size; micro-composites, macro-composites, and nanocomposites (Paul and Robeson 2008). The extremely high surface area, strong interaction between the matrix, and high stability of nanocomposites have revealed remarkable activity (Yu et al. 2006; Xu et al. 2015a). Notably, it was evinced that the combination of two active components dramatically enhances their catalytic activity (Lin et al. 2019a).

Nonetheless, the rapid growth of nanocomposites during the preparation results in hazardous environmental issues due to their complex decomposition (Ates et al. 2020). One of the most feasible solutions to this problem is utilizing templates to control the size and shape of nanocomposites and protect their surfaces, thereby preventing particle aggregation (Yadav et al. 2019). Diversified commercial templates have been utilized as functionalizing agents to ameliorate nanocomposites' morphology, size, and properties (Table 3). Still, they have revealed a fatal environmental risk due to their difficulty degrading or removing. Hence, synthesizing nanocomposites using bio-renewable resources like starch, chitin, vegetable oils, lignin, natural rubber, and cellulose has drawn vast concern to fabricating catalysts with no harsh synthetic approach (Borah et al. 2017). Such nanocomposite-based sustainable catalysts possess outstanding features, including easy preparation, excellent biocompatibility, low density, good biodegradability, low cost, flexibility,

and suitability for modifications (Fig. 9) (Ulu et al. 2018). However, these fabricated nanocomposites from bio-renewable resources still suffer drawbacks limiting their industrial applicability, such as low thermal, chemical, and mechanical stability (Ates et al. 2020).

Nanocomposites derived from bioresources have exhibited remarkable performance in diverse potential applications. For instance, Wang et al. (2019b) fabricated chelated copper onto polydopamine-coated sand composite (Cu-PDA@Sand) for the catalytic degradation of the anionic Congo red and cationic methylene blue as well as reduction of 4-nitrophenol. It was found that 4-nitrophenol was wholly reduced to 4-aminophenol within 13 min. Furthermore, the color of Congo red vanished after only 6 min, while the color of methylene blue dye disappeared after 9 min, suggesting the reduction of methylene blue (Kim et al. 2016; Subair et al. 2016). Moreover, to examine the applicability of copper onto polydopamine-coated sand composite in industrial applications, the long-term catalytic activity was studied after 30 days. It recorded a slight diminution in the apparent reaction rate of 4-nitrophenol, Congo red, and methylene blue (about 6%), inferring the stability of the copper onto polydopamine-coated sand composite. Interestingly, the reusability test showed that the catalytic activity of copper onto polydopamine-coated sand composite toward the reduction of 4-nitrophenol did not decrease yet, even after 20 cycles. These findings confirmed the superb catalytic activity, stability, and reusability of copper onto polydopamine-coated sand composite.

In another study, Hajipour and Malek (2021) inspected the catalytic performance of Co/N-heterocyclic carbene-supported magnetic chitosan composite (Co/NHC@mCs) toward Suzuki and Sonogashira reactions of aryl chlorides. Several key parameters were studied to determine the optimal condition for both reactions, including solvent, base, catalyst dose, and reaction temperature. It was recorded that Suzuki cross-coupling reaction of 1-chloro-4-nitrobenzene

with (4-methoxyphenyl) boronic acid achieved a high yield (90%) in polyethylene glycol as a reaction medium and at 70 °C within 8 h using 3 mol% of Co/NHC@mCs. On the other hand, the best yield (84%) in Sonogashira cross-coupling between 1-chloro-4-nitrobenzene and 1-ethynyl-4-methoxybenzene was obtained in polyethylene glycol at 100 °C, using 6 mol% of Co/NHC@mCs. Notably, both reactions proceeded without adding Co/NHC@mCs, and no product was obtained in these cases. Importantly, the recyclability test pointed out the propitious recyclability of Co/NHC@mCs since its catalytic activity dwindled to only 7% after the seven cycles. Furthermore, the used Co/NHC@mCs were characterized by transmission electron microscope, and scanning electron microscope displayed no change in the morphology compared to the fresh Co/NHC@mCs. Additionally, the Co-leaching amount that inductively coupled plasma mass spectrometry recorded was less than 2%. At the same time, X-ray diffraction revealed no change in the peak intensity after using Co/NHC@mCs for 7 cycles. These results suggested the excellent efficiency, stability, and reusability of Co/NHC@mCs. In addition to the sustainability of the earth-abundant Co-based catalyst instead of the high-cost Pt-based catalysts.

In this perspective, Mohammadinezhad and Akhlaghinia (2017) fabricated a costless and efficient nanocatalyst ( $\text{Fe}_3\text{O}_4@$ Boehmite- $\text{NH}_2$ -CoII) for both Heck–Mizoroki and Suzuki–Miyaura reactions. The transmission electron microscope image showed the core–shell structure of  $\text{Fe}_3\text{O}_4@$ Boehmite- $\text{NH}_2$ -CoII, where  $\text{Fe}_3\text{O}_4$  is the core and Boehmite is the shell. Furthermore, the particle size of  $\text{Fe}_3\text{O}_4@$ Boehmite- $\text{NH}_2$ -CoII was found to be in the range of 13–54 nm. Field emission scanning electron microscope revealed an excellent distribution of  $\text{Fe}_3\text{O}_4@$ Boehmite- $\text{NH}_2$ -CoII with an average particle size of 20–30 nm. To determine the optimum conditions of the Suzuki–Miyaura coupling reaction between 4-iodobenzene and phenylboronic acid, the effect of solvents was studied in the presence of dimethyl sulfoxide, n-hexane, polyethylene glycol, n-hexane, toluene, tetrahydrofuran, n-hexane, ethanol, acetonitrile, and water. It was found that water could be utilized as a benign, costless, efficient solvent for the reaction. Furthermore, the optimal dose of  $\text{Fe}_3\text{O}_4@$ Boehmite- $\text{NH}_2$ -CoII was 0.33 mol%, while the further increase in the catalyst dose (22 mol%) did not change the rate or the yield of the reaction. However, the lower catalyst dose (0.22 mol%) significantly diminished the reaction yield. Moreover, to prove the synergistic effect between the components of the catalyst, the reaction has proceeded in the presence of pristine  $\text{CoCl}_2\cdot 6\text{H}_2\text{O}$ ,  $\text{Fe}_3\text{O}_4$ , magnetic  $\text{Fe}_3\text{O}_4@$ Boehmite,  $\text{Fe}_3\text{O}_4@$ Boehmite-Pr-Cl, and  $\text{Fe}_3\text{O}_4@$ Boehmite- $\text{NH}_2$  as catalysts, revealing incomplete

coupling between 4-iodobenzene and phenylboronic acid with conversion yields of 40, 20, 20, 5, 5 and 5% after 24 h, respectively.

In another study, Basaveni et al. (2019) fabricated nickel (Ni) nanoparticle-based catalyst encapsulated in a supporting and stabilizing matrix hyperbranched poly-aromatic polymer anchored poly-aromatic polymer for the catalytic transfer hydrogenation of alkenes and nitroarenes. The hyperbranched poly-aromatic polymer matrix acted as a control matrix for the nickel nanoparticles' particle size. The nickel nanoparticles' size was controlled by encapsulation into the cavities of hyperbranched poly-aromatic polymer that prevent their aggregations. The Ni-hyperbranched poly-aromatic polymer had high activity and good air stability. The catalytic transfer hydrogenation was carried out under base-free conditions without the need for high pressure, highly acidic conditions, or a strongly flammable hydrogen source. The Ni-hyperbranched poly-aromatic polymer catalytic system showed good tolerance toward alkyne, hydroxyl, or halogen substituents.

## Enzymes

Enzyme biocatalysis has drawn vast attention in industrial applications, such as producing antibiotic precursors and synthesizing valuable chemical products such as acrylamide, detergents, and others (Ottone et al. 2021; Madhavan et al. 2021). Enzymes are biological catalysts that constitute a complex protein chain connected to active metal sites offering unique selectivity toward the substrate molecules and good catalytic activity (Yi et al. 2021; Nazor et al. 2021). Besides, enzymes have demonstrated excellent catalytic activity in various chemical conversions from simple hydrolysis to reaction syntheses, outperforming other traditional chemical processes (Bell et al. 2021). Therefore, enzymes have been involved in many applications, as listed in Table 4. Thanks to their intrinsic properties, high selectivity and turnover number, cost-effectiveness, sustainability, and eco-friendly advantage (Zhang et al. 2021a). Owing to the biodegradability and sustainability of enzymes, they have been extensively utilized in environmental applications such as the bioremediation of water and soil pollution (Singh et al. 2021; Sellami et al. 2022). Additionally, enzymes have exhibited an auspicious catalytic performance in the biorefinery of waste polysaccharides and agro-industrial residues into valuable products such as bioplastics, biofuels, and sweeteners (Shiva et al. 2022; Mirpoor et al. 2021; Baptista et al. 2021) as well as the revalorization of lignocellulose or cellulose wastes into costless biofuels (Fig. 10) (Mathew et al. 2021; Li et al. 2021). Notably, the high reaction

**Table 4** Sustainable enzyme-based catalysts and their immobilization support, applications, and recyclability

Enzyme	Immobilization support	Application	Recyclability	Reference
Horseradish peroxidase	Modified graphene oxide	Biodegradation of phenol	70% after 10 cycles	Besharati Vineh et al. (2018)
Horseradish peroxidase	Ca-alginate beads	Biodegradation of synthetic dyes	>40% efficiency after 7 cycles	Bilal et al. (2016)
Laccase	Polymer-containing cyclic carbonate	Biodegradation of bisphenol A & Congo red	53% (bisphenol A) and 67% (Congo red) after 10 cycles	Bayramoglu et al. (2018)
Peroxidase	Dopamine-modified, chitosan-coated, halloysite nanotube porous microspheres	Biodegradation of dyes mixture	57.6% efficiency after 6 cycles	Ren et al. (2022)
Phosphotri-esterase	Pluronic F127 forming cross-linked enzyme-polymer conjugates	Biodegradation of malathion	–	Cheng et al. (2018b)
Polyphenol oxidase	Chitosan/organic rectorite	Biodegradation of phenolic compounds	60.3 ± 1.5% efficiency after 10 cycles	Zhong et al. (2021)
Laccase	Bentonite-derived mesoporous materials	Biodegradation of tetracycline	36% efficiency after 5 cycles	Wen et al. (2019)
Laccase	Magnetic nanoparticles (Fe <sub>3</sub> O <sub>4</sub> )	Biodegradation of sulfonamides	–	Shi et al. (2014)
Chloroperoxidase and glucose peroxidases (Co-immobilized)	Graphene oxide functionalized composite of iron oxide	Biodegradation of orange G	38.5% efficiency after 6 cycles	Gao et al. (2019)
Laccase	Graphene-oxide zeolite nanocomposite	Biodegradation of direct red 23	95% efficiency after 5 cycles	Mahmoodi and Saifur-Dastgerdi (2020)
Manganese peroxidase	Chitosan functionalized iron oxide nanoparticles	Biodegradation of reactive orange and methylene blue	85 ± 2% (methylene blue), 86 ± 2% (reactive orange) efficiencies after 5 cycles	Siddeeq et al. (2020)
Laccase	Chitosan	Biodegradation of bisphenol A	71.2% efficiency after 10 cycles	Bilal et al. (2019b)
Peroxidase	Chitosan	Biodegradation of reactive blue 4, reactive blue 19, and methyl orange	>55% efficiency after 11 cycles	Ma et al. (2018)
Horseradish peroxidase	β-cyclodextrin–chitosan complex	Biodegradation of Azo dye	58% efficiency after 6 cycles	Karim et al. (2012)
Laccase	Chitosan-clay composite beads	Biodegradation of Remazol brilliant blue R, methyl red, and reactive black 5 dye	42% efficiency after 15 cycles	Mehandia et al. (2020)
Horseradish peroxidase	Zinc oxide nanowires/macroporous Silicon dioxide composite	Biodegradation of acetone-ethanol-butanol: ABE-113, ABK-10 BX	79.4% (ABE-113) and 71.1% (ABK-10 BX) efficiencies after 12 cycles	Sun et al. (2017)
Laccase	Core-shell magnetic copper alginate beads	Biodegradation of remazol brilliant blue R and tricosan	89.6% tricosan after 8 h 54.2–75.8% Remazol brilliant blue R after 4 h	Le et al. (2016)
Pectinase	Polyacrylamide gel	Biodegradation of industrial effluent	50% efficiency after 7 cycles	Rehman et al. (2020)
Peroxidase and syringaldehyde	Calcium alginate beads	Biodegradation of indole	91.8% efficiency after 4 cycles	Liu et al. (2021a)
Horseradish peroxidase	Chitosan	Biodegradation of reactive black 5, Crystal Violet, Congo Red, And Remazol Brilliant Blue	64.9% efficiency after 6 cycles	Bilal et al. (2017d)

Table 4 (continued)

Enzyme	Immobilization support	Application	Recyclability	Reference
Ginger peroxidase	Alginate-guar gum, agarose-guar gum hydrogels	Biodegradation of textile effluent	68% (alginate-guar gum) and 55% (agarose-guar gum) efficiencies after 10 cycles	Ali and Husain (2018)
Laccase	Copper alginate	Biodegradation of indigo	–	Teerapatsakul et al. (2017)
Peroxidase	Calcium alginate-pectin	Biodegradation of direct red, direct blue	–	Satar and Husain (2011)
Peroxidase	Calcium alginate	Biodegradation of Direct azo dye	36% efficiency after 5 cycles	Boucherit et al. (2013)
Peroxidase	Chitosan	Biodegradation of methyl orange, Congo red, and trypan blue	50% efficiency after 4 cycles	Pandey et al. (2017)
$\beta$ -Glucosidase	Magnetic chitosan microspheres	Biorefinery of pretreated corn straw to reduce sugar	84.4% efficiency after 8 cycles	Zheng et al. (2013)
Cellulase from <i>Alternaria alternata</i>	Iron oxide magnetic nanoparticles	Biorefinery of sugarcane bagasse powder pretreated with acid into glucose	52% efficiency after 3 cycles	Ingle et al. (2017)
Cellulase (cellic CTec2)	Magnetic graphene oxide	Biorefinery of pretreated sugarcane Bagasse into ethanol	27% efficiency after 10 cycles	Paz-Cedeno et al. (2021)
Cellulase from <i>Trichoderma reesei</i>	Silica functionalized gold nanoparticles	Biorefinery of bamboo chopstick Powder into glucose	> 99% efficiency after 6 cycles	Cheng and Chang (2013)
$\beta$ -Glucosidase	Calcium alginate entrapment	Biorefinery of hydrothermally pretreated barley straw into ethanol	–	Tsai and Meyer (2014)
Xylanase	Calcium alginate three-dimensional printed support	Biorefinery of corn cob into xylo-oligo saccharides	60% efficiency after 7 cycles	Jiang et al. (2020)
Laccase	chitosan coated Fe <sub>3</sub> O <sub>4</sub> @SiO <sub>2</sub>	Biorefinery of sweet sorghum stover into biohydrogen	70% efficiency after 8 cycles	Shanmugam et al. (2020)
Xylanase and $\beta$ -xylosidase	Co-immobilized on chitosan	Biorefinery of oat spelled xylan into xylobiose and xylotriiose	94% efficiency after 13 cycles	Maalej-Achouri et al. (2009)
Cellulase, pectinase, and hemicellulose	Alginate	Biorefinery of flaxseeds	–	Long et al. (2011)
Cellulase (ParsiCell)	Graphene oxide reinforced hydrogels	Biorefinery of carboxymethyl cellulose into glucose	51% efficiency after 4 cycles	Ariaeenejad et al. (2020)
Cellulase	UiO-66-NH <sub>2</sub>	Biorefinery of carboxymethyl cellulose into glucose	> 72% efficiency after 10 cycles	Ahmed et al. (2018)
$\beta$ -Glucosidase	Cu-MOF	Biorefinery of carboxymethyl cellulose into glucose	70% retained efficiency after 8 cycles	Wang et al. (2019c)

Enzymes-bioremediation of wastewater showed remarkable proficiency against a wide range of resistant pollutants, including oil, grease, and micropollutants, i.e., pharmaceuticals, pesticides, plastics, personal care products, and others, under mild conditions

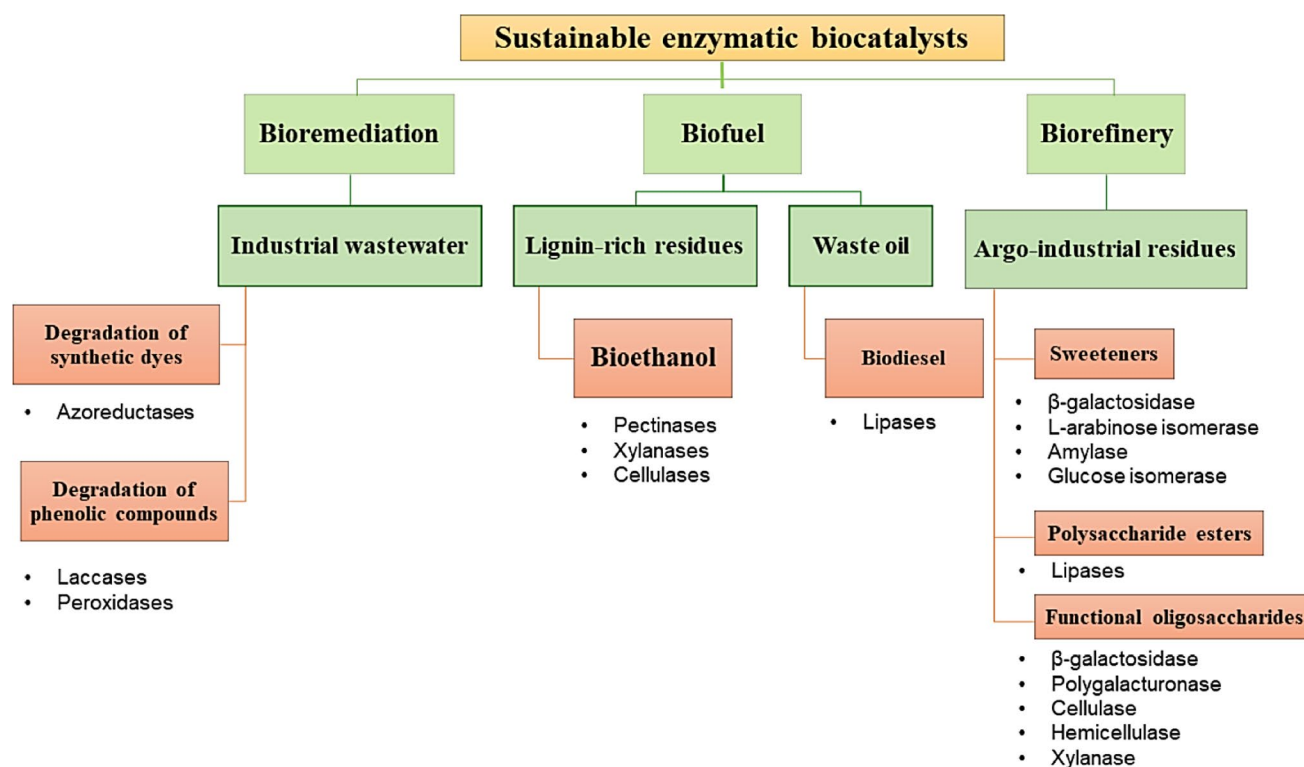


**Fig. 10** Applications of enzymatic biocatalysis for sustainability. Enzymes are utilized in the bioremediation of industrial wastewater and biofuel production from lignin residues and waste oil. Many

enzymes are used in the biorefinery field. Enzymes have shown excellent activity in chemical conversion processes

kinetics, selectivity, cost-effectiveness, recyclability, and non-toxicity of enzymes render them promising candidates in wastewater remediation.

Due to the extensive production of oils, greases, and fats over the past few years, estimated as 20–3.8 million metric tons of edible vegetable oils in 2018 (Luo et al. 2020), large amounts of waste oil containing organic and inorganic loads have been disposed into the aquatic environment, producing filamentous microorganism blooms onto the water's surface (Feng et al. 2021). Activated sludge was involved in mitigating such aquatic problems, but the floating oil effluent limited performance, causing poor sedimentation and reduced sludge biomass (Cammarota and Freire 2006). Lipases exhibited efficient biodegradation of triglycerides (i.e., vegetable oils, fats, greases) rather than traditional activated sludge. For example, Meng and co-workers investigated the anaerobic degradation of three different types of triglycerides (animal fat, vegetable oil, and floatable grease) involving lipase derived from three different sources, namely *Aspergillus* (lipase I), *Candida* (lipase II), and *Porcine pancreatic* (lipase III) (Meng et al. 2017). Lipase I and II showed an efficient biodegradation rate under appropriate hydrolysis conditions (24 h, 1000–1500  $\mu\text{L}$  of lipase volume, and 40–50  $^{\circ}\text{C}$ ), producing byproducts of long chains of fatty acids.

In contrast, lipase III showed a modest biodegradation performance. These findings confirmed the influence of the enzyme's source on their activity. In another attempt, Theerachat et al. (2017) exhibited excellent degradation efficiency (93%) of palm oil mill effluent with a high oil concentration (7762  $\text{mg L}^{-1}$ ) using lipase derived from *Candida rugosa*-cultured yeast cells. However, these enzymatic treatments were considered primary processes and needed to be accompanied by another treatment process, such as activated sludge or anaerobic fermentation, to attain complete treatment of the fatty acids and glycerol byproducts.

Despite the harsh removal of many micropollutants due to their resistance to natural biodegradation, toxicity, and presence in nanogram or microgram concentrations in the aquatic medium, enzymes demonstrated proficient catalytic degradation performance against a diverse range of micropollutants such as pharmaceuticals, pesticides, phenolic compounds, and organic dyes. However, their vulnerable stability under extreme pH and temperature conditions and their poor reusability due to the difficult separation of enzymes from reaction media remain challenging. Accordingly, directed evolution and genetic engineering techniques (i.e., tuning the sequential structure of genes) have been conducted to boost enzymes' stability and catalytic performance (Saravanan et al. 2021; Palomo 2021). Recently,



researchers found that immobilization of enzymes into solid support such as organics (natural or synthetic polymers), inorganics (silica, zeolites, graphene, titania, alumina), or organic–inorganic hybrid materials improves the catalytic performance of enzymes, the biocompatibility as well as the stability and the reusability considering the economic point of view (Ashkan et al. 2021; Zahirinejad et al. 2021). Notably, the immobilization strategy and the type of enzyme carrier represent crucial factors that directly affect the stability of the enzymes due to the possible undesired interactions with the solid support and the sluggish mass transfer of the target molecules retarding the catalytic interaction with enzymes (Nunes et al. 2021). In this context, Mahmoodi and Saffar-Dastgerdi (2020) developed a novel biocatalyst of laccase covalently immobilized onto zeolite (NZ)-graphene oxide (GO) for the effective removal of Direct red 23 organic pollutants. Covalent immobilization of laccase through salinization and crosslinking of the surface support via (3-aminopropyl) trimethoxy and glutaraldehyde, respectively, provided super stability and higher loading of the enzyme. Laccase covalently immobilized onto zeolite (NZ)-graphene oxide (GO) exhibited higher degradation efficiency by increasing the graphene oxide content from 3 to 7% due to the accelerated electron transfer from the enzyme to the support. Besides, graphene oxide content the loading amount of enzyme (350 mg/g) compared to bare zeolite support (180 mg/g) (i.e., 1.7 times higher than zeolite). This was attributed to the increased surface area of the NZ-GO nanocomposite support concerning bare zeolite, enabling a greater loading amount of enzyme.

Interestingly, Laccase covalently immobilized onto zeolite (NZ)-graphene oxide (GO) demonstrated remarkable retained efficiency of 95% over 5 cycles, verifying the outstanding stability of the immobilized laccase. Additionally, the immobilized enzyme revealed its superior storage stability than the free enzyme, achieving higher catalytic activity of 83% after 8 days of incubation comparable to the latter (60%). It is worth noting that covalent immobilization passively affects the catalytic activity of enzymes due to the conformational distortion and change in the chemical structure of enzymes after covalent attachment.

In this stream, Ahmed et al. (2018) exhibited an innovative strategy to immobilize cellulase for sustainable cellulose biorefinery into valuable products. Considering the advantage of enzyme immobilization via physical adsorption, retaining the structured entity, and catalytic activity of enzymes, cellulase was successfully immobilized onto UiO-66-NH<sub>2</sub> (cellulase@UiO-66-NH<sub>2</sub>) under mild conditions. Brunauer–Emmett–Teller (BET) measurements declared cellulase@UiO-66-NH<sub>2</sub> possessed a lower specific surface area (269.3 m<sup>2</sup> g<sup>-1</sup>) than pristine UiO-66-NH<sub>2</sub> (593 m<sup>2</sup> g<sup>-1</sup>), attributed to the pore-clogging by the loaded enzymes, confirming the successful immobilization approach. In fact,

UiO-66-NH<sub>2</sub> offered large numbers of -NH<sub>2</sub> adsorptive sites compared with UiO-66 and achieved a greater cellulase loading capacity (350 mg/g) than UiO-66 (102 mg/g). Cellulase@UiO-66-NH<sub>2</sub> accomplished outstanding hydrolysis of cellulose (85%) rather than free cellulase (60%) under conditions of 80 °C and pH = 3–6 in 30 min due to the extra stability of the immobilized cellulase. Besides, cellulase@UiO-66-NH<sub>2</sub> demonstrated 72% conversion efficiency after 10 cycles, outperforming covalently loaded cellulase onto Fe<sub>3</sub>O<sub>4</sub>@UiO-66-NH<sub>2</sub> via precipitation and glutaraldehyde crosslinking that attained 70% after only 5 cycles. These findings established that physical adsorption is a decent strategy for improving the catalytic performance of immobilized enzymes.

## Synthesis of environmental catalysts

The methods to prepare environmental catalysts are essential determinants of their catalytic behavior. Integrating green chemistry principles during large-scale syntheses, such as moderating energy input, organic solvent issues, and problematic wastes, is a significant challenge (Rodríguez-Padrón et al. 2019a). Jahangiri et al. (2014) defined a triangular concept to be tailored in catalyst design to achieve optimal performance, which included: (1) chemical-physical properties (i.e., surface area, porosity, dimension, acidity, composition, density), (2) catalytic properties (i.e., activity, selectivity, stability), and (3) mechanical properties (i.e., strength, attrition).

Furthermore, these materials' electronic and optical properties can be crucial in catalyst optimization (Rodríguez-Padrón et al. 2019a). Each catalyst's synthesis may involve a series of complex processes, some of which may be unknown (Schwarz et al. 1995). A minor alteration in the preparation details can result in a significant change in the final catalyst properties. Typically, the trial-and-error method was determined to be a viable solution. The conventional procedures for environmental catalyst preparation are precipitation (Geus and Van Dillen 2008; Wang et al. 2021c; Munnik et al. 2015), impregnation (via deposition, grafting, ion exchange, and others) (Munnik et al. 2015; Hafdi et al. 2021; Baeza et al. 2016), precipitation-impregnation (Ayati et al. 2014; Orooji et al. 2021), sol–gel (Mahy et al. 2021; Esposito 2019), chemical deposition (Tuna et al. 2022), hydrothermal (Mamaghani et al. 2019; Ayati et al. 2015), microwave-assisted (Ahmad and Hossain 2022), along with other methods (Zhang 2020; Yin et al. 2022). Because of its ease of use and low cost, precipitation is the most commonly used in preparing environmental catalysts (Rajput et al. 2022), where anions and cations combine in solution and form insoluble solids or supersaturated forms. Reagent addition, precipitate formation by pH, temperature and/or

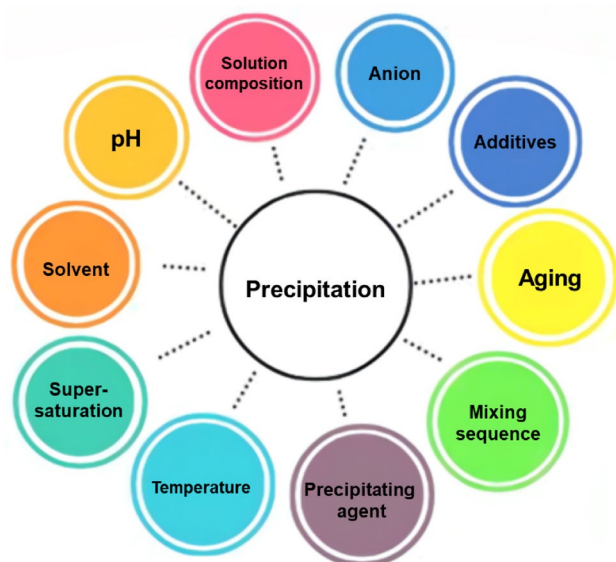


**Fig. 11** Parameters affecting the catalyst characteristics using the precipitation method. All these parameters must be optimized to obtain the catalyst-specific features. They can impact the nucleation and/or crystal growth of structures. So, the size and porosity of catalysts can be tuned by the variation of these parameters. Amongst, the solution composition and precipitating agent play the central role. For instance, the type of precipitation agent, such as sodium carbonate, sodium bicarbonate, sodium hydroxide, and ammonium carbonate, significantly impacts the final catalyst's characteristics

concentration adjustment, flocculation, sedimentation, and solid–liquid separation are all steps involved (Rajput et al. 2022; Wang et al. 2005), as shown in Fig. 11. It typically suffered from the separation of the product after precipitation and large volumes of salt-containing solutions (Hutchings and Védrine 2004). It has been extensively used to synthesize single-component, supported, and mixed catalysts (Perego and Villa 1997). For example, Chetri et al. (2014) successfully used this method to fabricate core–shell  $\text{TiO}_2/\text{SnO}_2$  and  $\text{SnO}_2/\text{TiO}_2$  nanocomposites with high potential for dye degradation under visible light irradiation. Magdalane et al. (2019) prepared the tin (IV) oxide/titanium dioxide nanostructure via a low-temperature precipitation method using tin chloride and titanium isopropoxide as main precursors and starch as a template.

Coprecipitation is one of the most practical approaches for fabricating bi-metallic catalysts (Munnik et al. 2015; Yao et al. 2018). The coprecipitation technique and deposition–precipitation for the fabrication of supported bimetallic catalysts are illustrated in Fig. 12. In this approach, the nucleation and growth of combined active metal and support are obtained in a single step in the solutions containing both active metal and support salts (Benhiti et al. 2020; Chen et al. 2016).

Impregnation is another method for improving the dispersion of an active phase on either inert or active

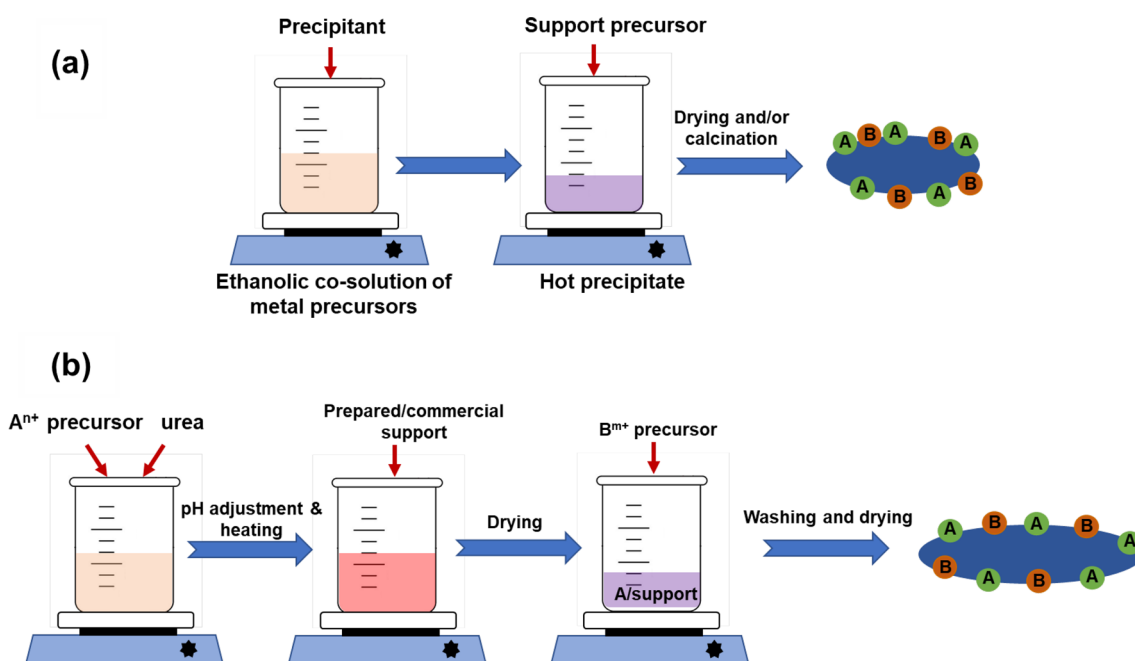


**Fig. 12** Synthesis of a supported bimetallic catalyst via a coprecipitation and **b** deposition precipitation. The support precursor is added to precipitated metal precursors in the coprecipitation approach. In contrast, the support material is added to the pH-adjusted metal precursor

and urea solution in the deposition precipitation technique. After drying, the second metal is deposited by deposition precipitation with urea

support that already possesses desired porous texture and mechanical toughness (Hutchings and Védrine 2004). It involves three steps (1) contacting the support with the solution containing a precursor, (2) drying, and (3) activating by calcination, reduction, or other suitable treatment (Hutchings and Védrine 2004; Perego and Villa 1997). The impregnation method can be divided into equivalent impregnation, using a particular carrier quality, and excessive impregnation, employing more than the amount of impregnation liquid metal salt solution volume. The impregnation method produces a catalyst with large particle size, easy recovery, and reagent-saving advantages. Alumina is commonly used support (Kim et al. 2022; Lericci et al. 2022), and silica (Xu et al. 2016; Gai et al. 2022), titania (Huang et al. 2022; Lincho et al. 2021; Martín-Hernández et al. 2012), carbon nanotubes (Afifeh et al. 2019; Li et al. 2022), metal–organic frameworks (Beni et al. 2020), cerium(III) oxide (Liu et al. 2015; Wang et al. 2016b), are some other employed supports in the synthesis of environmental catalysts via the impregnation way.

Actual ion exchange reactions between the precursor ions and those of the support surface are required for effective interaction in the impregnation process. By adding other competitive adsorption and exchange ions, the exchange process can be delayed to improve dispersion on the support. In preparing supported Pt<sup>0</sup> particles, for example, Cl<sup>-</sup> or NH<sup>4+</sup> ions are commonly added to the precursor solutions to improve particle dispersion (Hutchings and Védrine 2004). The literature (Schwarz et al. 1995; Hutchings and Védrine 2004; Quiton et al. 2021) examines the impact of several effective parameters in the impregnation approach.

The mechanochemistry synthesis of catalysts for environmental applications has also gained the scientific community's interest as a promising strategy (He et al. 2020a; Muñoz-Batista et al. 2018). This alternative solvent-free route has the advantages of high versatility, simplicity, and reproducibility (Rodríguez et al. 2007). It relies on directly absorbing mechanical energy by reagents, usually solids, during milling or grinding (Głowniak et al. 2021). Several mechanochemical methodologies, including top-down and bottom-up, have been developed based on milling equipment to transform precursors into the desired structures.

The commonly laboratory-level mechanochemistry synthesis are planetary ball mills, shaker mills, and attritor mills (Yin et al. 2022). Each mill possesses its advantages and disadvantages, which are extensively compared in the review articles (Yin et al. 2022; Espro and Rodríguez-Padrón 2021). Various mechanochemical synthesis techniques have recently progressed, such as solid-state grinding and liquid-assisted grinding (Xu et al. 2015b).

The mechanochemical routes have been employed to fabricate various environmental catalysts (Ralphs et al. 2013;

Szczeńśniak et al. 2020). High efforts have been made in the mechanochemical approach to narrow titanium oxide and zinc oxide bandgap and improve its photocatalytic behavior through its anionic and cationic doping through a ball mill (Pillai et al. 2020; Wu et al. 2019a; Reddy et al. 2019), or it's incorporated with various semiconductors, such as iron(III) oxide/titanium oxide (Subramonian et al. 2017), hexagonal boron nitride/titanium oxide (Fu et al. 2013), vanadium(V) oxide/titanium oxide (Mondal et al. 2020), and silver phosphate/zinc oxide (Liu et al. 2013a) hybrid composite. This considerable enhancement could be due to the decrease in particle size and therefore increase in surface area and enhancement of charge separation associated with the two components.

Similarly, by high-energy ball milling (8 days) and wet milling (1 h) to exfoliate graphite carbon nitride, higher photocatalytic efficiencies were achieved compared to that of pristine bulk (Ma et al. 2021). The different graphite carbon nitride heterojunctions could form under ball millings, such as ultrathin layer sheets (Wei et al. 2021b), sandwich-like three-dimensional structures (Ni et al. 2021), and multi-layer core–shell structures (Zhou et al. 2015). Also, the synthesis or decoration of carbonaceous material [e.g., graphite oxide (Ahmad et al. 2018), biochar (Yu et al. 2021a; Fawzy et al. 2021), and carbon nanotubes (Panahian and Arsalani 2017)] using high-energy ball milling provides a rapid and solventless process to intensify their environmental catalytic activity. Ball milling or liquid-assisted grinding was remarkably used as a promising alternative for metal–organic framework synthesis and modifications (Głowniak et al. 2021; Chen et al. 2019a; Stolar and Użarević 2020). Yin et al. (2022) well-reviewed the mechanochemical synthesis of various catalysts and reagents for water decontamination.

The conventional sol–gel process based on forming oxo bridges by hydrolysis and polycondensation of molecular precursors is a widely spread technique employed to synthesize inorganic and organic–inorganic hybrids catalytic materials (Debecker et al. 2013; Ciriminna et al. 2011). It has the inherent advantages of versatility, controlling the composition, structure, and morphology of the final materials, and high product homogeneity and purity, allowing the direct production of materials cast upon substrates (Agrafiotis et al. 2002). Due to the easy availability of molecular silicon sources with moderate reactivities, the most extensive research on the sol–gel synthesis of environmental catalysts has been conducted on silicate systems (e.g., tetraalkoxysilanes) (Kajihara 2013). The polycondensation and hydrolysis of tetraalkoxysilanes resulted in silica gels, which can be converted into silica glasses. It involves the partial hydrolysis of metallic alkoxides, condensation to create M–O–M bonds, and formation of sol by dealcoholation or dehydration, and finally, the formation of a cross-linked gel during aging or drying.

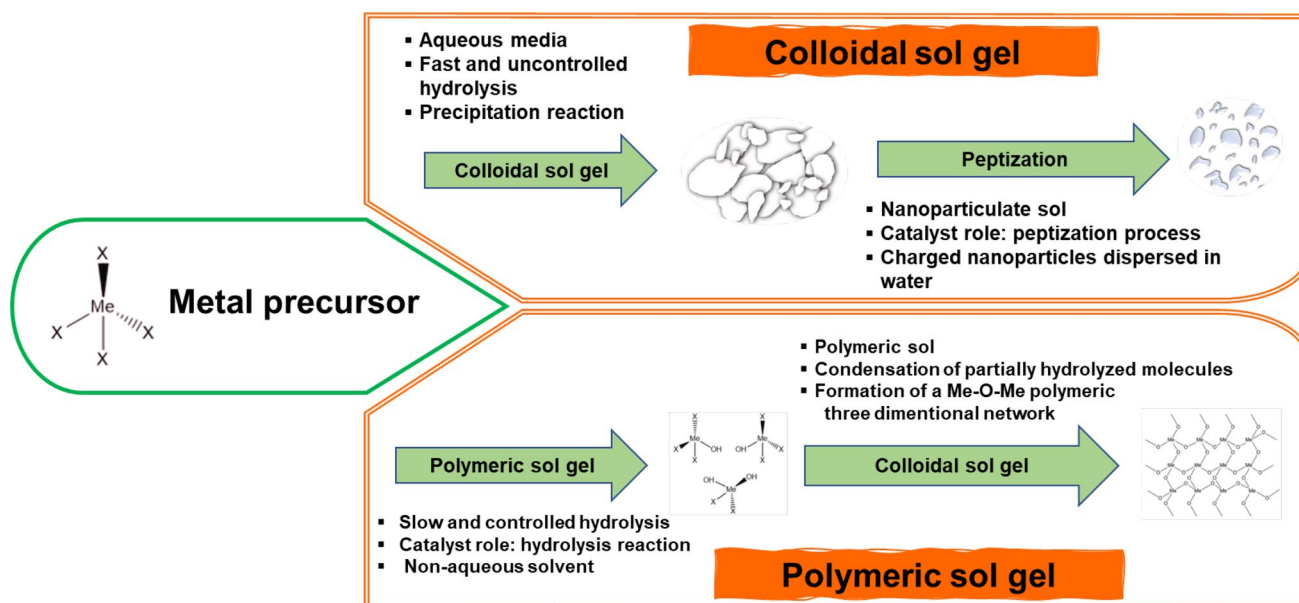


**Fig. 13** Comparison between colloidal and polymeric sol–gel methods. The sol–gel technique creates metal oxides, mainly silicon (Si) and titanium (Ti). During the procedure, monomers are transformed into a colloidal solution (sol), which serves as the precursor for an integrated network (or gel) of discrete particles or network polymers.

The most critical parameters in this process are the type and number of the alkyl group, water-to-alkoxide ratio, oxidation state and size of cation, pH, time, and temperature. Occasionally, chelating agents, such as glycol, acetylacetone, and acetyl acetoacetate, are exploited to prevent agglomeration and control crystallite morphology (Kazemi et al. 2020; Kim et al. 2020; Debecker 2018). The slow rate of hydrolysis and condensation resulted in sols. In contrast, precipitates form at slow hydrolysis and fast condensation, polymeric gels are synthesized at rapid hydrolysis and slow condensation (Hutchings and Védrine 2004), and colloidal gels are formed at fast hydrolysis and condensation processes. Figure 13 shows the differences between colloidal and polymeric sol–gel methods.

There are many studies carried out on the sol–gel synthesized dopants titanium oxide, such as Rh-doped titanium oxide-anatase nanoparticulate (Borlaf et al. 2012), Cerium-doped titanium oxide nanoparticulate (Xu et al. 2009), and some other metal cations (iron, silver, copper, zinc, chromium, aluminum, manganese or cobalt) doped titanium dioxide, to decrease the band gap of titanium dioxide and enhance its photocatalytic activity in degradation of different organic molecules (Mahy et al. 2018). For example, Ping et al. (2002) showed that the  $\text{Eu}^{3+}$  and  $\text{Fe}^{3+}$  doping of titanium dioxide nanoparticles improves the photoinduced charge separation in semiconductors and the interfacial charge transfer process at the semiconductor/solution interface. The sol–gel-assisted microwave or hydrothermal

In colloidal sol–gel, the hydrolysis of the metal precursor is fast and uncontrolled via the charge generated by the catalyst. On the other hand, in the polymeric route, the partial hydrolysis of the metal precursor is provoked by slow and controlled hydrolysis. The catalyst facilitates the hydrolysis reaction in this approach

treatment has also been employed to accelerate the synthesis and prepare the model catalysts with ordered mesoporosity (Debecker et al. 2013; Falk et al. 2017; Falk et al. 2018). Additionally, the binary and ternary oxide catalysts have been prepared by the sol–gel process, while by controlling the relative reactivities of the two alkoxides, the homogeneity of the mixed oxide gels can be engineered (Padmanabhan et al. 2022; Ramakrishnan et al. 2021; Mahdi et al. 2022; Shubha et al. 2022). As shown in Table 5, a large variety of catalytic materials were prepared by the sol–gel approach.

Hydrothermal synthesis is another method induced by temperature under aging in the presence of the mother liquor, used to modify precipitates, gels, or flocculates, and in particular, the preparation of mixed oxides zeolites, and other molecular sieves (Mamaghani et al. 2019; Yang et al. 2013). The concentration, pH, temperature, pressure, and time are the most crucial variable in given catalysts (Wang et al. 2021d, 2022). It is also carried out during other preparation procedures, such as precipitation, drying, washing, and extrusion (Ayati et al. 2015). The molecular sieve materials were well synthesized hydrothermally. It involves a classical precipitation method at a given pH under atmospheric pressure. For example, Khan et al. (2020) hydrothermally prepared the MFI TS-1 molecular sieve nanosheets using a tailored diquaternary ammonium surfactant as the structure-directing agent. Introducing  $\text{Ni}^{2+}$  cations at its ion-exchange sites remarkably enhanced its aerobic alcohol photo-oxidation. In another study, Zhou et al. (2022) synthesized the

**Table 5** Catalysts and photocatalysts prepared by the sol–gel method, adapted from Debecker and Mutin (2012)

Material	Route: precursor	Reaction catalyzed
Oxide and mixed oxide catalysts		
Nb–V(–Si) (niobium (Nb), vanadium (V), and silicon (Si))	Alkoxide route: (vanadyl isopropoxide (VO(OiPr) <sub>3</sub> , niobium(V) chloride (NbCl <sub>5</sub> ), tetraethyl orthosilicate (Si(OEt) <sub>4</sub> ))	Oxidative dehydrogenation of propane
V–Ti (vanadium (V) and titanium (Ti))	Ether route: vanadium oxytrichloride (VOCl <sub>3</sub> ), titanium tetrachloride (TiCl <sub>4</sub> ), diisopropyl ether (iPr <sub>2</sub> O)	Reduction of nitrogen oxides (NO <sub>x</sub> ) with ammonia (NH <sub>3</sub> )
V–Ti (vanadium (V) and titanium (Ti))	Ether route: vanadium oxytrichloride (VOCl <sub>3</sub> ), titanium tetrachloride (TiCl <sub>4</sub> ), diisopropyl ether (iPr <sub>2</sub> O)	Selective oxidation of hydrogen sulfide (H <sub>2</sub> S)
V–Ti(–W)(–Mo) (vanadium (V), titanium (Ti), tungsten (W), and molybdenum (Mo))	Ether route: Vanadium oxytrichloride (VOCl <sub>3</sub> ), titanium tetrachloride (TiCl <sub>4</sub> ), WCl <sub>5</sub> , molybdenum pentachloride (MoCl <sub>5</sub> ), diisopropyl ether (iPr <sub>2</sub> O)	Total oxidation
Ti–Si (titanium (Ti) and silicon (Si))	Alkoxide route: silicon tetrachloride (SiCl <sub>4</sub> ), titanium isopropoxide (Ti(OiPr) <sub>4</sub> ), tetraisopropyl orthosilicate (Si(OiPr) <sub>4</sub> )	Olefin epoxidation with organic hydroperoxides
Ti–Si (titanium (Ti) and silicon (Si))	Ether route: silicon tetrachloride (SiCl <sub>4</sub> ), titanium tetrachloride (TiCl <sub>4</sub> ), diisopropyl ether (iPr <sub>2</sub> O)	Mild oxidation with hydrogen peroxide
Ti–Si–MeSi and Ti–Si–Me <sub>3</sub> Si (titanium (Ti), silicon (Si), and either methyl/dichlorosilane (MeSi) or trimethylsilyl chloride (Me <sub>3</sub> Si), respectively)	Ether route: silicon tetrachloride (SiCl <sub>4</sub> ), titanium tetrachloride (TiCl <sub>4</sub> ), methyltrichlorosilane (MeSiCl <sub>3</sub> ) or trimethylsilyl chloride (Me <sub>3</sub> SiCl), diisopropyl ether (iPr <sub>2</sub> O)	Olefin epoxidation with organic hydroperoxides
Ti–Si (titanium (Ti) and silicon (Si))	Thermolysis: tris(tert-butoxy)siloxy complex (Ti[OSi(OtBu) <sub>3</sub> ] <sub>4</sub> )	Olefin epoxidation with organic hydroperoxides
Ta–Si (tantalum (Ta) and silicon (Si))	Thermolysis: tantalum complex (iPrO) <sub>2</sub> Ta[OSi(OtBu) <sub>3</sub> ] <sub>3</sub> (and Tert-butoxy orthosilicate (HOSi(OtBu) <sub>3</sub> ))	Olefin epoxidation with hydrogen peroxide and organic hydroperoxides
Cr–Si (chromium (Cr) and silicon (Si))	Thermolysis: tris(alkoxy)siloxochromium(IV) ((tBuO) <sub>3</sub> CrOSi(OtBu) <sub>3</sub> )	Oxidative dehydrogenation of propane
Co–Al (cobalt (Co) and aluminum (Al))	Ether route: aluminum trichloride (AlCl <sub>3</sub> ), CoCl <sub>2</sub> , diisopropyl ether (iPr <sub>2</sub> O)	Olefin epoxidation with iodosylbenzene
Co–Si–Al (cobalt (Co), silicon (Si), and aluminum (Al))	Ether route: silicon tetrachloride (SiCl <sub>4</sub> ), aluminum trichloride (AlCl <sub>3</sub> ), CoCl <sub>2</sub> , diisopropyl ether (iPr <sub>2</sub> O)	Mild oxidation with iodosylbenzene
Fe–Al (iron (Fe)-aluminum (Al))	Ether route: aluminum trichloride (AlCl <sub>3</sub> ), iron(III) chloride (FeCl <sub>3</sub> ), diisopropyl ether (iPr <sub>2</sub> O)	Mild oxidation with hydrogen peroxide
Mo–Al–Si (molybdenum (Mo)-aluminum (Al)-silicon (Si))	Ether route: molybdenum pentachloride (MoCl <sub>5</sub> ), silicon tetrachloride (SiCl <sub>4</sub> ), aluminum trichloride (AlCl <sub>3</sub> ), diisopropyl ether (iPr <sub>2</sub> O)	Alkene metathesis
Chlorinated tin dioxide	Benzyl alcohol route: Tin(IV) chloride (SnCl <sub>4</sub> ) in benzyl alcohol (BzOH)	Etherification, alkylation
Tungsten oxide (W <sub>18</sub> O <sub>49</sub> ) nanowires	Benzyl alcohol route: tungstenisopropoxide (W(OiPr) <sub>6</sub> ) in benzyl alcohol (BzOH)	Oligomerization of benzylic alcohols
Ag–Al(–Nb) (silver (Ag)-aluminum (Al)-niobium(Nb))	Ether route: aluminum trichloride (AlCl <sub>3</sub> ), silver chloride (AgCl), diisopropyl ether (iPr <sub>2</sub> O), Niobium(V) chloride (NbCl <sub>5</sub> )	Reduction of nitrogen oxides (NO <sub>x</sub> ) with decane
Pt–Al (Platinum (Pt)-Aluminum (Al))	Ether route: aluminum trichloride (AlCl <sub>3</sub> ), diisopropyl ether (iPr <sub>2</sub> O), (C <sub>6</sub> H <sub>5</sub> CN) <sub>2</sub> PtCl <sub>2</sub> or platinum(IV) bromide (PtBr <sub>4</sub> )	Not reported

Table 5 (continued)

Material	Route: precursor	Reaction catalyzed
Oxide and mixed oxide photocatalysts		
Titanium dioxide (TiO <sub>2</sub> )	Alkoxide route: titanium tetrachloride (TiCl <sub>4</sub> ), titanium isopropoxide (Ti(OiPr) <sub>3</sub> ) in hexane or hexane–triocetylphosphine oxide (TOPO) solutions	Photooxidation
Titanium dioxide (TiO <sub>2</sub> ) (spherical or nanorods)	Benzyl alcohol route: titanium tetrachloride (TiCl <sub>4</sub> ) in benzyl alcohol (BzOH)	Photooxidation
Titanium dioxide (TiO <sub>2</sub> )	Benzyl alcohol route: titanium tetrachloride (TiCl <sub>4</sub> ) in benzyl alcohol (BzOH)	Photooxidation
Titanium dioxide (TiO <sub>2</sub> )	Anhydride route: titanium isopropoxide (Ti(OiPr) <sub>3</sub> ), (CX <sub>3</sub> CO) <sub>2</sub> O, (X = H, F)	Photooxidation
Titanium dioxide (TiO <sub>2</sub> ) (nanorods)	Ester elimination route or carboxylic acid route titanium isopropoxide (Ti(OiPr) <sub>3</sub> ), oleic acid	Photocatalytic disinfection
Titanium dioxide (TiO <sub>2</sub> )	Benzyl alcohol route: titanium tetrachloride (TiCl <sub>4</sub> ) in benzyl alcohol (BzOH)	Photocatalytic disinfection
Layered titanate	Ether route: titanium tetrachloride (TiCl <sub>4</sub> ), in diglyme in the presence of borane-amine (BH <sub>3</sub> .amine) complex	Photooxidation
Titanium dioxide–silicon dioxide (TiO <sub>2</sub> –SiO <sub>2</sub> )	Formic acid route in supercritical carbon dioxide (scCO <sub>2</sub> ); tetraethyl orthosilicate (Si(OEt) <sub>4</sub> ), titanium isopropoxide (Ti(OiPr) <sub>3</sub> ), formic acid	Photooxidation
Triocetylphosphine oxide (TOPO)-capped (TiO <sub>2</sub> )	Alkoxide route: titanium tetrachloride (TiCl <sub>4</sub> ), titanium isopropoxide (Ti(OiPr) <sub>3</sub> ) in triocetylphosphine oxide (TOPO)	Photooxidation
Phosphate zirconium-doped titanium dioxide (Zr-doped TiO <sub>2</sub> )	Alkoxide route: titanium tetrachloride (TiCl <sub>4</sub> ), titanium isopropoxide (Ti(OiPr) <sub>3</sub> ), zirconium tetrachloride (ZrCl <sub>4</sub> ), zirconium (IV) isopropoxide isopropanol complex (Zr(OiPr) <sub>4</sub> , nPrOH) in triocetylphosphine oxide (TOPO)	Photooxidation
Iron-doped titanium dioxide (Fe-doped TiO <sub>2</sub> )	Alcohol route: titanium tetrachloride (TiCl <sub>4</sub> ), iron(III) nitrate (Fe(NO <sub>3</sub> ) <sub>3</sub> ) in tert-butanol (tBuOH)	Photooxidation
Iron, nitrogen-doped titanium dioxide (Fe, N-doped TiO <sub>2</sub> )	Alcohol route: titanium tetrachloride (TiCl <sub>4</sub> ), iron(III) nitrate (Fe(NO <sub>3</sub> ) <sub>3</sub> ) in tert-butanol (tBuOH)	Photooxidation
Zinc oxide (ZnO)	High-temperature decomposition of zinc acetate (Zn(OAc) <sub>2</sub> )	Photooxidation
Indium niobium oxide (InNbO <sub>4</sub> )	Benzyl alcohol route: indium(III) acetylacetonate (In(acac) <sub>3</sub> ), niobium(V) chloride (NbCl <sub>5</sub> ), in benzyl alcohol (BzOH)	Photooxidation

controllable MnSAPO-18 molecular sieves at the optimum crystallization time of 2 h for ammonia-selective catalytic reduction. This massive effort in hydrothermally synthesized materials resulted in numerous new structures with a large variety of monodisperse pore sizes, mono or tridimensional networks, and acidic or redox properties, which has opened tremendous hope for new catalysts.

While the synthesis and growth of nanostructures are highly sensitive to the reaction conditions, microwave and ultrasound irradiation's efficient and controlled energy can be a great promise (Gawande et al. 2014). Numerous studies have focused on the microwave-assisted method as a powerful approach (Kokel et al. 2017) in smart nanoarchitecture materials synthesis, particularly environmental catalysts (Kumar et al. 2020c). Compared to conventional heating, microwave heating operates in deep “inside-out,” high temperature and selective heating mode (Polshettiwar et al. 2009; Baig and Varma 2012) via the chemical polarity in the target compound (Kunal and Toops 2020). So, it is considered a fast, high-yield, high-purity product, highly reproducible, easily optimized, and more efficient synthesis route, which requires lower energy than the conventional methods.

A thorough review of the increasing growth of this research field and its performance is provided in the literature (Gawande et al. 2014; Kokel et al. 2017; State et al. 2019). Nanostructured photocatalysts, including oxides, sulfides, and nanocomposites, were fabricated using microwave-assisted methods (Singh et al. 2019). For instance, ceric oxide ( $\text{CeO}_2$ ),  $\text{Ce}_x\text{Sm}_{1-x}\text{O}_2$  (Polychronopoulou et al. 2017), and copper oxide ( $\text{CuO}$ )-promoted  $\text{CeO}_2\text{-M}_x\text{O}_y$  ( $\text{M} = \text{Zr, La, Pr, and Sm}$ ) (Reddy et al. 2012) were fabricated by microwave-assisted method and exploited for carbon monoxide oxidation. The tin dioxide quantum dots (Liu et al. 2013b), titanium dioxide-reduced graphene oxide ( $\text{TiO}_2\text{-rGO}$ ) photocatalyst, synthesized through the reduction of graphene oxide in titanium dioxide slurry (Yang et al. 2011),  $\text{ZnO-Y}_3\text{Al}_5\text{O}_{12}:\text{Ce}^{3+}$ ,  $\text{UiO-66-NH}_2$  (Solís et al. 2022), and dichalcogenide ( $\text{NiTe}_2$ ) (Hussain et al. 2022) some of the environmental photocatalysts were prepared under microwave conditions. (Yang et al. 2014) utilized the microwave-assisted hydrothermal route to prepare permeable titanium dioxide microspheres as an efficient photocatalyst to degrade a binary of chromium ( $\text{Cr(VI)}$ ) and methyl orange dye.

The uniform distribution of different metal oxides is a significant challenge in preparing improved mixed metal oxides catalysts. For example, due to the differences in salt solubility, preparing homogeneous mutual-dispersed catalysts is difficult through coprecipitation (Chen et al. 2017c). The double hydrolysis reaction is a simple, efficient, and environmentally friendly metathesis reaction involving the ionic compounds swapping their ionic partners (Bai et al. 2005). A low-cost and speedy preparation method was sought for thermally stable alumina-based two-component

and multi-component materials with high specific surface area and loading (Bai et al. 2005; Bai et al. 2009; Do et al. 2022). (Ullah et al. 2016) exploited the double hydrolysis method to synthesize  $\text{Ni/ZnO-Al}_2\text{O}_3$ , which exhibited improved reactive adsorption desulfurization behavior. In another study, Do et al. (2022) used this approach to prepare highly active Ru-free  $\text{Ni/Al}_2\text{O}_3$  for ammonia ( $\text{NH}_3$ ) decomposition. Recently, (Dong et al. 2022) reported the loading of  $\text{Nb}_2\text{O}_5$  nanoparticles on the surface of graphite carbon nitride using in-situ hydrolysis-calcination, which showed exemplary behavior in the rate of photocatalytic  $\text{NH}_3$  decomposition. The hydrolysis-driven method (Ling et al. 2021) was also reported in the highly efficient synthesis of homogeneous distributed Mn-Fe binary oxides, which showed a more exposed surface area and lower crystallinity.

The flame aerosol processes, including liquid-fed and vapor-fed, are the most well-known technologies for the large low-cost industrial-scale production of nanocatalysts (Sheng et al. 2018; Li et al. 2016b). As an important competitive advantage compared to traditional wet chemistry synthesis methods, this approach promotes the ability to form both active species and support in a single step (see Fig. 14) (Liu et al. 2021b). It gives further flexibility to tailor the catalyst structure with desirable performance (Zhao et al. 2019a; Schimmoeller et al. 2010; Schimmoeller et al. 2011). Its most notable challenges are the requirement of volatile metal precursors and achieving homogeneous distributions in multicomponent catalysts. Figure 15 shows a dependency on catalyst characteristics and flame synthesis parameters.

The liquid-fed flame aerosol is the most famous industrial continuous method for large-scale production of titanium dioxide, photocatalysts and fumed silica (Liu et al. 2021b; Teoh et al. 2010; Kho et al. 2010), and the vapor-fed flame aerosol was widely applied to synthesize high surface area oxides, such as iron(III) oxide, aluminum oxide (Pratsinis 1998), the aluminum oxide-supported (Jensen et al. 2003) and titanium dioxide-based (Almquist and Biswas 2002) catalysts. The liquid-fed flame aerosol can select a more comprehensive range of precursors (Sheng et al. 2018). It includes the sub-classes of flame spray pyrolysis and flame-assisted spray pyrolysis (Campagnoli et al. 2005), depending on the precursor solution combustion enthalpy, which is well-reviewed by Liu et al. (2021b). Most kinds of homogeneous and highly crystalline nanocatalysts in terms of composition have been prepared by flame spray pyrolysis by far (Sheng et al. 2018), particularly a wide spectrum of metal oxide and noble metal nanoparticles or composites, which are in growing in the catalytic processes. Some environmental catalysts prepared via flame aerosol processing are listed in Table 6. Some of the most recently synthesized photocatalysts and electrocatalysts prepared by flame spray pyrolysis are also presented in Table 7.

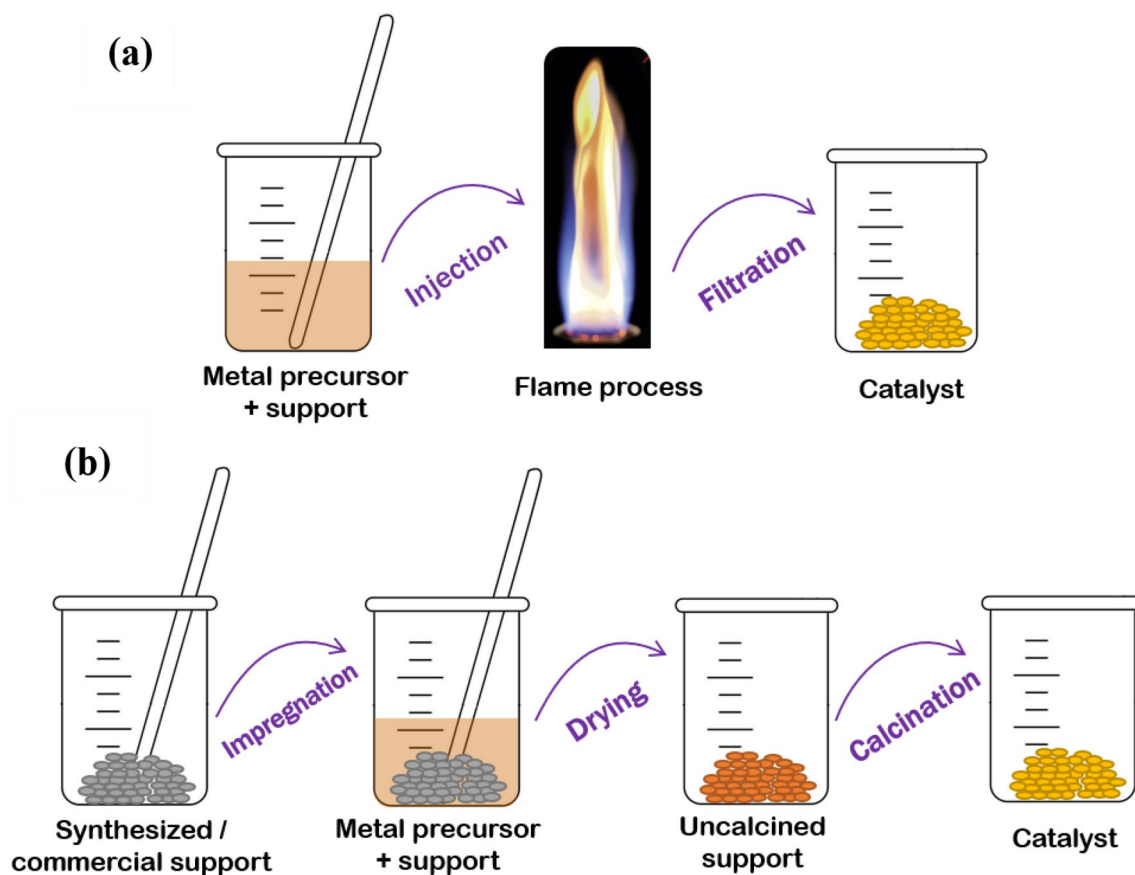


**Fig. 14** Catalyst synthesis procedures of the flame aerosol process (a) versus typical conventional wet impregnation methods (b). The use of flame aerosol processing provides additional freedom for customizing catalyst properties by adjusting a process parameter. The flame aero-

sol process approach allows active species to nucleate from individual atoms. Wet chemical techniques sometimes need several posttreatment procedures, such as solvent washing and calcination, which may modify the composition and structure of the catalyst

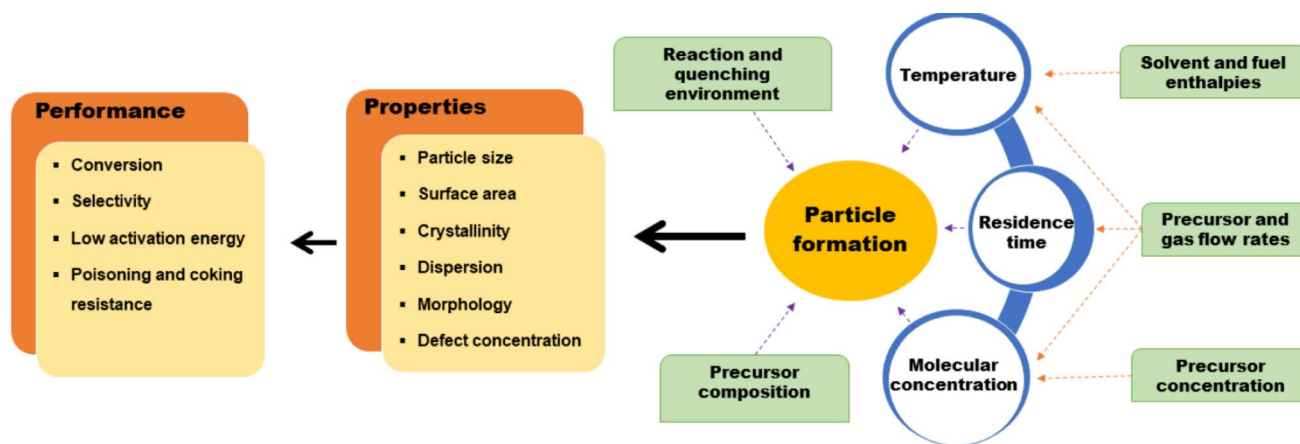


**Fig. 15** Effective process property parameters for catalyst design through flame aerosol processing. The flame temperature and residence time are the main factor affecting particle formation. However, they are individually dependent on some other factors. Therefore,

the actual relationship is much more complex. Their interpretation is essential to prepare nanocatalysts with desirable characteristics and behavior



**Table 6** Environmental catalysts synthesized by flame spray pyrolysis

Catalyst (actives/support)	Characteristics		Reaction	Optimized catalytic performance	Reference
	Particle size (nm) (actives/support)	Specific surface area ( $\text{m}^2 \text{g}^{-1}$ )			
Au–Pd/TiO <sub>2</sub> (gold–palladium/titanium dioxide)	1 ~ 2/17	104	Acetylene hydrogenation	45% C <sub>2</sub> H <sub>2</sub> conversion, 96% ethylene selectivity at 40 °C	Pongthawornsakun et al. (2018)
Pt/TiO <sub>2</sub> (platinum/titanium dioxide)	2.47/5 ~ 25	64	CO oxidation	T <sub>50</sub> ≈ 110 °C, T <sub>100</sub> ≈ 120 °C; CO reaction rate $0.13 \times 10^{-7} \text{ mol s}^{-1} \text{ g}_{\text{catalyst}}^{-1}$	Zhao et al. (2018)
Pt/Al <sub>2</sub> O <sub>3</sub> (platinum/aluminum oxide)	1.8 ~ 7.7/not reported	220	CO oxidation; NO oxidation	T <sub>50</sub> <sup>b</sup> ≈ 104 °C, T <sub>100</sub> ≈ 108 °C CO conversion; 70% NO conversion at 290 °C	Ogel et al. (2019)
Pt/TiO <sub>2</sub> (platinum/titanium dioxide)	1.2 ~ 5.45/not reported	64	CO oxidation	T <sub>100</sub> ≈ 100 °C after 300 °C calcination; T <sub>100</sub> ≈ 200 °C after 600 °C calcination;	Bi et al. (2019)
Pt/TiO <sub>2</sub> -Co (platinum/titanium dioxide–cobalt)	0.72/5 ~ 25	60	CO oxidation	T <sub>50</sub> ≈ 40 °C, T <sub>100</sub> ≈ 70 °C; CO reaction rate $5.46 \times 10^{-7} \text{ mol s}^{-1} \text{ g}_{\text{cat}}^{-1}$	
Pt/TiO <sub>2</sub> -N (platinum/titanium dioxide–nitrogen)	1.34 ~ 4.29/not reported	61	CO oxidation	T <sub>100</sub> ≈ 120 °C after 300 °C calcination; T <sub>100</sub> ≈ 150 °C after 600 °C calcination;	
CuO/TiO <sub>2</sub> (copper oxide/titanium dioxide)	< 4/15 ~ 20	70 ~ 98	CO oxidation	T <sub>50</sub> ≈ 92 °C, T <sub>100</sub> ≈ 120 °C	Chen et al. (2019b)
CuO/CeO <sub>2</sub> (copper oxide/ceric oxide)	NA/25.6 ~ 32.8	39 ~ 54	CO oxidation	T <sub>50</sub> ≈ 70 °C, T <sub>100</sub> ≈ 120 °C; keep 90% conversion for 23 h at 1.7% water vapor condition	Zhao et al. (2019b)
CuO/CeO <sub>2</sub> -Mn (copper oxide/ceric oxide–manganese)	NA/27 ~ 37	31 ~ 45	CO oxidation	T <sub>50</sub> ≈ 93 °C, T <sub>90</sub> ≈ 131 °C; keep 100% conversion for 9 h at 1.7% water vapor condition	Zhao et al. (2019a)
Hopcalite	5 ~ 10	111 ~ 178	CO oxidation in a humid atmosphere	T <sub>90</sub> ≈ 90 °C at dry condition; Keep above 50% CO conversion for 1 h in 75% humidity at 50 °C	Wegner et al. (2019)
Hopcalite	5.2 ~ 5.7	133 ~ 193	CO oxidation in a humid atmosphere	Keep above 65% CO conversion for 1 h in 75% humidity at 50 °C	Wegner et al. (2018)
Ru/SiO <sub>2</sub> -Al <sub>2</sub> O <sub>3</sub> (ruthenium/silicon dioxide–aluminum oxide)	5.4 ~ 7/18 ~ 22	133 ~ 243	Fischer–Tropsch synthesis	37% CO conversion at 240 °C	Wang et al. (2020)
LaCoO <sub>3</sub> (perovskite-type oxide)	6.14 ~ 9.39	23 ~ 95	CO oxidation	T <sub>100</sub> ≈ 175 °C	Angel et al. (2020)
La <sub>1-x</sub> A <sub>x</sub> BO <sub>3</sub> (perovskite-type oxide)	11 ~ 14	55 ~ 79	CO, NO, C <sub>x</sub> H <sub>y</sub> three-way oxidation	85% CO, 60% NO, 80% C <sub>x</sub> H <sub>y</sub> conversion at 500 °C	Simmanca et al. (2019)
Bi-Mo-Fe-Co oxide (Multicomponent oxide catalysts)	5 ~ 30	52	Propylene oxidation to acrolein and acrylic acid	90% propylene conversion, around 40% acrolein, and 50% acrylic acid selectivity at 330 °C	Sprenger et al. (2018)

Flame spray pyrolysis produced the majority of homogenous and highly crystalline nanocatalysts, especially a variety of metal oxide and noble metal nanoparticles or composites, which are increasingly used in catalytic processes. T, CO, and NO refer to temperature, carbon monoxide, and nitric oxide, respectively

**Table 7** Some recently used photocatalysts and electrocatalysts prepared by flame spray pyrolysis

Catalyst	Reaction	Structure			Optimal catalytic performance	Reference
		Dopant content (wt% or mol%)	Particle size (nm)	Specific surface area ( $\text{m}^2 \text{g}^{-1}$ )		
Zinc oxide (ZnO)	Carbon dioxide reduction	–	16.8~21.6	Not reported	$\text{H}_2:\text{CO} \approx 1$ with a current density of $40 \text{ mA cm}^{-2}$ at 2.6 V for 18 h	Daiyan et al. (2020)
Nitrogen-doped titanium dioxide (N-TiO <sub>2</sub> )	Phenol degradation	0.5~7	42~88	16~26	50% yield under six F8T5 ww lamps	Boningari et al. (2018a)
Nitrogen-doped titanium dioxide (N-TiO <sub>2</sub> )	Phenol degradation	–	6~88	17~22	50% yield under six F8T5 ww lamps	Smirniotis et al. (2018)
Sulfur-doped titanium dioxide (S-TiO <sub>2</sub> )	Acetaldehyde degradation	0.18~0.38	122~311	4.8~12.3	60% yield under six F8T5 ww lamps	Boningari et al. (2018b)
Palladium-doped titanium dioxide (Pd-TiO <sub>2</sub> )	NO <sub>x</sub> removal	0.1	–	87	80% NO conversion, 50% average NO <sub>x</sub> removal efficiency in 5 h under sunlight	Fujiwara and Pratsinis (2018)
Platinum-doped titanium dioxide (Pt-TiO <sub>2</sub> )	Steam reforming methanol	0.5	1.3/10~25	70	–	Chiarello et al. (2018)
Silver-doped titanium dioxide (Ag-TiO <sub>2</sub> )	Nitrate reduction	0.1	21	61	14.5% NO <sub>3</sub> <sup>3-</sup> conversion, 0.175 mmol/hour $\dot{g}_{\text{catalyst}}$ rate at 5.11 pH under 200 W Hg light	Bahadori et al. (2019)
Copper oxide-titanium dioxide (CuO-TiO <sub>2</sub> )	Water splitting hydrogen	2	6~40	144	112.6 $\mu\text{mol h}^{-1}$ h production rate under 300 W Xe lamp	Yang et al. (2018b)
Cerium-doped titanium dioxide (Ce-TiO <sub>2</sub> )	Methylene blue degradation	24	5~45	Not reported	70% methylene blue degradation efficiency after 3 h under 150 W Xe lamp	Mikaeili et al. (2018)
Tin dioxide (SnO <sub>2</sub> )	Carbon dioxide reduction	–	9~14	81~146	85% formate conversion with a current density of $-23.7 \text{ mA cm}^{-2}$ at $-1.1 \text{ V}$	Daiyan et al. (2019)
Iron-doping in double perovskite (PrBaCo <sub>2(1-x)</sub> Fe <sub>2x</sub> O <sub>6-<math>\delta</math></sub> )	Oxygen evolution reaction	–	5~30	43~56	50 mV dec <sup>-1</sup> Tafel slope, 19.7 A g <sup>-1</sup> current density at 1.55 V <sub>RHE</sub>	Kim et al. (2019)
Platinum on graphite carbon nitride (Pt-g-C <sub>3</sub> N <sub>4</sub> )	Water splitting hydrogen	3	10~20	81.85	41.18 $\mu\text{mol g}^{-1} \text{ h}^{-1}$ H <sub>2</sub> production rate under 400 W R7S lamp	Papailias et al. (2020)
Perovskite structures (LaCo <sub>1-x</sub> Fe <sub>x</sub> O <sub>3</sub> )	Oxygen evolution reaction	0~60 Fe	6~7	Not reported	10 mA cm <sup>-2</sup> current density at 1.64 V	Alkan et al. (2019)
	Ethanol oxidation				10 mA cm <sup>-2</sup> current density at 1.58 V	

H<sub>2</sub>, CO, NO, and ww refer to hydrogen, carbon monoxide, nitric oxide, and warm white, respectively

“–” not reported

## Analysis of catalyst structure

It is well established that the activity and the selection of a particular catalytic application of the catalyst strongly depend on its structure and intrinsic properties. On this basis, the structural characterization of a catalyst is a central topic to be considered. Moreover, different characterization techniques should be involved to assess the successful fabrication of heterogeneous catalysts and explore their inherent properties. Thus, the following section will discuss some intrinsic properties of heterogeneous

catalysts such as surface area, porosity, crystallinity, thermal stability, and electronic properties based on several characterization tools, including Brunauer–Emmett–Teller analysis, powder X-ray diffraction, thermogravimetric analysis, electron microscopy, and X-ray photoelectron spectroscopy as follows:

### Brunauer–Emmett–Teller isotherm analysis

The catalytic activity of heterogeneous catalysts is controlled by two intrinsic properties: (1) the high surface area

of the catalyst that offers large numbers of active sites, and so boosting the catalytic performance; and (2) the sufficient pore size of the catalyst that facilitates the diffusion of reactants to the internal active sites. Brunauer–Emmett–Teller isotherm measurement is the most commonly used tool to assess heterogeneous catalysts' specific surface area, pore volume, and pore size distribution. It measures the amount of nitrogen gas molecules adsorbed on the surface of porous material at liquid nitrogen temperature, so the sample capacity to adsorb certain amounts of nitrogen gas molecules represents the specific surface area. For instance, surface analysis shows a type I adsorption–desorption isotherm model with microporous nature of citrate-capped  $\text{Fe}_3\text{O}_4@\text{UiO}-66\text{-NH}_2$  nanocomposite (MU-2) (Prakash Tripathy et al. 2022). Remarkably, MU-2 exhibited higher specific surface area and pore sizes ( $572.13 \text{ m}^2/\text{g}$ ,  $1.65 \text{ \AA}$ ,  $6.72 \text{ \AA}$ ) than pristine  $\text{UiO}-66\text{-NH}_2$  ( $510.38 \text{ m}^2/\text{g}$ ,  $1.58 \text{ \AA}$ ,  $6.23 \text{ \AA}$ ), confirming the in situ growth of the  $\text{UiO}-66\text{-NH}_2$  particles onto the magnetic nanoparticles without clogging the metal–organic frameworks' pores. Accordingly, MU-2 demonstrated higher photocatalytic hydrogen evolution ( $417 \mu\text{mole h}^{-1}$ ) rate than  $\text{UiO}-66\text{-NH}_2$  ( $115 \mu\text{mole h}^{-1}$ ).

### Thermogravimetric analysis

Thermogravimetric analysis is the most commonly used tool to inspect the thermal stability of heterogeneous catalysts. The thermogravimetric analysis explores the weight loss (%) over different temperatures. The weight loss profile for a material is usually donated in the first derivative form, and the peak position refers to a specific component decomposition temperature (Zhang et al. 2019b). Notably, the thermal assessment environment (i.e., air, oxygen, nitrogen) plays a crucial role in the thermal behavior of the catalyst.

### Powder X-ray diffraction

It is noteworthy that the crystal phase directly influences heterogeneous catalysts' adsorption and catalytic performance. Besides, the catalytic process possibly changes the structural integrity and crystallinity of the catalyst. Powder X-ray diffraction provides a powerful route to recognize the crystallographic structure, purity, and crystal phase of the prepared catalysts, as well as the crystal phase stability and integrity after the catalytic process. In addition, powder X-ray diffraction can primarily measure the crystalline particle size using Scherrer's equation ( $D = K\lambda/\beta \cos\theta$ , where  $D$  represents the mean size of crystallite domains,  $K$  represents a dimensionless shape factor,  $\lambda$  represents X-ray wavelength,  $\beta$  represents the broadening of the diffraction peak at its half maximum, and  $\theta$  is the Bragg angle). Song et al. (2022b) studied the effect of different crystalline phases on the photocatalytic performance of Ni-MOF. Based on density functional theory

(DFT) calculations, Ni-MOF( $\text{H}_2\text{O}$ ) with rhombic crystalline phase attained more negative adsorption energy for carbon dioxide molecules ( $-0.85 \text{ eV}$ ) than monoclinic Ni-MOF ( $-0.62 \text{ eV}$ ).

Moreover, the Ni-C bond in Ni-MOF( $\text{H}_2\text{O}$ ) ( $1.87 \text{ \AA}$ ) was shorter than Ni-MOF ( $1.95 \text{ \AA}$ ). These findings verified the better carbon dioxide adsorption performance of Ni-MOF( $\text{H}_2\text{O}$ ) than Ni-MOF and the decisive role of the crystal phase differences. Accordingly, Ni-MOF( $\text{H}_2\text{O}$ ) accomplished 1.8 times higher photocatalytic conversion of carbon dioxide into carbon monoxide ( $34 \mu\text{mole}$  after 6 h) than Ni-MOF.

### Morphological characterization

Scanning electron microscopy has been commonly used to visualize the nanocatalyst's crystalline morphology and ascertain the catalyst's structural stability beyond the catalytic reaction. Wu et al. (2019b) used scanning electron microscopy to explore the morphology of Ni nanoparticles entrapped in microporous graphene-like carbon (Ni@MGC). Scanning electron microscope images depicted that the MGC support showed a crystalline morphology similar to NaY zeolite. Notably, Ni@MGC revealed structural defects after the catalytic carbon dioxide methanation process, which was attributed to the reaction of the carbon material with the by-product water at high temperatures. It should be noted that the electron beam scanning the surface of the specimen may cause damage, producing a distorted image. Field emission scanning electron microscope overcomes this issue, engaging a highly focused electron beam that raster the surface of the specimen, forming a spot ( $0.4\text{--}5 \text{ nm}$ ) and generating a high-quality three-dimensional image for the sample.

Transmission electron microscopy involves a highly accelerated electron beam that passes through a thin specimen or fine powder, providing information about the internal structure and morphology, size of tiny particles, dispersity of the metal nanoparticles onto a solid support, and the atomic arrangement.

### X-ray photoelectron spectroscopy

X-ray photoelectron spectroscopy is a non-destructive technique that studies the electronic state, composition, and content of the elements of the surface atoms. X-ray photoelectron spectroscopy can not only identify the elements but also can recognize the other elements bonded to these elements. Based on the photoelectric effect, X-ray photoelectron spectroscopy measures the kinetic energy and number of emitted core electrons from the surface atoms, giving a compositional analysis of the surface elements (i.e., element content and oxidation state). Furthermore, X-ray photoelectron

spectroscopy can elucidate the catalytic mechanisms and stability of the catalyst by tracking the change in the oxidation states of each element after the catalytic reaction. For example, Wang et al. studied the mechanism of the catalytic peroxymonosulfate activation using mesoporous carbon framework-supported Cu–Fe oxides (Wang et al. 2022b). The intensity of the two peaks corresponding to  $\text{Cu}^{2+}$  and  $\text{Cu}^+$  at 934.4 eV (26.2–12.4%) and 933 eV (36.4–47.5%) of Cu  $2p_{3/2}$  spectrum changed after the catalytic reaction. But, the Fe  $2p_{3/2}$  spectrum survey showed a slight change in the peak's intensity, revealing the remarkable activity of Cu instead of Fe within the mesoporous carbon support.

Moreover, the O 1s spectrum survey assured the catalytic contribution of the surface –OH groups, exhibiting observable changes in the terminal and bridging –OH groups at 532.9 eV and 531.2 eV, respectively. It is worth noting that X-ray photoelectron spectroscopy is a surface-sensitive technique that can only recognize the elemental composition of the atoms at only 0–10 nm depths. Nevertheless, X-ray photoelectron spectroscopy can identify the content and chemical composition of the deeper atomic layer using the ion-beam etching method. Such an approach has paved the way to study the electronic properties of several types of samples, such as thin films, graphene, and aligned carbon nanotubes at different depths.

## Applications

### Water remediation

In light of recent demographic developments, the global population is projected to increase by 29.9%, or 9.8 billion people, by 2025 (Bielecki et al. 2020). Similarly, numerous studies indicate that 30% of the world's population lacks access to safe drinking water (Wan and Wang 2021a, a, b, c, b). This is attributable to improperly discharging contaminated effluents into aquatic environments (Liu et al. 2021c). Organic and inorganic pollutants and dangerous biological infections are the primary contributors to water contamination (Lim et al. 2011). Heavy metals, dyes, and emerging organic contaminants (i.e., antibiotics, detergents, veterinary, pesticides, personal care, insecticides, oil spills, and food additives industries) are a diverse category of highly toxic water pollutants that have attracted significant attention from the legislative and scientific communities due to their widespread presence in the environment (Elgarahy et al. 2021a; Hüesker and Lepenies 2022; Cheng et al. 2020; Singh et al. 2020). Researchers have studied a multitude of operational methods, such as filtration (Zhang et al. 2021b), ion exchange (Liu et al. 2021d), coagulation (Cui et al. 2020), and chemical precipitation (Kalaitzidou et al. 2020) for wastewater treatment.

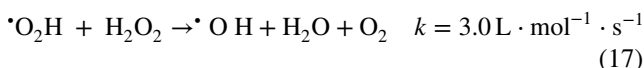
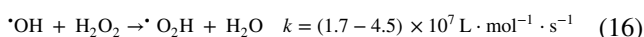
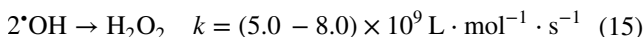
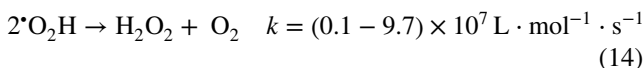
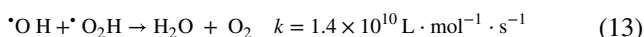
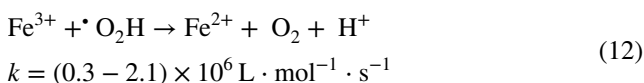
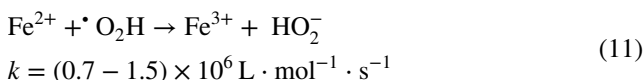
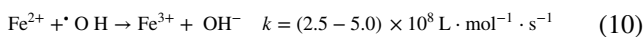
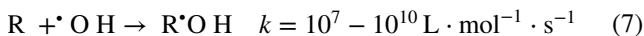
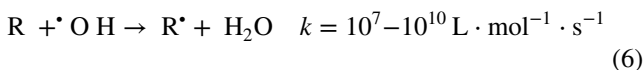
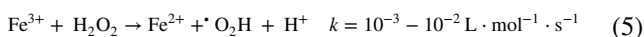
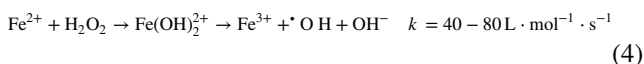
Recent years have seen the widespread application of environmental catalysis in various commercial and industrial sectors to protect the environment and enhance the quality of our lives. It can effectively mitigate water pollution, oxidize organic particles, reduce nitrogen oxide emissions from power plants, and regulate volatile organic compound emissions. Researchers have extensively researched water and wastewater remediation (Ali et al. 2021; Ihsanullah 2020). Among various scenarios, catalytic oxidation or reduction strategies (i.e., photocatalysis and advanced oxidation processes) have substantially progressed in treating wastewater containing pollutants (Kumar et al. 2020d; Russo 2021).

Advanced oxidation pathways (i.e., catalytic wet oxidation, electrochemical oxidation, sonochemical oxidation, photochemical oxidation, and ozone oxidation) can generate active transient species such as hydroxyl ( $\text{HO}\cdot$ ), chlorine ( $\text{Cl}\cdot$ ), alkoxy ( $\text{R}\cdot$ ), hydroperoxy ( $\text{HO}_2\cdot$ ), superoxide ( $\text{O}_2\cdot^-$ ), and sulfate ( $\text{SO}_4\cdot^-$ ), based on the employed catalyst or the oxidant type, and breakdown the hazardous pollutants into safe and biodegradable intermediate molecules (i.e., acetone, acetic, and oxalic acids) (Antonopoulou and Konstantinou 2019). Carbon dioxide, water, and inorganic ions are oxidation end products with no sludge formation. The process involving a catalyst may be suppressed whenever the catalyst is removed from the reaction or by the action of inhibitors (i.e., alcohols, phenols, and sugars, among others). The catalysis process can generally be classified as either homogenous or heterogeneous. During homogenous catalysis, the catalyst is dispersed in an aqueous solution or gas mixture with the reactants (i.e., a single phase of catalyst and reactants). In contrast, heterogeneous catalysis occurs when there are multiple phases (i.e., the catalyst is solid, and the reactants are liquid) (Antonopoulou et al. 2021). Advanced oxidation processes have evolved into promising wastewater remediation technologies in this context.

### Fenton catalysis

Because of its broad applicability, the Fenton catalysis process is regarded as one of the most promising advanced oxidation technologies for cleaning aquatic systems. These reactions generate transient species, primarily through decomposing the oxidant  $\text{H}_2\text{O}_2$  into hydroxyl radicals ( $\cdot\text{OH}$ ), which further attack and oxidize the target pollutants. Its distinguishing characteristics are its operational capabilities under ambient conditions, the nonselective nature of  $\cdot\text{OH}$  radicals, and the conversion of contaminants into harmless byproducts of carbon dioxide and  $\text{H}_2\text{O}$ . Combining these procedures with others, such as ultraviolet or sonic irradiation, which produce more  $\text{OH}\cdot$  and facilitate the regeneration of the  $\text{Fe}^{2+}$  catalyst from  $\text{Fe}^{3+}$ , can improve their efficacy (Bokare and Choi 2014; Ochando-Pulido et al. 2017). For instance, the mechanism of  $\text{OH}\cdot$  formation via Fenton

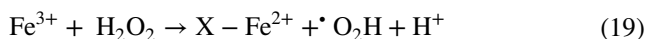
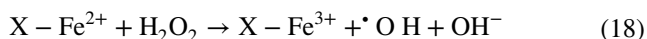
catalysis can be classified into homogenous and heterogeneous processes (Brink et al. 2017; Vorontsov 2019). In turn, the homogeneous process is subdivided into conventional and modified (i.e., Photo-Fenton, Electro-Fenton, Sono-Fenton, and combinations/hybrid Fenton pathways) processes (Zhang et al. 2019c; Nidheesh et al. 2018; Miklos et al. 2018), whereas the heterogeneous process utilizes zero-valent state metal catalysts, synthesized iron supporting catalysts, iron minerals and waste-derived catalysts, and nanomaterials (Thomas et al. 2021). The entire homogenous Fenton catalysis is highly complex, involving oxidation and coagulation processes as presented in Eqs. (4–17) (Babuponusami and Muthukumar 2014; Garcia-Segura et al. 2016).



Numerous variables (i.e., catalyst concentration, surface area, solution pH, oxidant, and ionic strength) significantly impact the efficacy of Fenton reactions. In addition to the differences in operational parameters and wastewater characteristics, the need for optimization studies before their use

in wastewater treatment is emphasized by the differences in operating parameters (Guo et al. 2018). Table 8 displays the wastewater remediation applications of homogenous (i.e., conventional and modified) Fenton catalysis processes.

The heterogeneous process operates on the same principles as the homogeneous process; however, the generation of  $\cdot\text{OH}$  is catalyzed on the surface of heterogeneous catalysts (X), as depicted in Eqs. (18–19). Both Fenton catalysis and reactant adsorption occur concurrently on the binding sites on the substrate's surface. After completing the process, the produced molecules are released (desorbed) from the binding sites, allowing new reactant molecules to bind to the vacant adsorptive sites (Queirós et al. 2015; Sreeja and Sosamony 2016).



The as-used catalyst should possess several desirable physicochemical properties, including cost-effectiveness, high reactivity for  $\cdot\text{OH}$  generation, a large surface area, a porous structure, physical and chemical stability, resistance to attrition and poisoning phenomena, and reusability. Table 9 summarizes the wastewater reclamation applications of the heterogeneous Fenton catalysis method. In addition, the heterogeneous Fenton process has several advantages over the widespread process, such as operational capacity over a broad pH range, a reduction in the formation of iron sludge and the associated cost issues, easy handling, and efficient recovery of as-used catalysts.

## Photocatalysis

Photocatalysis is a photo-promoted chemical reaction that occurs on the surface of the semiconductor substrate, i.e., photocatalyst, to produce reactive species, which are primarily forwarded to various applications, i.e., water pollutants degradation, microbes' disinfection, and hydrocarbon fuels production. The induced electrons ( $e^-$ ) and holes ( $h^+$ ) resulting from the photo-excitation state migrate to the surface of the catalyst, undergo a series of reactions, and produce non-selective oxidizing active radicals, which react with various water pollutants, i.e., heavy metals, organic dyes, pesticides, herbicides, phenols, antibiotics, and others, via various redox reactions (Ohtani 2013). One way to operate photocatalysis is to utilize solar energy to produce chemical energy from the collected solar energy, transfer the simulated electron through photocatalysis, and eliminate organic pollutants (Huang et al. 2021). Several variables influence the efficacy of the degradation process, including solution pH, system temperature, initial pollutant concentration, irradiation intensity, catalyst type, catalyst dose, radiant flux, and oxygen concentration (Anwer et al.

**Table 8** Applications of homogeneous (i.e., conventional and modified), Fenton catalysis process for wastewater remediation. BOD<sub>5</sub>, COD, BOD, AOX, and TOC refer to five-day biochemical oxygen demand, chemical oxygen demand, biological oxygen demand, adsorbable organic halides, and total organic carbon, respectively. H<sub>2</sub>O<sub>2</sub> refers to hydrogen peroxide

Wastewater type	Target parameter	Running condition	Removal (%)	Reference
Pulp bleaching wastewater	BOD <sub>5</sub> /COD	pH=2.0, time = 10.0 min, temperature = 60.0°C, [Fe <sup>2+</sup> ] concentration = 12.5 mM, and [H <sub>2</sub> O <sub>2</sub> ] = 169.0 mM	0.05–0.09	Ribeiro et al. (2020)
	COD		8.0	
	AOX		82.2	
	Color		2 folds higher	
Benzene dye production	BOD <sub>5</sub> /COD	pH=4.1, time = 60.0 min, temperature = 25.0°C, [Fe <sup>2+</sup> ] concentration = 360.0 mM, and [H <sub>2</sub> O <sub>2</sub> ] = 1000.0 mM	0.08–0.49	Guo et al. (2018)
	TOC		75.2	
	COD		85.3	
	Color		99.9	
Containers and drum cleaning	BOD <sub>5</sub> /COD	pH=3.0, time = 160.0 min, temperature = 25.0°C, [Fe <sup>2+</sup> ] concentration = 4.92 mM, and [H <sub>2</sub> O <sub>2</sub> ] = 1324.0 mM	0.38–0.42	Güneş et al. (2019)
	COD		86.8	
	BOD <sub>5</sub>		89.1	
	TOC		89.6	
Recovered paper mill wastewater	COD	pH=3.8, time = 60.0 min, temperature = 25.0°C, [Fe <sup>2+</sup> ] concentration = 3.60 mM, and [H <sub>2</sub> O <sub>2</sub> ] = 13.24 mM	63.0	Brink et al. (2017)
	Phenol		> 85.0	
Municipal landfill leachate	COD	pH=4.0, time = 24.0 h, temperature = 25.0°C, [Fe <sup>2+</sup> ] concentration = 24.35 mM, and [H <sub>2</sub> O <sub>2</sub> ] = 800.0 mM	94.0	Trapido et al. (2017)
	BOD <sub>5</sub>		99.0	
	Phenol		100	
Pharmaceutical	TOC	pH=3.3, time = 2.2 h, temperature = 25.0°C, [Fe <sup>2+</sup> ] concentration = 19.05 mM, and [H <sub>2</sub> O <sub>2</sub> ] = 384.0 mM	71.6	Xie et al. (2016)
	AOX		90.8	
Textile	Color	pH=3.5, time = 30.0 min, temperature = 25.0°C, [Fe <sup>2+</sup> ] concentration = 4.2 mM, and [H <sub>2</sub> O <sub>2</sub> ] = 4.0 mM	77.0	Bae et al. (2015)
	Aromatics		78.0	
	COD		84.0	
Slaughterhouse wastewater	COD	pH=3.0, time = 60.0 min, temperature = 25.0°C, [Fe <sup>2+</sup> ] concentration = 2.0 mM, and [H <sub>2</sub> O <sub>2</sub> ] = 130.0 mM, and ultrasound = 40.0 kHz	77.0	Rahmani et al. (2019)
Paper mill wastewater	TOC	pH=3.0, time = 12.0 h, temperature = 25.0°C, [Fe <sup>2+</sup> ] concentration = 0.5 mM, [H <sub>2</sub> O <sub>2</sub> ] = 0.0 mM, and Current Density = 20 mA cm <sup>-2</sup>	83.0	Klidi et al. (2019)
Pulp and paper mill wastewater	COD	pH=2.5, time = 20.0 min, temperature = 25.0°C, [Fe <sup>2+</sup> ] concentration = 0.0 mM, [H <sub>2</sub> O <sub>2</sub> ] = 29.41 mM, and Current intensity = 1.0 A	91.7	Altin et al. (2017)
Pulp bleaching wastewater	BOD <sub>5</sub> /COD	pH=2.0, time = 10.0 min, temperature = 60.0°C, [Fe <sup>2+</sup> ] concentration = 1.0 mM, [H <sub>2</sub> O <sub>2</sub> ] = 178.0 mM, and ultraviolet lamp = 150.0 W	0.05–0.09	Ribeiro et al. (2020)
	COD		20.0	
	Color		76.0	
	AOX		89.4	
Landfill leachate	BOD <sub>5</sub> /COD	pH=3.5, time = 45.0 min, temperature = 25.0°C, [Fe <sup>2+</sup> ] concentration = 1.07 mM, [H <sub>2</sub> O <sub>2</sub> ] = 264.7 mM, and Current Density = 2.3 A	0.18–0.40	Seibert et al. (2019)
	Suspended solids		26.3	
	BOD <sub>5</sub>		30.2	
	COD		68.0	
	Aromatics		89.2	
	Color		92.4	

2019; Adeel et al. 2021; Nisar et al. 2022). Equations (20–26) represent the overall photocatalysis process (Antonopoulou and Konstantinou 2019; Wang and Zhuan 2020).

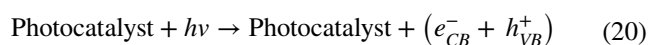
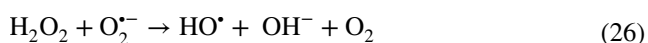
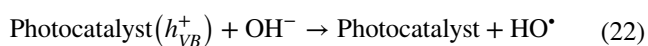
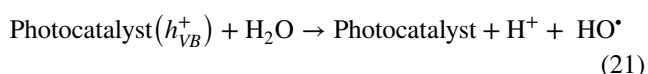


**Table 9** The applications of heterogeneous Fenton catalysis process for wastewater remediation. Several wastewater organics contents and other parameters can be reduced using catalysts

Wastewater type	Target parameter	Running condition	Removal (%)	Reference
Tannery wastewater	COD	pH = 4.8, time = 120.0 min, temperature = 25.0°C, mixed-iron coated olive stone catalyst dosage = 4 g L <sup>-1</sup> , and [H <sub>2</sub> O <sub>2</sub> ] = 37.42 mM	58.4	Vilardi et al. (2018)
	Phenol		59.2	
Olive mill wastewater	BOD <sub>5</sub> /COD	pH = 3.5, time = 60.0 min, temperature = 25.0°C, ion exchange dosage = 40.0 g L <sup>-1</sup> , [Fe <sup>2+</sup> ] concentration = 0.895 mM, and [H <sub>2</sub> O <sub>2</sub> ] = 735.3 mM	0.38–0.50	Reis et al. (2018)
	BOD <sub>5</sub>		75.0	
	COD		81.0	
	Phenol		97.0	
Pulp bleaching wastewater	COD	pH = 3.0, time = 120.0 min, temperature = 24.0°C, [Fe <sup>0</sup> ] concentration = 8.95 mM, and [H <sub>2</sub> O <sub>2</sub> ] = 29.41 Mm	58.4	Sevimli et al. (2014)
Textile wastewater	DOC	pH = 2.8, time = 74.0 min, temperature = 25.0°C, [Fe <sup>3+</sup> : oxalate] concentration = 1.79:5.37 mM, [H <sub>2</sub> O <sub>2</sub> ] = 53.0 Mm, and solar irradiation = 20.2 kJ L <sup>-1</sup>	74.0	Manenti et al. (2015)
	Color		100.0	
Textile wastewater	BOD <sub>5</sub> /COD	pH = 3.0, time = 30.0 min, temperature = 25.0°C, magnetic biochar composite catalyst concentration = 1.0 g L <sup>-1</sup> , and [H <sub>2</sub> O <sub>2</sub> ] = 8.824 Mm	0.26–0.68	Zhang et al. (2018a)
	COD		47.0	
	TOC		49.0	
Textile wastewater	BOD <sub>5</sub> /COD	pH = 3.5, hydraulic retention time = 60.0 min, temperature = 25.0°C, [Fe <sup>2+</sup> ] concentration = 0.36 mM, and [H <sub>2</sub> O <sub>2</sub> ] = 2.0 Mm	0.21–0.39	Karthikeyan et al. (2011)
	Suspended solids		6.3	
	BOD <sub>5</sub>		83.0	
	TOC		83.0	
	COD		91.0	
	Aromatics		100.0	
Plywood manufacturing wastewater	COD	pH = 3.0, time = 24.0 h, temperature = 22.0°C, [Fe <sup>2+</sup> ] concentration = 7.073 mM, and [H <sub>2</sub> O <sub>2</sub> ] = 90.62 Mm	80.0	Bolobajev et al. (2014)
Semicoke landfill leachate	BOD <sub>7</sub> /COD	pH = 3.0, time = 24.0 h, temperature = 22.0°C, [Fe <sup>2+</sup> ] concentration = 6.446 mM, and [H <sub>2</sub> O <sub>2</sub> ] = 59.29 Mm	20.0	Bolobajev et al. (2014)
	COD		65.0	

BOD<sub>5</sub>, COD, BOD, DOC, and TOC refer to five-day biochemical oxygen demand, chemical oxygen demand, biological oxygen demand, dissolved organic carbon, and total organic carbon, respectively. H<sub>2</sub>O<sub>2</sub> refers to hydrogen peroxide



First-generation, second-generation, and third-generation photocatalysts are distinguished from one another. Examples of first-generation photocatalysts include metal oxides, sulfides, phosphates, and nitride compounds. TiO<sub>2</sub>,

as previously mentioned, is the most common and well-known single-component (first-generation) type. The primary drawback of the first-generation kind is the large band gap (i.e., > 3 eV) and the rapid recombination of photoinduced (e<sup>-</sup>) and (h<sup>+</sup>), which reduces the catalytic efficiency (Li et al. 2015; Intarasuwan et al. 2017). Several second-generation photocatalyst modifications, such as heterojunction construction, co-catalyst loading, quantum dot sensitization, and metal oxide doping with metals/nonmetals, have been implemented to address the issues mentioned above (Luo et al. 2021). BiVO<sub>4</sub>/Ag<sub>3</sub>VO<sub>4</sub>, WO<sub>3</sub>/NiWO, graphite carbon nitride/Ag<sub>3</sub>VO<sub>4</sub>, and Bi<sub>2</sub>O<sub>2</sub>CO<sub>3</sub>/Bi<sub>2</sub>S are typical examples of second-generation photocatalysts used for photocatalytic degradation of methyl red, methylene blue, malachite green, and rhodamine B, with the activity of 78%, 92%, 97%, and 98%, respectively (Yan et al. 2016; Mohamed et al. 2014; Wang et al. 2014; Wang et al. 2013). However, the disadvantages of second-generation photocatalysts include difficulties

**Table 10** Applications of photocatalysis for the degradation of water pollutants

Target water pollutant	Photocatalyst material	Surface area (m <sup>2</sup> g <sup>-1</sup> )	Band gap energy (eV)	Degradation (%)	Reference
Ciprofloxacin	Photocatalyst/cadmium sulfide (Bi <sub>3</sub> TaO <sub>7</sub> /CdS)	32.87	2.98	27.0	Xu et al. (2020)
Methylene blue dye	Carbon nanotubes (CNTs)/ titanium dioxide (TiO <sub>2</sub> )/ silver (Ag) nanoparticles/surfactant nanocomposites	146.0	2.25	100.0	Azzam et al. (2019)
Phenol	Graphite carbon nitride on carbon nanotubes/ BiVO <sub>4</sub>	34.99	2.70	75.0	Samsudin et al. (2019)
Gemifoxacin	Zn-layered double hydroxide composite	95.76	1.83	60.4	Gholami et al. (2020)
Chromium (VI)	Titanium dioxide @carbon/cadmium sulfide (TiO <sub>2</sub> @C/CdS)	81.06	3.14	96.0	Yin et al. (2020)
Methylene blue dye	Copper sulfide—cadmium sulfide nanocomposite (CuS-CdS)	27.11	2.2	99.0	Mahanthappa et al. (2019)
Tetracycline	Calcite/titanium dioxide (TiO <sub>2</sub> )	130.33	–	90.6	Belhouchet et al. (2019)
Glyphosate	Bismuth oxybromide (BiOBr)/magnetite (Fe <sub>3</sub> O <sub>4</sub> )	47.38	1.75	97.0	Cao et al. (2019)
Phenol	Cerium oxide	–	–	92.24	Ahmad et al. (2020)
Malathion	Tungsten trioxide/titanium dioxide (WO <sub>3</sub> /TiO <sub>2</sub> )	99.3	3.11	63.0	Ramos-Delgado et al. (2013)
Iodosulphurum	Nitrogen-doped titanium dioxide (TiO <sub>2</sub> )	150.0	–	74.0	Kralchevska et al. (2012)
Acephate	Mesoporous material/ cobalt tetraoxide (MCM-41/Co <sub>3</sub> O <sub>4</sub> )	608	1.51	81.0	AbuKhadra et al. (2020)
Sulphamethaxazole	Zinc oxide (ZnO) nanostructures	7.5	–	84.0	Makropoulou et al. (2020)

Catalysts can be used to degrade antibiotics, several dyes, pesticides, heavy metals, and other chemical contaminants. “–” not reported

in separation and recovery of as-used photocatalysts, high operational costs (i.e., high energy and pressure requirements), and the possibility of catalyst leaching into the aqueous medium, and a decrease in the catalytic activity of reusable photocatalysts (Munshi et al. 2017). Immobilizing photocatalysts on solid substrates has been proposed to overcome these obstacles with photocatalysts of the third generation. Metallic nanocrystals, carbon nitrides, and boron nitrides are some of their varieties. The photocatalysis applications for the degradation of various water pollutants are presented in Table 10.

## Electrocatalysis

Electrocatalysis is a chemical-free electrochemical process in which an electrode at the electrode–electrolyte interface serves as both an electron donor or acceptor and a catalyst (i.e., accelerates the rate of charge transfer). Similar to the photocatalytic process, where the cathodes and anodes represent the reduction and oxidation reaction sites, respectively. The only variation is when reduction and oxidation reactions occur separately on separate electrodes. Electrocatalysts are substrates that can reduce the activation energy of a reaction

by modulating the binding energies without altering the thermodynamics of the reaction (Qian et al. 2021). The homogeneous electrocatalysts are not commercially applicable but are of scientific interest. Generally, high-quality catalysts should be cost-effective, chemically and physically stable, and possess excellent porosity for efficient mass transfer. Enzymes and inorganic coordination complexes are homogenous electrocatalyst examples, whereas nanomaterials, metal–organic frameworks, and carbon-based materials are heterogenous electrocatalyst examples (Khan et al. 2018b).

## Biomass valorization and product upgrading

Sustainability is the development that meets the current generation's needs without compromising the ability of future generations to meet their own needs. The role of environmental catalysis in achieving sustainability is crucial. The valorization of biomass is one of the most significant issues addressed by environmental catalysis (Rodríguez-Padrón et al. 2019b). Biomass is one of the most abundant and renewable sources of energy. The majority of biomass, about 60–80% is composed of carbohydrates, which can be divided into structural polysaccharides such as chitin, cellulose, and hemicellulose, and storage carbohydrates, i.e.,



starch, sucrose, and inulin (Sheldon 2016). Lignocellulosic biomass, the fibrous substance that makes up plant cell walls, is composed of lignin, hemicellulose, and cellulose of (10–25%), (15–30%), and (40–60%), respectively (Wang et al. 2017b; Osman et al. 2020b). Due to its accessibility, biomass feedstock has become one of the most valuable sources for obtaining alternative fuels and commodity chemical compounds, including alcohols, alkanes, biohydrocarbons, glycerol, succinic acid, lactic acid, olefins, levulinic acid, vanillin, muconic acid, furfural, sorbitol, and others (Bayu et al. 2019; Elgarahy et al. 2021b). Since then, biomass valorization has been regarded as an intriguing subject. The effective upcycling of waste biomass (such as corn stover, rice husks, and wheat straw) into valuable biofuels, biomaterials, and commodity chemicals can be accomplished via so-called chemo-catalytic and bio-catalytic strategies, depending on the biomass type, availability, desired end products, and process economics. The pretreatment (fractionation process) is an essential step for modifying the lignocellulosic structure into the primary constituents, thereby generating highly reactive lignocellulosic materials for subsequent catalytic upgrading to valuable biofuels and chemicals (Jing et al. 2019).

Chemical pretreatments, e.g., acid, alkaline, organosolv, ionic liquid, co-solvent, and deep eutectic solvents, physical pretreatments, e.g., steam explosion, ammonia fiber explosion, liquid hot water, and supercritical fluid, and biological pretreatment stages can be distinguished, i.e., enzymatic, and whole microbes (Bhatia et al. 2020; Chuetor et al. 2021). By utilizing thermochemical treatments, e.g., pyrolysis and gasification, and biological treatment, e.g., hydrolysis, fermentation, and anaerobic digestion, lignocellulosic feedstock valorization by fractionation, depolymerization, and upgrading can be accomplished (Akor et al. 2021). Each product of pyrolysis and gasification, such as bio-oil and syngas, can be further processed to generate liquid fuels or leading chemicals. Syngas can be used as a fermentation feedstock to produce acids, diols, and other compounds (Widayatno et al. 2016; Kurnia et al. 2017).

The lignocellulosic feedstock can also be hydrolyzed into lignin, cellulose, hemicellulose, and residual proteins. Their further hydrolysis may yield the monosaccharides pentose (C5) and hexose (C6), which constitute their primary structural components. Several platform lignin-derived commodities can be obtained via aqueous phase reforming, i.e., alkanes, hydrolysis, i.e., hydroxymethylfurfural, and separate hydrolysis and the fermentation/simultaneous saccharification and fermentation by diverting (processing) the intermediates resultant monosaccharides, i.e., acids, alcohols, and diols (Ishola et al. 2013). The use of catalysts, i.e., homogeneous, heterogeneous, and enzymatic, has a significant effect on optimizing process parameters and enhancing the distribution and quality of the products. Typically, an

efficient catalyst should be supported by three essential characteristics: activity, stability, and selectivity. For instance, various types of catalysts have been adopted, including alkali or alkaline metals, activated carbon, fly ash, dolomite, zeolites, i.e., natural, hierarchical, two-dimensional, and three-dimensional, and others (Yu et al. 2021b; Duan et al. 2021; Islam 2020; Mardiana et al. 2022; Trinh and Chang 2021; Gao et al. 2011; El-Nahas et al. 2020).

Biofuels, e.g., bio-ethanol, biodiesel, jet fuel, bio-butanol, and biogas, as well as petroleum hydrocarbons, e.g., ethylene, propylene, butenes, butadiene, ethanol, propanol, butanols, furfural, gasoline, kerosene, aromatics (BTX), isoprene, isobutene, butadiene, and farnesene, can be produced through depolymerization, isomerization, epimerization, dehydration and hydration, retro-aldol, and reduction or oxidation reactions, operated by diverse chemo-catalytic and bio-catalytic pathways (Yang et al. 2016b; Delidovich and Palkovits 2016; Bayu et al. 2018). Moreover, the resultant monosaccharide sugar units produced from the depolymerization of biomass content can be converted into countless value-added chemicals such as hydroxymethylfurfural, levulinic acid, 2,5-Furandicarboxylic acid,  $\gamma$ -valerolactone (GVL), and others (Mariscal et al. 2016).

Lignin is considered one of the most promising renewable resources for producing abundant bio-products such as aerogels, bioplastics, carbon-derived materials, dye dispersants, guaiacol, and vanillin. In addition, the lignin content can serve as a suitable carbon precursor for producing various carbonaceous nanomaterials, including carbon nanotubes, fullerene, graphene, and graphene quantum dots. Due to their unique properties, these materials have gained great attention and are employed in various industrial sectors of energy storage materials, i.e., supercapacitors, photocatalysts, and lithium-ion batteries. Alternatively, lignin-based compounds, such as sodium lignosulfonate and hydroxypropyl sulfated alkaline lignin, can be used as dyes dispersing substrates due to their high adsorption dispersive efficiency, potent thermal stability, and durability (Liu et al. 2019). Economically, biodegradable lignin-based bioplastics are viewed as a viable alternative to non-biodegradable conventional plastics, i.e., petroleum-based polymers, due to the presence of multiple reactive moieties, i.e., carboxyl and hydroxyl, reasonable glass transition temperatures, and their thermoplastic properties. Aerogels are a distinct class of advanced solid-state materials with exceptional physicochemical properties, such as an open mesoporous framework, a large surface area, enormous pore volumes, and a very low density. They can be used in numerous industries, such as adsorbents, acoustics, electromagnetic interference shielding, and others (Cho et al. 2018).

It is believed that biomass-derived cellulose is the most sustainable material capable of producing inexpensive bio-derived ionic liquids, i.e., cellulose-tetrabutylammonium bromide and cationic cellulosic poly ionic liquid. They

have proven to be effective carbon dioxide absorbers with enhanced recyclability. In addition, they have exceptional loading capacities for various water pollutants, superior selectivity, accelerated loading rates, and excellent recyclability. In addition, biocompatible cellulose-based composites can be utilized as catalysts, supercapacitors, drug carriers, antibacterial, and batteries, among other applications (Suhas et al. 2016). Due to their low cost, large surface area, potential for functionalization, and fluorescence, carbon dots derived from cellulose could be utilized in several scientific fields, including biosensors, bioimaging, photocatalysis, solar cells, and optoelectronic devices. Cellulose-based aerogels are primarily used in thermal insulators, electrode materials, and wastewater treatment applications due to their hydrophilicity, biodegradability, low thermal conductivity, sonic velocity, and refractive index (Long et al. 2018).

Compared to lignocellulosic and cellulosic bioproducts, hemicellulose-derived bioproducts are the most limited. Due to their cost-effectiveness, biocompatibility, and renewability, they are ideally suited for certain potential applications, such as the production of pharmaceutical carriers. The hemicellulose-based films are excellent packaging materials, wound dressings, and drug capsules. In addition, hemicellulose-derived hydrogels served as pharmaceutically viable candidates for drug delivery systems due to their tolerance to various pH, solvent composition, temperature, and ionic strength variables (Sun et al. 2013). In addition, the biosorbents derived from hemicellulose exhibit significant adsorption capacities for various water pollutants (i.e., dyes, heavy metals, phenol, and others) (Xiang et al. 2022).

## Biofuel and hydrogen production

### Biofuel production

Biomass is viewed as a promising resource for producing biofuels, one of the best alternatives to fossil fuels for sustainable energy production. Attempting to generate energy from biomass components (such as lignin, cellulose, and hemicellulose, among others) simultaneously reduces waste production and satisfies our future energy demand. Biomass can be converted into valuable biofuels such as bioethanol, biodiesel, and biohydrogen via multiple bio-refinery and bio-transformation scenarios. Biomass is a renewable, sustainable, and cost-effective resource (Cai et al. 2017; Li et al. 2018b; Al-Mawali et al. 2021; Al-Muhtaseb et al. 2021). Due to the inexhaustible supply of feedstock, biofuels can be utilized in various contexts. Depending on feedstock type, biofuels can be divided into the first, second, third, and fourth generations (Osman et al. 2021a). The first generation is produced directly from edible biomass (starch), whereas the second generation uses non-edible biomass, i.e., crop wastes. Marine-derived raw materials, i.e., algal

biomass, can be incorporated into the third generation of biofuel production. Lastly, the fourth-generation harnesses bioengineered (genetically modified) microorganisms to produce biofuels (Osman et al. 2021a).

To produce biofuels, thermochemical, i.e., combustion, hydrothermal liquefaction, torrefaction, pyrolysis, and gasification, biochemical, i.e., anaerobic digestion and microbial fermentation, and chemical, i.e., transesterification, conversion techniques are widely utilized (Osman et al. 2021b; Najeeb et al. 2021). Using either homogeneous or heterogeneous catalysts throughout the process, the catalytic conversion of biomass is a rapid and effective expanding technique for biofuel production. Homogeneous catalysts, e.g., acid and base catalysts, enzyme-based biocatalysts, e.g., lipase-based and acyl acceptor catalysts, and heterogeneous catalysts are among the various types of catalysts, i.e., solid acid catalysts, solid base catalysts, and ion exchange resin catalysts. The heterogeneous solid acid catalysts are divided into metal-based and carbon-based catalysts. In contrast, the heterogeneous solid base catalysts are divided into oxide-based, boron-based, carbon-based, and waste-derived catalysts (Vasić et al. 2020). They have been studied to convert biomass into biofuels efficiently. Fundamentally, there are challenges associated with using homogeneous catalysts, such as the energy-intensive separation process. However, they yield better yields in a shorter amount of time.

In contrast, heterogeneous catalysts are inexpensive and environmentally benign materials with simple product separation, but they pose a challenge for rational nanoscale catalyst design (Najeeb et al. 2021; Bohlouli and Mahdavian 2021). Typically, homogeneous catalysts are used to convert biomass into biofuels. The primary disadvantages of these homogeneous catalysts are soap production under alkaline catalytic conditions and the caustic nature of the acidic catalyst. Typically, the reaction rate of biocatalysts is slow, but they have high selectivity for product synthesis and minimal environmental impact. Heterogeneous catalysis is chosen over homogeneous and biocatalyst catalysis because it is more effective in selectivity and reactivity. In the presence of heterogeneous catalysts, thermochemical processes may improve product selectivity and increase energy efficiency by decreasing activation energy.

The catalytic pyrolysis process has been identified as an efficient and effective method for producing biochar, liquid oil, and syngas from biomass in an oxygen-free environment using supporting catalysts. Approximately 40% of the produced biofuels (crude bio-oil) contain oxygenated compounds. In addition to its physicochemical properties, the bio-oil production yield depends heavily on the feedstock source and the various operational parameters, i.e., heating temperature, heating rate, inert gas type, inert gas flow rate, and others. Numerous studies have applied solid acid catalysts such as silica (Tan et al. 2018), zeolites (Paysepar et al.

2018), Nickel-supported catalysts (Santamaria et al. 2019), and silicoaluminophosphate (SAPO) catalysts (Chen et al. 2018) during the conversion of biomass into hydrocarbons (i.e., pyrolysis) with varying selectivity. The gasification of biomass is a subject of significant scientific interest at present. Producing gaseous fuel by burning biomass in a gasification medium, i.e., air, oxygen, and steam, at high temperatures, i.e., 500–1500 °C, and pressures, i.e., 30–40 bars, maximizes the released gas.

Several studies have been performed on biomass gasification (Zhu and Zhuang 2012). Calcined dolomites or their related minerals, i.e., magnesite, calcite, and limestone, are frequently employed for hot gas cleaning (Gil et al. 1999). Some common catalysts (such as Ni- and Re-based catalysts) are also used to limit the coke production from tar (Kıpçak and Akgün 2018; Jin et al. 2018). Moreover, the introduced noble metal Rh catalyst admirably decreased the tar content in the product (Zhang et al. 2018b). Various types of catalysts such as native/modified zeolites, metal oxides, metal phosphates, metal–organic frameworks, and siliceous supporting materials are used to decompose biomass feedstock at moderate running (hydrothermal conditions) temperatures into phenolic compounds and sugars, i.e., mono- or oligosaccharides, which are then catalyzed to produce C<sub>5</sub>–C<sub>6</sub> sugars (Li et al. 2016c; Huang and Fu 2013).

In the transesterification process, the triglycerides in vegetable oils, animal fats, or waste cooking oil feedstocks typically react with alcohols, i.e., methanol, ethanol, butanol, and hexanol, via a series of chemical reactions in the presence of an acid or base catalyst to form fatty acid methyl esters (FAME biodiesel) and glycerol (reaction byproduct). Diverse critical parameters, including catalyst loading, catalyst porosity, catalyst surface area, catalyst particle size, hydrophilic or hydrophobic characteristics of catalyst, calcination temperature, leaching phenomenon, reaction time, working temperatures, alcoholic factor, blending and stirring, and alcohol: oil molar ratios, have a significant impact on the biodiesel production yield and quality (Kumar and Ali 2013; Dhamodaran et al. 2017). The catalyst in the reaction provides a greater number of active sites for the catalytic reaction process, resulting in increased catalytic activity and a higher biodiesel conversion yield. However, adequate quantities of as-used catalysts must be optimized to prevent an uncontrollable increase in the viscosity of the alcohol-oil mixture. To purify its stream, produced crude diesel must be neutralized and passed through various cleaning-up scenarios (such as dry-washing, membrane extraction, water washing, and washing with adsorbent or water) (Bertram et al. 2009). Viscosity kinetics and dynamics, density, acid or neutralization number, cetane number, cloud point, and pour point should be thoroughly investigated (Agarwal and Das 2001). Table 11 displays a variety of distinct biodiesel production catalysts currently in use.

## Hydrogen production

Due to limited fossil fuel suppliers, rising energy demand, and the urgent need to protect diverse forms of life on our planet to mitigate the effects of climate change, recent efforts have been concentrated on exploiting various renewable resources, e.g., solar and wind. Converting renewable natural resources into valuable, transportable fuels is an attractive concept (Avcıoğlu et al. 2019). From this point of view, hydrogen appears to be one of the promising fuels due to its zero emissions and subsequent reacquisition of chemical energy during combustion (Eljack and Kazi 2021). Hydrogen production from various feedstock such as non-renewables, i.e., natural gas, or renewables, i.e., biomass, organic solid wastes, and water, can be carried out through a variety of methods, including thermochemical (i.e., pyrolysis, gasification, catalytic reforming, partial oxidation, and chemical looping), biological (i.e., direct/indirect biophotolysis, dark/photo fermentation, enzymatic, and electrochemical (i.e., water electrolysis)). The downstream reformat gas can be purified to produce hydrogen with a reduced carbon monoxide content, making it suitable for further applications (Carneiro and Gomes 2019; Morosuk and Tsatsaronis 2019).

In general, the decomposition of water through water electrolysis, whether powered by electricity or solar energy, can be divided into oxygen evolution reaction and hydrogen evolution reaction. Anodes and cathodes undergo oxidation–reduction reactions that result in the release of oxygen and hydrogen gases, respectively. The released hydrogen can be used solely as fuel or combined with oxygen to produce oxyhydrogen gas, which is then used for welding and other industrial applications (Wang et al. 2021e). Slow reaction kinetics of oxygen evolution reaction and hydrogen evolution reaction attributable to high overpotentials, a metric for kinetic energy barriers, is one of the most significant operational obstacles to water splitting (Suen et al. 2017). Catalysis plays a vital role in the energy cycle described previously during the water electrolysis process.

There are currently three significant electrolysis scenarios: proton exchange membrane (acidic condition), high-temperature solid oxide water electrolysis (high temperature), and alkaline electrolysis (alkaline conditions) (Wang et al. 2021e). Therefore, developing novel, highly effective, and stable electrocatalysts is suitable for different process parameters (i.e., working media, temperature, and others) and contain the proper stimulator species to accelerate reaction kinetics by enhancing their physicochemical properties is a significant challenge. The hydrogen evolution reaction electrocatalysts are separated into noble-metal-based (palladium, platinum, rhodium, ruthenium, iridium) and non-noble metal-based electrocatalysts. Many critical parameters for activity (i.e., exchange current density, overpotential, and Tafel slope), stability (i.e., current/potential over time),

**Table 11** Catalysts for biodiesel production

Feedstock	Catalyst/source	Operational parameters				Production (%)	Reference
		Methanol-to-oil molar ratio	Catalyst loading (wt%)	Temperature (°C)	Reaction time (min)		
Waste frying oil	NaOH	7.5: 1.0	0.5	50.0	30.0	96.0	Uzun et al. (2012)
Mahua oil	Mn-doped ZnO nanocatalyst	7.0: 1.0	8.0	50.0	50.0	97.0	Baskar et al. (2017)
Soybean oil	CaO@NaY zeolite	9.0: 1.0	3.0	65.0	180.0	95.0	Wu et al. (2013)
Soybean oil	Sodalite	12.0: 1.0	4.0	65.0	120.0	95.5	Manique et al. (2017)
Castor oil	La <sub>2</sub> O <sub>3</sub> /NaY zeolite	15.0: 1.0	10.0	70.0	50.0	84.6	Du et al. (2018)
Sunflower oil	Ba–Sr/ZSM-5	9.0: 1.0	3.0	60.0	180.0	87.7	Feyzi and Khajavi (2014)
Soybean oil	H <sub>4</sub> [W <sub>12</sub> SiO <sub>40</sub> ]@zeolite H $\beta$	4.0: 1.0	0.2	65.0	480.0	95.0	Narkhede and Patel (2013)
Waste sunflower oil	KOH/zeolite	11.5: 1.0	6.0	50.0	120.0	96.7	Al-Jammal et al. (2016)
Vegetable oil	CaO/activated carbon	40.0: 111.0	–	120.0	420.0	>90.0	Konwar et al. (2018)
Corn oil	KOH/activated carbon	3.0: 1.0	0.75	62.5	60.0	92.0	Narowska et al. (2019)
Bitter almond oil	Potassium acetate/activated carbon	9.0: 1.0	2.50	65.0	150.0	93.21	Fadhil et al. (2016)
Palm oil	Ag@ZnO	10.0: 1.0	10.0	60.0	60.0	97.0	Laskar et al. (2020)
Sunflower oil	Mg–Al HT	48.0: 1.0	2.0	60.0	480.0	92.0	Navajas et al. (2018)
Soybean oil	Zn–Al HT	26.0: 1.0	–	140.0	60.0	76.0	Liu et al. (2014b)
Stearic acid	ZrO <sub>2</sub> @SiO <sub>2</sub>	120.0: 1.0	10.0	120.0	180.0	48.6	Ibrahim et al. (2019)
Soybean oil	CaO	8.0: 1.0	10.0	65.0	180.0	90.0	Ayodeji et al. (2018)
Sunflower	CaO	11.0: 1.0	5.0	60.0	3.0	83.2	Fayyazi et al. (2018)
Palm oil	CaO/coconut waste	24.0: 1.0	5.0	65.0	180.0	81.0	Sulaiman and Ruslan (2017)
<i>Azadirachta indica</i> oil	Ripe plantain fruit peel	1.0: 0.73	0.65	65.0	57.0	99.2	Etim et al. (2018)

The catalyst in the reaction increases the number of active sites, leading to a higher conversion yield of biodiesel. However, the amount of catalyst used must be optimized to prevent an increase in the mixture's viscosity. NaOH, CaO, ZnO, La<sub>2</sub>O<sub>3</sub>, KOH, SiO<sub>2</sub> and ZrO<sub>2</sub> refer to sodium hydroxide, calcium oxide, zinc oxide, lanthanum oxide, potassium hydroxide, silica and zirconium oxide, respectively

and efficiency are used to evaluate the performance of the employed catalyst (i.e., faradaic efficacy and turnover frequency) (Wang et al. 2021e). Table 12 shows different as-used catalysts for hydrogen evolution reactions through water electrolysis.

Both catalytic reforming and catalytic cracking are used to convert hydrocarbons into valuable products. Using mild temperatures and pressures in the presence of catalysts, catalytic cracking is the process by which larger hydrocarbon compounds are broken down into smaller (cracked) hydrocarbon molecules. While catalytic reforming (i.e., steam reforming, autothermal reforming, aqueous phase reforming, partial oxidation, and dry reforming) is the process by which

hydrocarbons are reconfigured to form different valuable (reformate) products with the aid of a catalyst, reforming is the rearrangement of hydrocarbons into different products (Naikoo et al. 2021). Among various hydrocarbons, methane, the primary component of natural gas and biogas, can be an abundant source of hydrogen production. Compared to steam methane reforming (63.3 kJ/mol hydrogen), methane cracking with a lower energy requirement (37.8 kJ/mol hydrogen) provides a more sustainable hydrogen production approach because it does not produce carbon monoxide or carbon dioxide emissions. However, catalysts with a low tendency for carbon formation, long-term stability, and high catalytic and reforming efficiencies are strongly suggested. Various

**Table 12** Catalysts for hydrogen evolution reaction through the water electrolysis process

Cathode electrocatalyst material	Electrolyte/anode used in the electrolysis cell	Overpotential (mV) at 10 mA cm <sup>-2</sup>	Cell voltages (V) (at 10 mA cm <sup>-2</sup> )	Reference
NiCoP/CC	NiCoP/CC	44/62	1.52	Du et al. (2017)
MoS <sub>2</sub> /NiFe-LDH	MoS <sub>2</sub> /NiFe-LDH	110.0	1.57	Xiong et al. (2019)
Co-P	Co-P	94.0	1.47	Jiang et al. (2015)
Ni/NiFe	Ni/NiFe	100.0	1.56	Wu et al. (2018)
NiCoFe-PS	NiCoFe-PS	195.0	1.52	Yao et al. (2019)
Ruthenium dioxide cluster	Ruthenium dioxide cluster	33/20/98	1.51	Park et al. (2019)
NiMoCo	NiMoCo	40.0	1.56	Hu et al. (2019)
NSP-Ni <sub>3</sub> FeN	NSP-Ni <sub>3</sub> FeN	45.0	1.495	Wang et al. (2016c)
Ni <sub>3</sub> N	Ni <sub>3</sub> N	47.0	1.503	Hu et al. (2020)
Ni <sub>2</sub> P/Ni <sub>0.96</sub> S/NF	Ni <sub>2</sub> P/Ni <sub>0.96</sub> S/NF	72.0	1.453	He et al. (2020b)
PrGO/NiCoP	PrGO/NiCoP	106.0	1.56	Dong et al. (2019)
NiCoSe <sub>2-x</sub> N-C	NiCoSe <sub>2-x</sub> N-C	89.0	1.53	Li et al. (2018c)
Ni/Ni <sub>2</sub> P	Ni/Ni <sub>2</sub> P	92.0	1.55	Sun et al. (2018)

It is desirable to use highly efficient catalysts to reduce the overpotentials of oxygen evolution reaction and hydrogen evolution reaction to improve oxygen and hydrogen production yields. LDH, NSP, NF, PrGO, and NiCoP are layered double hydroxide, nanoparticle-Stacked Porous, Ni foam, reduced graphene oxide, and Ni-Co phosphides, respectively

catalyst types have been developed for catalytic and reforming processes, including metal (i.e., noble and transition)-based catalysts and carbon (i.e., activated carbon and carbon black). Tables 13 and 14 detail various catalysts used in catalytic cracking and reforming.

## Conclusion

Recent advancements in photocatalysis, biocatalysis and electrocatalysis have been evaluated, and the challenges faced in environmental catalysis have been identified. Research is currently focused on developing efficient photocatalysts through doping, coupling with other nanomaterials, precipitation with metal particles, crystal growth designs, and heterojunctions. Heterojunction-based photocatalysts promise to improve photocatalytic activity for environmental pollution degradation, hydrogen production, and carbon dioxide reduction. However, the practical application of photocatalysis is currently limited due to insufficient activity, poor stability, and high cost. Electrocatalysts have been evaluated for environmental remediation applications, but limited efforts have been made to assess the toxicity of pollutants that are not efficiently mineralized. Developing novel, highly effective, and stable electrocatalysts

suitable for various process parameters and containing the proper stimulator species to accelerate reaction kinetics by enhancing their physicochemical properties is a significant challenge.

In biocatalysis, enzymes found in soil, such as lipases, dehydrogenases, ureases, and catalases, have been used as bioindicators for evaluating pollution. However, lipase-based biosensors for bioremediation are not yet suitable for commercial use and require further research. Protein modeling and computational design have been utilized to improve known enzymatic functions and design new catalytic enzymes. New protein engineering tools, such as computational protein design, next-generation sequencing, and machine learning, will also aid in developing new enzymatic activities.

Materials such as biomass-derived carbon materials, metal-organic frameworks, non-noble metals, and nanocomposites have also been discussed as catalysts. The preparation and catalytic applications of these materials, as well as their impact on the circular economy, have been evaluated. The preparation of metal-organic frameworks via solvent-free methods is currently a popular research topic. Enzymes have also been discussed as sustainable catalysts with various supports and catalytic applications. The relationship between the chemical structure of

**Table 13** Catalysts for methane cracking

Feed composition	Operating temperatures (°C)	Catalyst name	Preparation method	Maximum methane (%)	Hydrogen yield (%)	References
Methane	700	10% Ni/TiO <sub>2</sub>	Sol-gel	–	43.0	Pudukudy et al. (2017)
Methane	700	Ni-Fe/ Santa Barbara Amorphous-15 (SBA-15)	Wet impregnation	35.0	52.0	Pudukudy et al. (2015)
Nitrogen: methane (19:1)	850	Shengli lignite char	Pyrolysis	86.0	88.0	Wei et al. (2011)
Methane	700	40% Ni- zeolite (ZSM-5(25))	Wet impregnation	–	77.0	Awadallah et al. (2016)
Methane	800	Fe-SiO <sub>2</sub>	Sol-gel	–	58.0	Pudukudy and Yaakob (2015)
Methane	600	50% Ni/TiO <sub>2</sub>	Sol-gel	–	45.0	Pudukudy et al. (2017)
	650			–	53.0	
	700			–	56.0	
Methane	700	50% Ni-25% CeO <sub>2</sub> /Al <sub>2</sub> O <sub>3</sub>	Wet impregnation	–	53.0	Ahmed et al. (2016)
Nitrogen: methane (1:9)	500	12.5%Ni-12.4%Co/La <sub>2</sub> O <sub>3</sub>	Co-precipitation	21.0	–	Khan et al. (2016)
	600			54.0	–	
	700			82.0	–	
Methane	700	Co-Fe/ Santa Barbara Amorphous-15 (SBA-15)	Wet impregnation	34.0	51.0	Pudukudy et al. (2015)
Nitrogen: methane (19:1)	850	Xiaolongtan lignite char	Pyrolysis	80.0	82.0	Wei et al. (2011)
	850	Jincheng anthracite char		35.0	27.0	

Various biofuels can be synthesized into hydrogen using a catalyst-induced reforming process, including bioethanol, methanol, ethanol, bio-oil, and others. “–” not reported. CeO<sub>2</sub>, Al<sub>2</sub>O<sub>3</sub>, ZrO<sub>2</sub> and La<sub>2</sub>O<sub>3</sub> refer to cerium(IV) oxide, aluminum oxide, zirconium oxide, and lanthanum oxide, respectively

sustainable catalysts and their end-application and catalytic performance has been critically evaluated.

The production of shape-controlled metal nanoparticles remains challenging. Several methods have been developed to synthesize stable metal nanoparticles with a defined shape, including the addition of inorganic capping agents, organic ligands, colloids, polymers, and core-shell materials. Using functionalizing agents improves nanocomposites' morphology, size, and properties, but their inability to degrade or be eliminated poses a significant environmental threat. Consequently, there is a growing interest in synthesizing nanocomposites from renewable resources such as starch, chitin, vegetable oils, lignin, natural rubber, and cellulose. The sensitivity of enzymes to extreme pH and temperature conditions and their poor reusability continues to be

obstacles in enzyme-based catalysts. Techniques of directed evolution and genetic engineering have been employed to improve enzymes' stability and catalytic performance.

Integrating green chemistry principles into large-scale synthesis is a significant challenge, including moderating energy input, addressing organic solvent issues, and managing problematic wastes. As an alternative, solvent-free routes such as mechanochemistry synthesis offer high versatility, simplicity, and reproducibility. Additionally, microwave and ultrasound irradiation can provide highly efficient and precisely controlled energy for the synthesis and growth of nanostructures. However, preparing enhanced mixed metal oxide catalysts with a uniform distribution of various metal oxides remains challenging.

**Table 14** Performance of diverse catalysts during oxygenates reforming processes for hydrogen production

Feedstock	Temperature (°C)	Catalyst name	Ethanol, water, and oxygen (C <sub>2</sub> H <sub>6</sub> O/H <sub>2</sub> O/O <sub>2</sub> ) (molar ratio)	% ethanol (XC <sub>2</sub> H <sub>6</sub> O)	% hydrogen selectivity	Reference
Bioethanol	600	Ni/CeO <sub>2</sub> -ZrO <sub>2</sub> and Rh-Ni/CeO <sub>2</sub> -ZrO <sub>2</sub>	1:9:0.35	91.0 –100.0	3.5–4.6	Mondal et al. (2015)
Bioethanol	150–350	Ni/La <sub>2</sub> O <sub>3</sub> -Al <sub>2</sub> O <sub>3</sub> and Ni/CeO <sub>2</sub> -Al <sub>2</sub> O <sub>3</sub>	43.69 g/L	90.0	63.6	Dan et al. (2015)
Methanol	200–350	Cu/Zn-Al <sub>2</sub> O <sub>3</sub>	–	51.87	75.4	Hammoud et al. (2015)
Ethanol	250–750	CZ91NiCo	1:6	90.0	80.0	Moretti et al. (2015)
Bio-oil	700	Ce-Ni/Co/Al <sub>2</sub> O <sub>3</sub>	Liquid-hourly space velocity (LHSV) of 0.23 h <sup>-1</sup>	94.1	83.8	Xie et al. (2015)
Ethylene glycol	600	1.25 wt% Ni–3.75 wt% Pt/Al <sub>2</sub> O <sub>3</sub>	1:9	40.0	30.0	Larimi and Khorasheh 2018
	600	2.5 wt% Ni–2.5 wt% Pt/Al <sub>2</sub> O <sub>3</sub>	1:9	50.0	40.0	
	600	3.75 wt% Ni–1.25 wt% Pt/Al <sub>2</sub> O <sub>3</sub>	1:9	60.0	44.0	
	600	5 wt% Ni/Al <sub>2</sub> O <sub>3</sub>	1:9	36.0	20.0	
	600	5 wt% Pt/Al <sub>2</sub> O <sub>3</sub>	1:9	30.0	30.0	
Acetic acid	450–650	Ni/Ce <sub>0.75</sub> Zr <sub>0.25</sub> O <sub>2</sub>	Weight hourly space velocity (WHSV) = 134 h <sup>-1</sup>	100.0	High	Phongprueksathat et al. (2019)

Methane can be utilized as feedstock that is converted by catalysts into hydrogen in various methane-cracking processes. Methane cracking can provide a more sustainable hydrogen production approach because it does not produce carbon monoxide or carbon dioxide emissions. “–” not reported. TiO<sub>2</sub>, SiO<sub>2</sub>, CeO<sub>2</sub>, Al<sub>2</sub>O<sub>3</sub> and La<sub>2</sub>O<sub>3</sub> refer to titanium dioxide, silica, cerium(IV) oxide, aluminum oxide, and lanthanum oxide, respectively

**Acknowledgements** Prof David W. Rooney and Dr Ahmed I. Osman wish to acknowledge the support of The Bryden Centre project (Project ID VA5048). The Bryden Centre project is supported by the European Union’s INTERREG VA Programme, managed by the Special EU Programmes Body (SEUPB). Dr Park acknowledged that this work was supported by the Brain Pool program funded by the Ministry of Science and ICT through the National Research Foundation of Korea (Grant Number: 2021H1D3A2A02081973).

**Disclaimer** The views and opinions expressed in this review do not necessarily reflect those of the European Commission or the Special EU Programmes Body (SEUPB).

## Declarations

**Conflict of interest** The authors declare no conflict of interest.

**Open Access** This article is licensed under a Creative Commons Attribution 4.0 International License, which permits use, sharing, adaptation, distribution and reproduction in any medium or format, as long as you give appropriate credit to the original author(s) and the source, provide a link to the Creative Commons licence, and indicate if changes were made. The images or other third party material in this article are included in the article’s Creative Commons licence, unless indicated otherwise in a credit line to the material. If material is not included in the article’s Creative Commons licence and your intended use is not permitted by statutory regulation or exceeds the permitted use, you will need to obtain permission directly from the copyright holder. To view a copy of this licence, visit <http://creativecommons.org/licenses/by/4.0/>.

## References

- Abd El-Monaem EM et al (2022) Floatable cellulose acetate beads embedded with flower-like zwitterionic binary MOF/PDA for efficient removal of Tetracycline. *J Colloid Interface Sci* 620:333–345. <https://doi.org/10.1016/j.jcis.2022.04.010>
- AbuKhadra MR et al (2020) Enhanced photocatalytic degradation of acephate pesticide over MCM-41/Co<sub>3</sub>O<sub>4</sub> nanocomposite synthesized from rice husk silica gel and Peach leaves. *J Hazard Mater* 389:122129. <https://doi.org/10.1016/j.jhazmat.2020.122129>
- Adeel M et al (2021) Synthesis and characterization of Co-ZnO and evaluation of its photocatalytic activity for photodegradation of methyl orange. *ACS Omega* 6(2):1426–1435. <https://doi.org/10.1021/acsomega.0c05092>
- Affes M et al (2017) Effect of bacterial lipase on anaerobic co-digestion of slaughterhouse wastewater and grease in batch condition and continuous fixed-bed reactor. *Lipids Health Dis* 16:1–8
- Afifeh MR et al (2019) A green approach to the facile synthesis of colloidal platinum nanoparticles by Preyssler polyoxometalate. *J Nanostruct* 9:249–257
- Agarwal AK, Das LM (2001) Biodiesel development and characterization for use as a fuel in compression ignition engines. *J Eng Gas Turbin Power* 123(2):440–447. <https://doi.org/10.1115/1.1364522>
- Agrafiotis C et al (2002) Evaluation of sol-gel methods for the synthesis of doped-ceria environmental catalysis systems. Part I: preparation of coatings. *J Eur Ceram Soc* 22:15–25. [https://doi.org/10.1016/S0955-2219\(01\)00246-1](https://doi.org/10.1016/S0955-2219(01)00246-1)

- Ahmad H, Hossain MK (2022) Supported nanocatalysts: recent developments in microwave synthesis for application in heterogeneous catalysis. *Mater Adv* 3:859–887. <https://doi.org/10.1039/D1MA00840D>
- Ahmad J et al (2018) Fabrication of highly photocatalytic active anatase TiO<sub>2</sub>-graphene oxide heterostructures via solid phase ball milling for environmental remediation. *Surf Interface* 13:186–195. <https://doi.org/10.1016/j.surf.2018.09.010>
- Ahmad T et al (2020) Phytosynthesis of cerium oxide nanoparticles and investigation of their photocatalytic potential for degradation of phenol under visible light. *J Mol Struct*. <https://doi.org/10.1016/j.molstruc.2020.128292>
- Ahmed W et al (2016) Ni/CeO<sub>2</sub>-Al<sub>2</sub>O<sub>3</sub> catalysts for methane thermo-catalytic decomposition to CO<sub>x</sub>-free H<sub>2</sub> production. *Int J Hydrog Energy* 1217:128292. <https://doi.org/10.1016/j.ijhydene.2016.08.177>
- Ahmed IN et al (2018) Hydrolysis of cellulose using cellulase physically immobilized on highly stable zirconium based metal-organic frameworks. *Biores Technol* 270:377–382. <https://doi.org/10.1016/j.biortech.2018.09.077>
- Ai L et al (2018) Bamboo-structured nitrogen-doped carbon nanotube coencapsulating cobalt and molybdenum carbide nanoparticles: an efficient bifunctional electrocatalyst for overall water splitting. *ACS Sustain Chem Eng* 6:9912–9920. <https://doi.org/10.1021/acssuschemeng.8b01120>
- Akor CI et al (2021) Thermokinetic study of residual solid digestate from anaerobic digestion. *Chem Eng J* 406:127039. <https://doi.org/10.1016/j.cej.2020.127039>
- Akpan U, Hameed B (2011) Photocatalytic degradation of 2, 4-dichlorophenoxyacetic acid by Ca–Ce–W–TiO<sub>2</sub> composite photocatalyst. *Chem Eng J* 173:369–375
- Alamgholiloo H et al (2021) A facile strategy for designing core-shell nanocomposite of ZIF-67/Fe<sub>3</sub>O<sub>4</sub>: a novel insight into ciprofloxacin removal from wastewater. *Process Saf Environ Prot* 147:392–404
- Alcalde M et al (2006) Environmental biocatalysis: from remediation with enzymes to novel green processes. *Trends Biotechnol* 24:281–287
- Ali M, Husain Q (2018) Guar gum blended alginate/agarose hydrogel as a promising support for the entrapment of peroxidase: Stability and reusability studies for the treatment of textile effluent. *Int J Biol Macromol* 116:463–471. <https://doi.org/10.1016/j.ijbiomac.2018.05.037>
- Ali N et al (2021) Deployment of metal-organic frameworks as robust materials for sustainable catalysis and remediation of pollutants in environmental settings. *Chemosphere* 272:129605. <https://doi.org/10.1016/j.chemosphere.2021.129605>
- Al-Jammal N et al (2016) Manufacturing of zeolite based catalyst from zeolite tuft for biodiesel production from waste sunflower oil. *Renewable Energy*. <https://doi.org/10.1016/j.renene.2016.03.018>
- Alkan B et al (2019) Spray-flame-synthesized LaCo<sub>1-x</sub>Fe<sub>x</sub>O<sub>3</sub> perovskite nanoparticles as electrocatalysts for water and ethanol oxidation. *ChemElectroChem* 6:4266–4274. <https://doi.org/10.1002/celec.201900168>
- Al-Mawali KS et al (2021) Life cycle assessment of biodiesel production utilising waste date seed oil and a novel magnetic catalyst: a circular bioeconomy approach. *Renew Energy* 170:832–846. <https://doi.org/10.1016/j.renene.2021.02.027>
- Almqvist CB, Biswas P (2002) Role of synthesis method and particle size of nanostructured TiO<sub>2</sub> on its photoactivity. *J Catal* 212:145–156. <https://doi.org/10.1006/jcat.2002.3783>
- Al-Muhtaseb A, Ala'a H et al (2021) Circular economy approach of enhanced bifunctional catalytic system of CaO/CeO<sub>2</sub> for biodiesel production from waste loquat seed oil with life cycle assessment study. *Energy Convers Manag* 236:114040
- Altin A et al (2017) Treatment of kraft pulp and paper mill wastewater by electro-fenton/electro-coagulation process. *J Environ Protect Ecol* 18(2):652–661
- Angel S et al (2020) Spray-flame synthesis of La(Fe, Co)O<sub>3</sub> nanoperovskites from metal nitrates. *AIChE J* 66:16748. <https://doi.org/10.1002/aic.16748>
- Ani I et al (2018) Photocatalytic degradation of pollutants in petroleum refinery wastewater by TiO<sub>2</sub>- and ZnO-based photocatalysts: recent development. *J Clean Prod* 205:930–954
- Ansari A, Nematollahi D (2020) Convergent paired electrocatalytic degradation of p-dinitrobenzene by Ti/SnO<sub>2</sub>-Sb/β-PbO<sub>2</sub> anode. A new insight into the electrochemical degradation mechanism. *Appl Catal B Environ* 261:118226. <https://doi.org/10.1016/j.apcatb.2019.118226>
- Antoniadou M et al (2011) Photocatalysis and photoelectrocatalysis using (CdS-ZnS)/TiO<sub>2</sub> combined photocatalysts. *Appl Catal B* 107:188–196
- Antonopoulou M et al (2021) An overview of homogeneous and heterogeneous photocatalysis applications for the removal of pharmaceutical compounds from real or synthetic hospital wastewaters under lab or pilot scale. *Sci Total Environ* 7:65. <https://doi.org/10.1016/j.scitotenv.2020.144163>
- Antonopoulou M, Konstantinou I (2019) AOPs methods for the removal of taste and odor compounds. In: Applications of advanced oxidation processes (AOPs) in drinking water treatment, pp 179–210. [https://doi.org/10.1007/978\\_2017\\_119](https://doi.org/10.1007/978_2017_119)
- Anwer H et al (2019) Photocatalysts for degradation of dyes in industrial effluents: opportunities and challenges. *Nano Res* 12:345. <https://doi.org/10.1007/s12274-019-2287-0>
- Ariaeenejad S et al (2020) Stable cellulase immobilized on graphene oxide@CMC-g-poly(AMPS-co-AAm) hydrogel for enhanced enzymatic hydrolysis of lignocellulosic biomass. *Carbohydr Polym* 230:115661. <https://doi.org/10.1016/j.carbpol.2019.115661>
- Arunachalam P et al (2021) Recent developments in the use of heterogeneous semiconductor photocatalyst based materials for a visible-light-induced water-splitting system—a brief review. *Catalysts* 11:160
- Ashkan Z et al (2021) Immobilization of enzymes on nanoinorganic support materials: an update. *Int J Biol Macromol* 168:708–721. <https://doi.org/10.1016/j.ijbiomac.2020.11.127>
- Ates B et al (2020) Chemistry, structures, and advanced applications of nanocomposites from biorenewable resources. *Chem Rev* 120:9304–9362
- Ates B, et al (2017) Biomedical applications of hybrid polymer composite materials. In: Hybrid polymer composite materials. Elsevier, pp 343–408
- Avcioglu AO et al (2019) Assessment of the energy potential of agricultural biomass residues in Turkey. *Renew Energy*. <https://doi.org/10.1016/j.renene.2019.01.053>
- Awadallah AE et al (2016) Effect of crystalline structure and pore geometry of silica based supported materials on the catalytic behavior of metallic nickel particles during methane decomposition to CO<sub>x</sub>-free hydrogen and carbon nanomaterials. *Int J Hydrog Energy*. <https://doi.org/10.1016/j.ijhydene.2016.07.081>
- Ayati A et al (2014) Novel Au NPs/preyssler acid/TiO<sub>2</sub> nanocomposite for the photocatalytic removal of azo dye. *Sep Pur Technol* 133:415–420
- Ayati A et al (2015) Phosphotungstic acid (PTA) in the synthesis of 3D CdS superstructures by diffusion assisted hydrothermal method. *Adv Powder Technol* 26:1495–1503
- Ayodeji AA et al (2018) Data on CaO and eggshell catalysts used for biodiesel production. *Data Brief*. <https://doi.org/10.1016/j.dib.2018.06.028>
- Azzam EMS et al (2019) Enhancement the photocatalytic degradation of methylene blue dye using fabricated CNTs/TiO<sub>2</sub>/AgNPs/



- Surfactant nanocomposites. *J Water Process Eng* 28:345. <https://doi.org/10.1016/j.jwpe.2019.02.016>
- Babuponnusami A, Muthukumar K (2014) A review on Fenton and improvements to the Fenton process for wastewater treatment. *J Environ Chem Eng*. <https://doi.org/10.1016/j.jece.2013.10.011>
- Bae W et al (2015) Characterization of refractory matters in dyeing wastewater during a full-scale Fenton process following pure-oxygen activated sludge treatment. *J Hazard Mater* 287:421–428. <https://doi.org/10.1016/j.jhazmat.2015.01.052>
- Baeza A et al (2016) Magnetite and metal-impregnated magnetite catalysts in organic synthesis: a very old concept with new promising perspectives. *ChemCatChem* 8:49–67. <https://doi.org/10.1002/cctc.201500854>
- Bahadori E et al (2019) Semi-batch photocatalytic reduction of nitrates: role of process conditions and Co-catalysts. *ChemCatChem* 11:4642–4652. <https://doi.org/10.1002/cctc.201900890>
- Bai P et al (2005) Facile synthesis of thermally stable mesoporous crystalline alumina by using a novel cation–anion double hydrolysis method. *Mater Lett* 59:3128–3131. <https://doi.org/10.1016/j.matlet.2005.05.033>
- Bai P et al (2009) Cation–anion double hydrolysis derived mesoporous  $\gamma$ - $\text{Al}_2\text{O}_3$  as an environmentally friendly and efficient aldol reaction catalyst. *J Mater Chem* 19:1554–1563. <https://doi.org/10.1039/B819993K>
- Baig RBN, Varma RS (2012) Alternative energy input: mechanochemical, microwave and ultrasound-assisted organic synthesis. *Chem Soc Rev* 41:1559–1584. <https://doi.org/10.1039/C1CS15204A>
- Baptista SL et al (2021) Galactose to tagatose isomerization by the l-arabinose isomerase from *Bacillus subtilis*: a biorefinery approach for *Gelidium sesquipedale* valorisation. *LWT* 151:112199. <https://doi.org/10.1016/j.lwt.2021.112199>
- Basahel SN et al (2015) Influence of crystal structure of nanosized  $\text{ZrO}_2$  on photocatalytic degradation of methyl orange. *Nanoscale Res Lett* 10:1–13
- Basaveni S et al (2019) Ni nanoparticles on polyaromatic hyperbranched polymer support as a mild, tunable, and sustainable catalyst for catalytic transfer hydrogenation. *J Nanopart Res* 21:1–14
- Baskar G et al (2017) Optimization and kinetics of biodiesel production from Mahua oil using manganese doped zinc oxide nanocatalyst. *Renew Energy* 103:641–646. <https://doi.org/10.1016/j.renene.2016.10.077>
- Bayramoglu G et al (2018) Cyclic-carbonate functionalized polymer brushes on polymeric microspheres: Immobilized laccase for degradation of endocrine disturbing compounds. *J Ind Eng Chem* 60:407–417. <https://doi.org/10.1016/j.jiec.2017.11.028>
- Bayu A et al (2018) An effective heterogeneous catalyst of [BMIM]3PMo12O40 for selective sugar epimerization. *ChemPlusChem* 83(5):383–389. <https://doi.org/10.1002/cplu.20180154>
- Bayu A et al (2019) Reaction pathways and selectivity in chemo-catalytic conversion of biomass-derived carbohydrates to high-value chemicals: a review. *Fuel Process Technol* 196:106162. <https://doi.org/10.1016/j.fuproc.2019.106162>
- Belhouchet N et al (2019) Photocatalytic degradation of tetracycline antibiotic using new calcite/titania nanocomposites. *J Photochem Photobiol A Chem*. <https://doi.org/10.1016/j.jphotochem.2018.12.016>
- Bell EL et al (2021) Biocatalysis. *Nat Rev Methods Primers* 1:1–46. <https://doi.org/10.1038/s43586-021-00044-z>
- Bendi R, Imae T (2013) Renewable catalyst with Cu nanoparticles embedded into cellulose nano-fiber film. *RSC Adv* 3:16279–16282
- Benhiti R et al (2020) Synthesis, characterization, and comparative study of MgAl-LDHs prepared by standard coprecipitation and urea hydrolysis methods for phosphate removal. *Environ Sci Pollut Res* 27:45767–45774. <https://doi.org/10.1007/s11356-020-10444-5>
- Beni FA et al (2020) UV-Switchable phosphotungstic acid sandwiched between ZIF-8 and Au nanoparticles to improve simultaneous adsorption and UV light photocatalysis toward Tetracycline degradation. *Micropor Mesopor Mater* 303:110275
- Bertram B, et al (2009) Purification of biodiesel with adsorbent materials. US Patent 7,635,398. 2
- Besharati Vineh M et al (2018) Stability and activity improvement of horseradish peroxidase by covalent immobilization on functionalized reduced graphene oxide and biodegradation of high phenol concentration. *Int J Biol Macromol* 106:1314–1322. <https://doi.org/10.1016/j.ijbiomac.2017.08.133>
- Bhadra S et al (2008) One-pot copper nanoparticle-catalyzed synthesis of S-aryl- and S-vinyl dithiocarbamates in water: high diastereoselectivity achieved for vinyl dithiocarbamates. *Green Chem* 10:1224–1230
- Bhatia SK et al (2020) Recent developments in pretreatment technologies on lignocellulosic biomass: EFFECT of key parameters, technological improvements, and challenges. *Bioresour Technol* 300:122724. <https://doi.org/10.1016/j.biortech.2019.122724>
- Bi W et al (2019) In-situ synthesized surface N-doped Pt/TiO<sub>2</sub> via flame spray pyrolysis with enhanced thermal stability for CO catalytic oxidation. *Appl Surf Sci* 481:360–368. <https://doi.org/10.1016/j.apsusc.2019.03.129>
- Bielecki M et al (2020) Demographics and the natural interest rate in the euro area. *Eur Econ Rev* 129:103535. <https://doi.org/10.1016/j.eurocorev.2020.103535>
- Bilal M et al (2016) Horseradish peroxidase-assisted approach to decolorize and detoxify dye pollutants in a packed bed bioreactor. *J Environ Manag* 183:836–842. <https://doi.org/10.1016/j.jenvman.2016.09.040>
- Bilal M et al (2017a) Bio-based degradation of emerging endocrine-disrupting and dye-based pollutants using cross-linked enzyme aggregates. *Environ Sci Pollut Res* 24:7035–7041. <https://doi.org/10.1007/s11356-017-8369-y>
- Bilal M et al (2017b) Bio-catalytic performance and dye-based industrial pollutants degradation potential of agarose-immobilized MnP using a packed bed reactor system. *Int J Biol Macromol* 102:582–590. <https://doi.org/10.1016/j.ijbiomac.2017.04.065>
- Bilal M et al (2017c) Immobilized ligninolytic enzymes: An innovative and environmental responsive technology to tackle dye-based industrial pollutants—a review. *Sci Total Environ* 576:646–659. <https://doi.org/10.1016/j.scitotenv.2016.10.137>
- Bilal M et al (2017d) Enhanced bio-catalytic performance and dye degradation potential of chitosan-encapsulated horseradish peroxidase in a packed bed reactor system. *Sci Total Environ* 575:1352–1360. <https://doi.org/10.1016/j.scitotenv.2016.09.215>
- Bilal M et al (2018) State-of-the-art protein engineering approaches using biological macromolecules: a review from immobilization to implementation view point. *Int J Biol Macromol* 108:893–901. <https://doi.org/10.1016/j.ijbiomac.2017.10.182>
- Bilal M et al (2019) Immobilization of fungal laccase on glutaraldehyde cross-linked chitosan beads and its bio-catalytic potential to degrade bisphenol A. *Biocatal Agric Biotechnol* 19:101174. <https://doi.org/10.1016/j.bcab.2019.101174>
- Bilal M et al (2019) Multifunctional metal–organic frameworks-based biocatalytic platforms: recent developments and future prospects. *J Market Res* 8:2359–2371
- Bohlouli A, Mahdavian L (2021) Catalysts used in biodiesel production: a review. *Biofuels* 12(8):885–898. <https://doi.org/10.1080/17597269.2018.1558836>
- Bokare AD, Choi W (2014) Review of iron-free Fenton-like systems for activating H<sub>2</sub>O<sub>2</sub> in advanced oxidation processes. *J Hazard Mater* 275:345. <https://doi.org/10.1016/j.jhazmat.2014.04.054>

- Bolobajev J et al (2014) Reuse of ferric sludge as an iron source for the Fenton-based process in wastewater treatment. *Chem Eng J* 255:8–13. <https://doi.org/10.1016/j.cej.2014.06.018>
- Boningari T et al (2018a) Novel one-step synthesis of nitrogen-doped TiO<sub>2</sub> by flame aerosol technique for visible-light photocatalysis: effect of synthesis parameters and secondary nitrogen (N) source. *Chem Eng J* 350:324–334. <https://doi.org/10.1016/j.cej.2018.05.122>
- Boningari T et al (2018b) Novel one-step synthesis of sulfur doped-TiO<sub>2</sub> by flame spray pyrolysis for visible light photocatalytic degradation of acetaldehyde. *Chem Eng J* 339:249–258. <https://doi.org/10.1016/j.cej.2018.01.063>
- Borah R et al (2017) Banana pulp extract mediated synthesis of Cu<sub>2</sub>O nanoparticles: an efficient heterogeneous catalyst for the ipso-hydroxylation of arylboronic acids. *Tetrahedron Lett* 58:1211–1215
- Bordbar M et al (2018) Melissa *Officinalis* L. leaf extract assisted green synthesis of CuO/ZnO nanocomposite for the reduction of 4-nitrophenol and Rhodamine B. *Sep Purif Technol* 191:295–300
- Borlaf M et al (2012) Synthesis and characterization of TiO<sub>2</sub>/Rh<sup>3+</sup> nanoparticulate sols, xerogels and cryogels for photocatalytic applications. *J Sol-Gel Sci Technol* 63:408–415. <https://doi.org/10.1007/s10971-012-2802-y>
- Boucherit N et al (2013) Degradation of direct azo dye by *Cucurbita pepo* free and immobilized peroxidase. *J Environ Sci* 25:1235–1244. [https://doi.org/10.1016/S1001-0742\(12\)60102-8](https://doi.org/10.1016/S1001-0742(12)60102-8)
- Boudjemaa A (2020) History, progress, and development of electrocatalysis. In: *Methods for electrocatalysis*, pp 401–424
- Boyjoo Y et al (2021) Engineering nanoreactors for metal–chalcogen batteries. *Energy Environ Sci* 14:540–575. <https://doi.org/10.1039/D0EE03316B>
- Bresolin B-M et al (2020) Recent progresses on metal halide perovskite-based material as potential photocatalyst. *Catalysts* 10:709
- Brink A et al (2017) The Fenton oxidation of biologically treated paper and pulp mill effluents: a performance and kinetic study. *Process Saf Environ Protect.* <https://doi.org/10.1016/j.psep.2017.02.011>
- Byrne C et al (2018) Recent advances in photocatalysis for environmental applications. *J Environ Chem Eng* 6:3531–3555
- Cai J et al (2017) Review of physicochemical properties and analytical characterization of lignocellulosic biomass. *Renew Sustain Energy Rev* 76:309–322. <https://doi.org/10.1016/j.rser.2017.03.072>
- Cammarota M, Freire D (2006) A review on hydrolytic enzymes in the treatment of wastewater with high oil and grease content. *Biores Technol* 97:2195–2210
- Campagnoli E et al (2005) Effect of preparation method on activity and stability of LaMnO<sub>3</sub> and LaCoO<sub>3</sub> catalysts for the flameless combustion of methane. *Appl Catal B: Environ* 55:133–139. <https://doi.org/10.1016/j.apcatb.2004.07.010>
- Campelo JM et al (2009) Sustainable preparation of supported metal nanoparticles and their applications in catalysis. *ChemSusChem Chem Sustainab Energy Mater* 2:18–45
- Cao S et al (2015) Polymeric photocatalysts based on graphitic carbon nitride. *Adv Mater* 27:2150–2176
- Cao L et al (2019) Efficient photocatalytic degradation of herbicide glyphosate in water by magnetically separable and recyclable BiOBr/Fe<sub>3</sub>O<sub>4</sub> nanocomposites under visible light irradiation. *Chem Eng J* 368:212–222. <https://doi.org/10.1016/j.cej.2019.02.100>
- Carlesi Jara C et al (2007) Electrochemical removal of antibiotics from wastewaters. *Appl Catal B* 70:479–487. <https://doi.org/10.1016/j.apcatb.2005.11.035>
- Carneiro MLNM, Gomes MSP (2019) Energy, exergy, environmental and economic analysis of hybrid waste-to-energy plants. *Energy Convers Manag.* <https://doi.org/10.1016/j.enconman.2018.10.007>
- Cavaleiro A et al (2013) Biochemical methane potential of raw and pre-treated meat-processing wastes. *Biores Technol* 129:519–525
- Cha BJ et al (2019) Hydrophilic surface modification of TiO<sub>2</sub> to produce a highly sustainable photocatalyst for outdoor air purification. *Appl Surf Sci* 479:31–38
- Chagas PMB et al (2019) Use of an environmental pollutant from hexavalent chromium removal as a green catalyst in the Fenton process. *Sci Rep* 9:1–15
- Chandra R, Nath M (2017) Multi-core–shell TiO<sub>2</sub>NPs@ ZIF-8 composite for enhanced photocatalytic degradation and adsorption of methylene blue and rhodamine-B. *Chem Select* 2:7711–7722
- Chandra R et al (2019) Multi-core-shell composite SnO<sub>2</sub>NPs@ ZIF-8: potential antiviral agent and effective photocatalyst for wastewater treatment. *Environ Sci Pollut Res* 26:23346–23358
- Chang K et al (2014) MoS<sub>2</sub>/graphene cocatalyst for efficient photocatalytic H<sub>2</sub> evolution under visible light irradiation. *ACS Nano* 8:7078–7087
- Chen G (2004) Electrochemical technologies in wastewater treatment. *Sep Purif Technol* 38:11–41
- Chen J et al (2015) Electrochemical degradation of chloramphenicol with a novel Al doped PbO<sub>2</sub> electrode: Performance, kinetics and degradation mechanism. *Electrochim Acta* 165:277–287. <https://doi.org/10.1016/j.electacta.2015.02.029>
- Chen F et al (2016) Characteristics and catalytic properties of Ni/CaA-IO<sub>x</sub> catalyst for hydrogen-enriched syngas production from pyrolysis-steam reforming of biomass sawdust. *Appl Catal B Environ* 183:168–175. <https://doi.org/10.1016/j.apcatb.2015.10.028>
- Chen J et al (2017a) Greening the processes of metal–organic framework synthesis and their use in sustainable catalysis. *ChemSuschem* 10:3165–3187
- Chen J et al (2017b) Hydrolysis driving redox reaction to synthesize Mn–Fe binary oxides as highly active catalysts for the removal of toluene. *Chem Eng J* 330:281–293. <https://doi.org/10.1016/j.cej.2017.07.147>
- Chen L et al (2017c) Controllable design of tunable nanostructures inside metal–organic frameworks. *Chem Soc Rev* 46:4614–4630
- Chen X et al (2018) Catalytic fast pyrolysis of cellulose to produce furan compounds with SAPO type catalysts. *J Analyt Appl Pyrolysis* 129:53–60. <https://doi.org/10.1016/j.jaap.2017.12.004>
- Chen D et al (2019a) Mechanochemical synthesis of metal–organic frameworks. *Polyhedron* 162:59–64. <https://doi.org/10.1016/j.poly.2019.01.024>
- Chen X et al (2019b) Flame spray pyrolysis synthesized CuO–TiO<sub>2</sub> nanoparticles for catalytic combustion of lean CO. *Proc Combust Inst* 37:5499–5506. <https://doi.org/10.1016/j.proci.2018.05.102>
- Cheng C, Chang K-C (2013) Development of immobilized cellulase through functionalized gold nano-particles for glucose production by continuous hydrolysis of waste bamboo chopsticks. *Enzyme Microb Technol* 53:444–451. <https://doi.org/10.1016/j.enzmictec.2013.09.010>
- Cheng H et al (2018a) Cross-linked enzyme-polymer conjugates with excellent stability and detergent-enhanced activity for efficient organophosphate degradation. *Bioresour Bioprocess* 5:49. <https://doi.org/10.1186/s40643-018-0236-2>
- Cheng L et al (2018b) CdS-based photocatalysts. *Energy Environ Sci* 11:1362–1391
- Cheng D et al (2020) A critical review on antibiotics and hormones in swine wastewater: water pollution problems and control approaches. *J Hazard Mater* 387:121682. <https://doi.org/10.1016/j.jhazmat.2019.12.1682>
- Chetri P et al (2014) Structural, optical and photocatalytic properties of TiO<sub>2</sub>/SnO<sub>2</sub> and SnO<sub>2</sub>/TiO<sub>2</sub> core–shell nanocomposites: an experimental and DFT investigation. *Chem Phys* 434:1–10. <https://doi.org/10.1016/j.chemphys.2014.02.007>
- Chiarello GL et al (2018) In situ attenuated total reflection infrared spectroscopy study of the photocatalytic steam reforming of

- methanol on Pt/TiO<sub>2</sub>. *App Surf Sci* 450:146–154. <https://doi.org/10.1016/j.apsusc.2018.04.167>
- Cho M et al (2018) Skipping oxidative thermal stabilization for lignin-based carbon nanofibers. *ACS Sustain Chem Eng* 6(5):6434–6444. <https://doi.org/10.1021/acssuschemeng.8b00209>
- Chu S et al (2017) The path towards sustainable energy. *Nat Mater* 16:16–22
- Chuetor S et al (2021) Evaluation of rice straw biopowder from alkaline-mechanical pretreatment by hydro-textural approach. *Bioresour Technol* 32:3. <https://doi.org/10.1016/j.biortech.2020.124619>
- Ciriminna R et al (2011) From molecules to systems: sol–gel microencapsulation in silica-based materials. *Chem Rev* 111:765–789. <https://doi.org/10.1021/cr100161x>
- Clark JH et al (2016) Circular economy design considerations for research and process development in the chemical sciences. *Green Chem* 18:3914–3934. <https://doi.org/10.1039/C6GC00501B>
- Cliffe MJ et al (2012) Accelerated aging: a low energy, solvent-free alternative to solvothermal and mechanochemical synthesis of metal–organic materials. *Chem Sci* 3:2495–2500
- Comminellis C (1994) Electrocatalysis in the electrochemical conversion/combustion of organic pollutants for waste water treatment. *Electrochim Acta* 39:1857–1862. [https://doi.org/10.1016/0013-4686\(94\)85175-1](https://doi.org/10.1016/0013-4686(94)85175-1)
- Cui H et al (2020) Application progress of enhanced coagulation in water treatment. *RSC Adv* 10(34):20231–20244. <https://doi.org/10.1039/d0ra02979c>
- Daiyan R et al (2019) Modulating activity through defect engineering of tin oxides for electrochemical CO<sub>2</sub> reduction. *Adv Sci* 6:1900678. <https://doi.org/10.1002/advs.201900678>
- Daiyan R et al (2020) Uncovering atomic-scale stability and reactivity in engineered zinc oxide electrocatalysts for controllable syngas production. *Adv Energy Mater* 10:2001381. <https://doi.org/10.1002/aenm.202001381>
- Dan M et al (2015) From wood wastes to hydrogen - Preparation and catalytic steam reforming of crude bio-ethanol obtained from fir wood. *Renew Energy* 74:27–36. <https://doi.org/10.1016/j.renene.2014.07.050>
- de Amorim KP et al (2013) Electrochemical degradation of sulfamethoxazole and trimethoprim at boron-doped diamond electrode: performance, kinetics and reaction pathway. *Sep Purif Technol* 120:319–327. <https://doi.org/10.1016/j.seppur.2013.10.010>
- De Wolf S et al (2012) High-efficiency silicon heterojunction solar cells: a review. *Green* 2:7–24
- Debecker DP (2018) Innovative sol-gel routes for the bottom-up preparation of heterogeneous catalysts. *Chem Record* 18:662–675. <https://doi.org/10.1002/tcr.201700068>
- Debecker DP, Mutin PH (2012) Non-hydrolytic sol–gel routes to heterogeneous catalysts. *Chem Soc Rev* 41:3624–3650. <https://doi.org/10.1039/C2CS15330K>
- Debecker DP et al (2013) Mesoporous mixed oxide catalysts via non-hydrolytic sol–gel: a review. *Appl Catal A Gen* 451:192–206. <https://doi.org/10.1016/j.apcata.2012.11.002>
- Delidovich I, Palkovits R (2016) Catalytic isomerization of biomass-derived aldoses: a review. *Chemsuschem* 9(6):547–561. <https://doi.org/10.1002/cssc.201501577>
- Devi TB et al (2019) Biomass derived activated carbon loaded silver nanoparticles: an effective nanocomposites for enhanced solar photocatalysis and antimicrobial activities. *J Ind Eng Chem* 76:160–172. <https://doi.org/10.1016/j.jiec.2019.03.032>
- Dhakshinamoorthy A, Garcia H (2014) Metal–organic frameworks as solid catalysts for the synthesis of nitrogen-containing heterocycles. *Chem Soc Rev* 43:5750–5765
- Dhamodaran G et al (2017) A comparative study of combustion, emission, and performance characteristics of rice-bran-, neem-, and cottonseed-oil biodiesels with varying degree of unsaturation. *Fuel* 187:296–305. <https://doi.org/10.1016/j.fuel.2016.09.062>
- Din MI et al (2018) Single step green synthesis of stable nickel and nickel oxide nanoparticles from *Calotropis gigantea*: catalytic and antimicrobial potentials. *Environ Nanotechnol Monitor Manag* 9:29–36
- Ding D et al (2020) Nitrogen-doping positively whilst sulfur-doping negatively affect the catalytic activity of biochar for the degradation of organic contaminant. *Appl Catal B Environ* 263:118348. <https://doi.org/10.1016/j.apcatb.2019.118348>
- Do J-L, Friščić T (2017) Mechanochemistry: a force of synthesis. *ACS Cent Sci* 3:13–19
- Do QC et al (2022) Facile one-pot synthesis of Ni-based catalysts by cation-anion double hydrolysis method as highly active Ru-free catalysts for green H<sub>2</sub> production via NH<sub>3</sub> decomposition. *Appl Catal B Environ* 307:121167. <https://doi.org/10.1016/j.apcatb.2022.121167>
- Dong T et al (2019) Hierarchical nickel-cobalt phosphide hollow spheres embedded in P-doped reduced graphene oxide towards superior electrochemistry activity *Carbon* 149:222–233. <https://doi.org/10.1016/j.carbon.2019.04.050>
- Dong Q et al (2022) In situ fabrication of niobium pentoxide/graphitic carbon nitride type-II heterojunctions for enhanced photocatalytic hydrogen evolution reaction. *J Colloid Interf Sci* 608:1951–1959. <https://doi.org/10.1016/j.jcis.2021.10.161>
- Du C et al (2017) Nest-like NiCoP for highly efficient overall water splitting. *ACS Catal* 7(6):4131–4137. <https://doi.org/10.1021/acscatal.7b00662>
- Du L et al (2018) Transesterification of castor oil to biodiesel using NaY zeolite-supported La<sub>2</sub>O<sub>3</sub> catalysts. *Energy Convers Manag* 173:728–734. <https://doi.org/10.1016/j.enconman.2018.07.053>
- Duan D et al (2021) Activated carbon from lignocellulosic biomass as catalyst: a review of the applications in fast pyrolysis process. *J Analyt Appl Pyrolys* 158:105246. <https://doi.org/10.1016/j.jaap.2021.105246>
- Dutta V et al (2021) An overview on WO<sub>3</sub> based photocatalyst for environmental remediation. *J Environ Chem Eng* 9:105018
- Elbanna O et al (2016) Facile preparation of nitrogen and fluorine codoped TiO<sub>2</sub> mesocrystal with visible light photocatalytic activity. *Appl Catal B* 192:80–87
- Elgarahy AM et al (2021a) A critical review of biosorption of dyes, heavy metals and metalloids from wastewater as an efficient and green process. *Clean Eng Technol* 4:100209. <https://doi.org/10.1016/j.clet.2021.100209>
- Elgarahy AM et al (2021b) Thermochemical conversion strategies of biomass to biofuels, techno-economic and bibliometric analysis: a conceptual review. *J Environ Chem Eng* 9:106503. <https://doi.org/10.1016/j.jece.2021.106503>
- Eljack F, Kazi M-K (2021) Prospects and challenges of green hydrogen economy via multi-sector global symbiosis in qatar. *Front Sustain* 1:612762. <https://doi.org/10.3389/frsus.2020.612762>
- El-Nahas S et al (2020) Facile and affordable synthetic route of nano powder zeolite and its application in fast softening of water hardness. *J Water Process Eng* 33:101104. <https://doi.org/10.1016/j.jwpe.2019.101104>
- Esposito S (2019) “Traditional” sol-gel chemistry as a powerful tool for the preparation of supported metal and metal oxide catalysts. *Mater* 12:668
- Espro C, Rodríguez-Padrón D (2021) Re-thinking organic synthesis: mechanochemistry as a greener approach. *Curr Opin Green Sustain Chem* 30:100478. <https://doi.org/10.1016/j.cogsc.2021.100478>
- Etim AO et al (2018) Potential of ripe plantain fruit peels as an eco-friendly catalyst for biodiesel synthesis: optimization by artificial

- neural network integrated with genetic algorithm. Sustainability (switzerland) 10(3):707. <https://doi.org/10.3390/su10030707>
- Fadhil AB et al (2016) Potassium acetate supported on activated carbon for transesterification of new non-edible oil, bitter almond oil. Fuel 170:130–140. <https://doi.org/10.1016/j.fuel.2015.12.027>
- Falk G et al (2017) Microwave-assisted synthesis of Nb<sub>2</sub>O<sub>5</sub> for photocatalytic application of nanopowders and thin films. J Mater Res 32:3271–3278. <https://doi.org/10.1557/jmr.2017.93>
- Falk GS et al (2018) Microwave-assisted synthesis of TiO<sub>2</sub> nanoparticles: photocatalytic activity of powders and thin films. J Nanopart Res 20:1–10
- Farghali M et al (2022) Integration of biogas systems into a carbon zero and hydrogen economy: a review. Environ Chem Lett 20:2853–2927. <https://doi.org/10.1007/s10311-022-01468-z>
- Fawzy S et al (2021) Industrial biochar systems for atmospheric carbon removal: a review. Environ Chem Lett 19:3023–3055. <https://doi.org/10.1007/s10311-021-01210-1>
- Fayyazi E et al (2018) Optimization of biodiesel production over chicken eggshell-derived CaO catalyst in a continuous centrifugal contactor separator. Ind Eng Chem Res 57(38):12742–12755. <https://doi.org/10.1021/acs.iecr.8b02678>
- Feng D et al (2012) Zirconium-metalloporphyrin PCN-222: mesoporous metal-organic frameworks with ultrahigh stability as biomimetic catalysts. Angew Chem Int Ed 51:10307–10310
- Feng D et al (2013) Construction of ultrastable porphyrin Zr metal-organic frameworks through linker elimination. J Am Chem Soc 135:17105–17110
- Feng S et al (2021) Roles and applications of enzymes for resistant pollutants removal in wastewater treatment. Bioresour Technol 335:125278. <https://doi.org/10.1016/j.biortech.2021.125278>
- Feyzi M, Khajavi G (2014) Investigation of biodiesel production using modified strontium nanocatalysts supported on the ZSM-5 zeolite. Ind Crops Prod 58:298–304. <https://doi.org/10.1016/j.indcrop.2014.04.014>
- Field CB et al (1998) Primary production of the biosphere: integrating terrestrial and oceanic components. Science 281:237–240. <https://doi.org/10.1126/science.281.5374.237>
- Fu X et al (2013) Ball milled h-BN: an efficient holes transfer promoter to enhance the photocatalytic performance of TiO<sub>2</sub>. J Hazard Mater 244–245:102–110. <https://doi.org/10.1016/j.jhazmat.2012.11.033>
- Fujishima A, Honda K (1972) Photolysis-decomposition of water at the surface of an irradiated semiconductor. Nature 238:37–38
- Fujiwara K, Pratsinis SE (2018) Single Pd atoms on TiO<sub>2</sub> dominate photocatalytic NO<sub>x</sub> removal. Appl Catal B Environ 226:127–134. <https://doi.org/10.1016/j.apcatb.2017.12.042>
- Gai X et al (2022) Preparation of Ni-Co/SiO<sub>2</sub> catalyst by ammonia reflux impregnation and its CH<sub>4</sub>-CO<sub>2</sub> reforming reaction performance. Fuel 316:123337. <https://doi.org/10.1016/j.fuel.2022.123337>
- Gao B et al (2011) Adsorption-photocatalytic degradation of acid red 88 by supported TiO<sub>2</sub>: effect of activated carbon support and aqueous anions. Chem Eng J 171:1098–1107. <https://doi.org/10.1016/j.cej.2011.05.006>
- Gao F et al (2019) Enhancing the catalytic performance of chloroperoxidase by co-immobilization with glucose oxidase on magnetic graphene oxide. Biochem Eng J 143:101–109. <https://doi.org/10.1016/j.bej.2018.12.013>
- Garcia-Segura S et al (2016) Fluidized-bed fenton process as alternative wastewater treatment technology—a review. J Taiwan Inst Chem Engineers. 67:345. <https://doi.org/10.1016/j.jtice.2016.07.021>
- Gawande MB et al (2014) Microwave-assisted chemistry: synthetic applications for rapid assembly of nanomaterials and organics. Acc Chem Res 47:1338–1348. <https://doi.org/10.1021/ar400309b>
- Geng A et al (2020) Using wood flour waste to produce biochar as the support to enhance the visible-light photocatalytic performance of BiOBr for organic and inorganic contaminants removal. Chemosphere 250:126291. <https://doi.org/10.1016/j.chemosphere.2020.126291>
- Geus JW, Van Dillen AJ (2008) Preparation of supported catalysts by deposition-precipitation. Prep Solid Catal 460:487. <https://doi.org/10.1002/9783527619528.ch4f>
- Gholami P et al (2020) Photocatalytic degradation of gemifloxacin antibiotic using Zn-Co-LDH@biochar nanocomposite. J Hazard Mater 382:121070. <https://doi.org/10.1016/j.jhazmat.2019.12.1070>
- Ghorbani-Choghamarani A et al (2021) Facile synthesis of Fe<sub>3</sub>O<sub>4</sub>@GlcA@Ni-MOF composites as environmentally green catalyst in organic reactions. Environ Technol Innov 24:102050
- Ghosh BK et al (2015) Preparation of Cu nanoparticle loaded SBA-15 and their excellent catalytic activity in reduction of variety of dyes. Powder Technol 269:371–378
- Gil J et al (1999) Biomass gasification with air in a fluidized bed: effect of the in-bed use of dolomite under different operation conditions. Ind Eng Chem Res 38:4226–4235. <https://doi.org/10.1021/ie980802r>
- Głowniak S et al (2021) Mechanochemistry: toward green synthesis of metal-organic frameworks. Mater Today 46:109–124. <https://doi.org/10.1016/j.mattod.2021.01.008>
- Gong Q et al (2019) Core-shell structured Fe<sub>3</sub>O<sub>4</sub>@GO@MIL-100 (Fe) magnetic nanoparticles as heterogeneous photo-Fenton catalyst for 2, 4-dichlorophenol degradation under visible light. J Hazard Mater 371:677–686
- Gopinath CS, Nalajala N (2021) A scalable and thin film approach for solar hydrogen generation: a review on enhanced photocatalytic water splitting. J Mater Chem A 9:1353–1371
- Guesh K et al (2017) Sustainable preparation of MIL-100 (Fe) and its photocatalytic behavior in the degradation of methyl orange in water. Cryst Growth Des 17:1806–1813
- Güneş E et al (2019) Characterization and treatment alternatives of industrial container and drum cleaning wastewater: comparison of Fenton-like process and combined coagulation/oxidation processes. Sep Purif Technol 209:426–433. <https://doi.org/10.1016/j.seppur.2018.07.060>
- Guo Y et al (2018) Treatment of real benzene dye intermediates wastewater by the Fenton method: characteristics and multi-response optimization. RSC Adv 8(1):80–90. <https://doi.org/10.1039/c7ra09404c>
- Hachemi L et al (2017) Lipolytic bacteria use as bio-decontaminating natural in the water purification stations. Int J Biol Macromol 105:873–878
- Hafdi H et al (2021) Nickel sulfide impregnated on natural phosphate: characterization and applications in photocatalytic degradation of indigocarmine dye. Opt Quant Electron 53:183. <https://doi.org/10.1007/s11082-021-02811-4>
- Hajipour AR, Malek SS (2021) Magnetic chitosan-functionalized cobalt-NHC: synthesis, characterization and catalytic activity toward Suzuki and Sonogashira cross-coupling reactions of aryl chlorides. Mol Catal 508:111573
- Hammoud D et al (2015) Steam reforming of methanol over x% Cu/Zn-Al 400 500 based catalysts for production of hydrogen: preparation by adopting memory effect of hydrotalcite and behavior evaluation. Int J Hydrog Energy. <https://doi.org/10.1016/j.ijhydene.2014.09.080>
- Han L et al (2020) Stable and efficient single-atom Zn catalyst for CO<sub>2</sub> reduction to CH<sub>4</sub>. J Am Chem Soc 142:12563–12567. <https://doi.org/10.1021/jacs.9b12111>
- He F, Zhao D (2008) Hydrodechlorination of trichloroethene using stabilized Fe-Pd nanoparticles: reaction mechanism and effects

- of stabilizers, catalysts and reaction conditions. *Appl Catal B* 84:533–540
- He H et al (2020a) Use mechanochemical activation to enhance interfacial contaminant removal: A review of recent developments and mainstream techniques. *Chemosphere* 243:125339. <https://doi.org/10.1016/j.chemosphere.2019.125339>
- He M et al (2020b) Low-Cost Ni<sub>2</sub>P/Ni<sub>0.96</sub>S heterostructured bifunctional electrocatalyst toward highly efficient overall urea-water electrolysis. *ACS Appl Mater Interfaces* 12:456. <https://doi.org/10.1021/acsami.9b14350>
- Herranz S et al (2018) Multiplex environmental pollutant analysis using an array biosensor coated with chimeric hapten-dextran-lipase constructs. *Sens Actuat B Chem* 257:256–262. <https://doi.org/10.1016/j.snb.2017.10.134>
- Hitam CN, Jalil A (2020) A review on exploration of Fe<sub>2</sub>O<sub>3</sub> photocatalyst towards degradation of dyes and organic contaminants. *J Environ Manag* 258:110050
- Hoag GE et al (2009) Degradation of bromothymol blue by 'greener' nano-scale zero-valent iron synthesized using tea polyphenols. *J Mater Chem* 19:8671–8677
- Hojamberdiev M et al (2020) SnO<sub>2</sub>@ ZnS photocatalyst with enhanced photocatalytic activity for the degradation of selected pharmaceuticals and personal care products in model wastewater. *J Alloy Compd* 827:154339
- Hosseini SE, Wahid MA (2016) Hydrogen production from renewable and sustainable energy resources: Promising green energy carrier for clean development. *Renew Sustain Energy Rev* 57:850–866
- Hu X et al (2016) Hierarchical manganese dioxide/poly(3,4-ethylenedioxythiophene) core-shell nanoflakes on ramie-derived carbon fiber for high-performance flexible all-solid-state supercapacitor. *ACS Sustain Chem Eng* 4:1201–1211. <https://doi.org/10.1021/acssuschemeng.5b01263>
- Hu Y-H et al (2018) TiO<sub>2</sub>@ UiO-68-CIL: a metal-organic-framework-based bifunctional composite catalyst for a one-pot sequential asymmetric Morita-Baylis-Hillman reaction. *Inorg Chem* 58:4722–4730
- Hu K et al (2019) Boosting electrochemical water splitting: via ternary NiMoCo hybrid nanowire arrays. *J Mater Chem A* 7(5):2156–2164. <https://doi.org/10.1039/c8ta11250a>
- Hu S et al (2020) Novel MOF-derived nickel nitride as high-performance bifunctional electrocatalysts for hydrogen evolution and urea oxidation. *ACS Sustain Chem Eng* 8(19):7414–7422. <https://doi.org/10.1021/acssuschemeng.0c01450>
- Huang YB, Fu Y (2013) Hydrolysis of cellulose to glucose by solid acid catalysts. *Green Chem*. <https://doi.org/10.1039/c3gc40136g>
- Huang G et al (2016) Polydimethylsiloxane coating for a palladium/MOF composite: highly improved catalytic performance by surface hydrophobization. *Angew Chem* 128:7505–7509
- Huang Q et al (2021) Applications and Fundamentals of photocatalysis with solar energy. In: Bashir S (ed) *Advances in sustainable energy*. Springer, Cham, pp 27–66. [https://doi.org/10.1007/978-3-030-74406-9\\_2](https://doi.org/10.1007/978-3-030-74406-9_2)
- Huang Y et al (2022) Rearrangement of  $\alpha$ -terpineol by using PTA/TiO<sub>2</sub> catalyst synthesized by ultrasonic-assisted impregnation method. *Tetrahedron* 108:132659. <https://doi.org/10.1016/j.tet.2022.132659>
- Hüesker F, Lepenies R (2022) Why does pesticide pollution in water persist? *Environ Sci Policy*. <https://doi.org/10.1016/j.envsci.2021.11.016>
- Hussain T et al (2022) Microwave-assisted synthesis of NiTe<sub>2</sub> photocatalyst as a facile and scalable approach for energy-efficient photocatalysis and detoxification of harmful organic dyes. *Sep Pur Technol* 282:120025. <https://doi.org/10.1016/j.seppur.2021.120025>
- Hutchings GJ, Védrine JC (2004) Heterogeneous catalyst preparation. In: Lv X (ed) *Basic principles in applied catalysis*. Springer Series in Chemical Physics. Springer, Berlin, Heidelberg, pp 215–258
- Ibrahim MM et al (2019) Influence of support on physicochemical properties of ZrO<sub>2</sub> based solid acid heterogeneous catalysts for biodiesel production. *Catal Commun* 122:10–15. <https://doi.org/10.1016/j.catcom.2019.01.008>
- Ihsanullah I (2020) MXenes (two-dimensional metal carbides) as emerging nanomaterials for water purification: Progress, challenges and prospects. *Chem Eng J* 388:124340. <https://doi.org/10.1016/j.cej.2020.124340>
- Ilies L et al (2020) *Earth-abundant metals in catalysis*, vol 9. Wiley, New York, pp 324–325
- Ingle AP et al (2017) Comparative evaluation of free and immobilized cellulase for enzymatic hydrolysis of lignocellulosic biomass for sustainable bioethanol production. *Cellulose* 24:5529–5540
- Intarasuwan K et al (2017) Photocatalytic dye degradation by ZnO nanoparticles prepared from X<sub>2</sub>C<sub>2</sub>O<sub>4</sub> (X = H, Na and NH<sub>4</sub>) and the cytotoxicity of the treated dye solutions. *Sep Purif Technol* 177:304–312. <https://doi.org/10.1016/j.seppur.2016.12.040>
- Ishola MM et al (2013) Simultaneous saccharification, filtration and fermentation (SSF): a novel method for bioethanol production from lignocellulosic biomass. *Bioresour Technol* 133:68–73. <https://doi.org/10.1016/j.biortech.2013.01.130>
- Islam MW (2020) A review of dolomite catalyst for biomass gasification tar removal. *Fuel* 267:117095. <https://doi.org/10.1016/j.fuel.2020.117095>
- Islam DA et al (2017) Ag-nanoparticle-anchored rGO-coated MIL-88B (Fe) hybrids as robust electrocatalysts for the highly efficient oxygen evolution reaction at neutral pH. *ChemElectroChem* 4:3110–3118
- Jahangiri H et al (2014) A review of advanced catalyst development for Fischer-Tropsch synthesis of hydrocarbons from biomass derived syn-gas. *Catal Sci Technol* 4:2210–2229. <https://doi.org/10.1039/C4CY00327F>
- Jensen JR et al (2003) A study of Cu/ZnO/Al<sub>2</sub>O<sub>3</sub> methanol catalysts prepared by flame combustion synthesis. *J Catal* 218:67–77. [https://doi.org/10.1016/S0021-9517\(03\)00047-2](https://doi.org/10.1016/S0021-9517(03)00047-2)
- Jiang J et al (2014) Superacidity in sulfated metal-organic framework-808. *J Am Chem Soc* 136:12844–12847
- Jiang N et al (2015) Electrodeposited cobalt-phosphorous-derived films as competent bifunctional catalysts for overall water splitting. *Angew Chem Int Edn* 127(21):6349–6352. <https://doi.org/10.1002/anie.201501616>
- Jiang Y et al (2017) In situ synthesis of core-shell Pt-Cu frame@ metal-organic frameworks as multifunctional catalysts for hydrogenation reaction. *Chem Mater* 29:6336–6345
- Jiang W et al (2020) 3D-printed xylanase within biocompatible polymers as excellent catalyst for lignocellulose degradation. *Chem Eng J* 400:125920. <https://doi.org/10.1016/j.cej.2020.125920>
- Jin R et al (2013) ZIF-8 crystal coatings on a polyimide substrate and their catalytic behaviours for the Knoevenagel reaction. *Dalton Trans* 42:3936–3940
- Jin F et al (2018) Effect of calcium addition on Mg-AlO<sub>x</sub> supported Ni catalysts for hydrogen production from pyrolysis-gasification of biomass. *Catal Today* 309:2–10. <https://doi.org/10.1016/j.cattod.2018.01.004>
- Jin M et al (2019) Solvent-free synthesis of CuO/HKUST-1 composite and its photocatalytic application. *Inorg Chem* 58:8332–8338
- Jing D, Guo L (2006) A novel method for the preparation of a highly stable and active CdS photocatalyst with a special surface nanostructure. *J Phys Chem B* 110:11139–11145
- Jing H-P et al (2014) Photocatalytic degradation of methylene blue in ZIF-8. *RSC Adv* 4:54454–54462
- Jing Y et al (2019) Catalytic production of value-added chemicals and liquid fuels from lignocellulosic biomass. *Green Energy Environ* 5:345. <https://doi.org/10.1016/j.chempr.2019.05.022>

- Julien PA et al (2017) Metal–organic frameworks meet scalable and sustainable synthesis. *Green Chem* 19:2729–2747
- Kadri T et al (2017) Biodegradation of polycyclic aromatic hydrocarbons (PAHs) by fungal enzymes: a review. *J Environ Sci* 51:52–74. <https://doi.org/10.1016/j.jes.2016.08.023>
- Kajihara K (2013) Recent advances in sol–gel synthesis of monolithic silica and silica-based glasses. *J Asia Ceramic Soc* 1:121–133. <https://doi.org/10.1016/j.jascer.2013.04.002>
- Kalaitzidou K et al (2020) Cost evaluation for Se(IV) removal, by applying common drinking water treatment processes: coagulation/precipitation or adsorption. *J Environ Chem Eng* 8(5):104209. <https://doi.org/10.1016/j.jece.2020.104209>
- Kamal T et al (2019) Bacterial cellulose as support for biopolymer stabilized catalytic cobalt nanoparticles. *Int J Biol Macromol* 135:1162–1170
- Kanmani P et al (2015) Utilization of coconut oil mill waste as a substrate for optimized lipase production, oil biodegradation and enzyme purification studies in *Staphylococcus pasteurii*. *Electron J Biotechnol* 18:20–28
- Karayilan M et al (2019) Catalytic metallopolymers from [2Fe–2S] clusters: artificial metalloenzymes for hydrogen production. *Angew Chem* 131:7617–7630
- Karim Z et al (2012) A  $\beta$ -cyclodextrin–chitosan complex as the immobilization matrix for horseradish peroxidase and its application for the removal of azo dyes from textile effluent. *Int Biodeterior Biodegradation* 72:10–17. <https://doi.org/10.1016/j.ibiod.2012.04.008>
- Karthikeyan S et al (2011) Treatment of textile wastewater by homogeneous and heterogeneous Fenton oxidation processes. *Desalination* 281:438–445. <https://doi.org/10.1016/j.desal.2011.08.019>
- Kazemi F et al (2020) Effects of chelating agents on the sol–gel synthesis of nano-zirconia: comparison of the Pechini and sugar-based methods. *Int J Miner Metall Mater* 27:693. <https://doi.org/10.1007/s12613-019-1933-3>
- Khan WU et al (2016) La<sub>2</sub>O<sub>3</sub> supported bimetallic catalysts for the production of hydrogen and carbon nanomaterials from methane. *Int J Hydrog Energy* 41(2):976–983. <https://doi.org/10.1016/j.ijhydene.2015.10.112>
- Khan SA et al (2018) Green synthesis of ZnO and Cu-doped ZnO nanoparticles from leaf extracts of *Abutilon indicum*, *Clerodendrum infortunatum*, *Clerodendrum inerme* and investigation of their biological and photocatalytic activities. *Mater Sci Eng C* 82:46–59
- Khan MA et al (2018) Recent progresses in electrocatalysts for water electrolysis. *Electrochem Energy Rev* 1:483–530. <https://doi.org/10.1007/s41918-018-0014-z>
- Khan I et al (2020) Synthesis of Ni<sup>2+</sup> cation modified TS-1 molecular sieve nanosheets as effective photocatalysts for alcohol oxidation and pollutant degradation. *Chin J Catal* 41:1589–1602. [https://doi.org/10.1016/S1872-2067\(20\)63555-0](https://doi.org/10.1016/S1872-2067(20)63555-0)
- Kho YK et al (2010) Photocatalytic H<sub>2</sub> evolution over TiO<sub>2</sub> nanoparticles. The synergistic effect of anatase and rutile. *J Phys Chem C* 114:2821–2829. <https://doi.org/10.1021/jp910810r>
- Kim SP et al (2016) Photocatalytic activity of SnO<sub>2</sub> nanoparticles in methylene blue degradation. *Mater Res Bull* 74:85–89
- Kim B-J et al (2019) Fe-doping in double perovskite PrBaCo<sub>2</sub>(1–x)Fe<sub>2x</sub>O<sub>6–δ</sub>: Insights into structural and electronic effects to enhance oxygen evolution catalyst stability. *Catal* 9:263
- Kim BG et al (2020) Chelating agent mediated sol-gel synthesis for efficient hole extracted perovskite photovoltaics. *J Phys Chem C* 124:25184–25195. <https://doi.org/10.1021/acs.jpcc.0c05804>
- Kim CH et al (2022) Enhanced activity of a WO<sub>x</sub>-incorporated Pt/Al<sub>2</sub>O<sub>3</sub> catalyst for the dehydrogenation of homocyclic LOHCs: effects of impregnation sequence on Pt–WO<sub>x</sub> interactions. *Fuel* 313:122654. <https://doi.org/10.1016/j.fuel.2021.122654>
- Kırpak E, Akgün M (2018) Biofuel production from olive mill wastewater through its Ni/Al<sub>2</sub>O<sub>3</sub> and Ru/Al<sub>2</sub>O<sub>3</sub> catalyzed supercritical water gasification. *Renew Energy* 124:155–164. <https://doi.org/10.1016/j.renene.2017.06.075>
- Klidi N et al (2019) Electrochemical treatment of paper mill wastewater by electro-Fenton process. *J Electroanal Chem* 841:166–171. <https://doi.org/10.1016/j.jelechem.2019.04.022>
- Klinowski J et al (2011) Microwave-assisted synthesis of metal–organic frameworks. *Dalton Trans* 40:321–330
- Kokel A et al (2017) Application of microwave-assisted heterogeneous catalysis in sustainable synthesis design. *Green Chem* 19:3729–3751. <https://doi.org/10.1039/C7GC01393K>
- Konwar LJ et al (2018) Activated carbon supported CaO from waste shells as a catalyst for biodiesel production. *Energy Sour Part A Recov Utiliz Environ Effects* 40(6):601–607. <https://doi.org/10.1080/15567036.2012.733483>
- Kralchevska R et al (2012) Photocatalytic degradation of the herbicide iodosulfuron by neodymium or nitrogen doped TiO<sub>2</sub>. *Mater Chem Phys*. <https://doi.org/10.1016/j.matchemphys.2012.02.025>
- Kuang Y et al (2013) Heterogeneous Fenton-like oxidation of monochlorobenzene using green synthesis of iron nanoparticles. *J Colloid Interface Sci* 410:67–73
- Kumar D, Ali A (2013) Transesterification of low-quality triglycerides over a Zn/CaO heterogeneous catalyst: kinetics and reusability studies. *Energy Fuels* 27:345. <https://doi.org/10.1021/ef400594t>
- Kumar S, Negi S (2015) Transformation of waste cooking oil into C-18 fatty acids using a novel lipase produced by *Penicillium chrysogenum* through solid state fermentation. *3 Biotech* 5:847–851
- Kumar S et al (2011) Use of evolutionary operation (EVOP) factorial design technique to develop a bioprocess using grease waste as a substrate for lipase production. *Biores Technol* 102:4909–4912
- Kumar A et al (2020a) Microwave chemistry, recent advancements, and eco-friendly microwave-assisted synthesis of nanoarchitectures and their applications: a review. *Mater Today Nano* 11:100076. <https://doi.org/10.1016/j.mtnano.2020.100076>
- Kumar R et al (2020b) Conducting polymers-based photocatalysis for treatment of organic contaminants in water. *Chem Eng J Adv* 4:100047. <https://doi.org/10.1016/j.cej.2020.100047>
- Kumar A et al (2020c) Microbial lipolytic enzymes–promising energy-efficient biocatalysts in bioremediation. *Energy* 192:116674
- Kumar NM et al (2020d) Micro-pollutants in surface water: Impacts on the aquatic environment and treatment technologies. In: *Current developments in biotechnology and bioengineering*. Elsevier, pp 41–62
- Kumari A et al (2017) Biodegradation of waste grease by *Penicillium chrysogenum* for production of fatty acid. *Biores Technol* 226:31–38
- Kunal P, Toops TJ (2020) A review of microwave-assisted synthesis-based approaches to reduce Pd-content in catalysts. *Catal* 10:991
- Kurnia I et al (2017) In-situ catalytic upgrading of bio-oil derived from fast pyrolysis of lignin over high aluminum zeolites. *Fuel Process Technol* 167:730–737. <https://doi.org/10.1016/j.fuproc.2017.08.026>
- Lan X et al (2016) Investigation of metal organic frameworks for the adsorptive removal of hydrochloride from dilute aqueous solution. *Microporous Mesoporous Mater* 231:40–46
- Lan G et al (2018) Wheat flour-derived N-doped mesoporous carbon extrudate as superior metal-free catalysts for acetylene hydrochlorination. *Chem Commun* 54:623–626. <https://doi.org/10.1039/C7CC09370E>
- Lanchas M et al (2012) A direct reaction approach for the synthesis of zeolitic imidazolate frameworks: template and temperature mediated control on network topology and crystal size. *Chem Commun* 48:9930–9932
- Larimi A, Khorasheh F (2018) Renewable hydrogen production by ethylene glycol steam reforming over Al<sub>2</sub>O<sub>3</sub> supported Ni-Pt

- bimetallic nano-catalysts. *Renew Energy* 128:188–199. <https://doi.org/10.1016/j.renene.2018.05.070>
- Laskar IB et al (2020) Zinc oxide supported silver nanoparticles as a heterogeneous catalyst for production of biodiesel from palm oil. *Environ Prog Sustain Energy*. <https://doi.org/10.1002/ep.13369>
- Le TT et al (2016) Degradation of synthetic pollutants in real wastewater using laccase encapsulated in core–shell magnetic copper alginate beads. *Biores Technol* 216:203–210. <https://doi.org/10.1016/j.biortech.2016.05.077>
- Lee KM et al (2016) Recent developments of zinc oxide based photocatalyst in water treatment technology: a review. *Water Res* 88:428–448
- Lei J et al (2020) Degradation of aqueous cefotaxime in electro-oxidation—electro-Fenton—persulfate system with Ti/CNT/SnO<sub>2</sub>–Sb–Er anode and Ni@NCNT cathode. *Chemosphere* 250:126163. <https://doi.org/10.1016/j.chemosphere.2020.126163>
- Lerici LC et al (2022) Fe-doped Al<sub>2</sub>O<sub>3</sub> nanoplateforms as efficient and recyclable photocatalyst for the dyes remediation. *J Photochem Photobiol A Chem* 426:113733. <https://doi.org/10.1016/j.jphotochem.2021.113733>
- Li K et al (2015) In-situ-reduced synthesis of Ti<sub>3</sub>+ self-doped TiO<sub>2</sub>/g-C<sub>3</sub>N<sub>4</sub> heterojunctions with high photocatalytic performance under LED light irradiation. *ACS Appl Mater Interfaces* 7(17):9023–9030. <https://doi.org/10.1021/am508505n>
- Li S et al (2016a) Flame aerosol synthesis of nanostructured materials and functional devices: processing, modeling, and diagnostics. *Prog Energy Combust Sci* 55:1–59. <https://doi.org/10.1016/j.peccs.2016.04.002>
- Li Z et al (2016b) Visible photocatalytic water splitting and photocatalytic two-electron oxygen formation over Cu- and Fe-doped g-C<sub>3</sub>N<sub>4</sub>. *J Phys Chem C* 120:56–63
- Li X et al (2016c) Furfural: a promising platform compound for sustainable production of C<sub>4</sub> and C<sub>5</sub> chemicals. *ACS Catal* 6:2345. <https://doi.org/10.1021/acscatal.6b01838>
- Li Z et al (2018a) Recent development on MoS<sub>2</sub>-based photocatalysis: a review. *J Photochem Photobiol C* 35:39–55
- Li J et al (2018b) NiCoSe<sub>2</sub>-x/N-doped C mushroom-like core/shell nanorods on N-doped carbon fiber for efficiently electrocatalyzed overall water splitting. *Electrochim Acta* 272:161–168. <https://doi.org/10.1016/j.electacta.2018.04.032>
- Li X et al (2018c) One-pot catalytic transformation of lignocellulosic biomass into alkylcyclohexanes and polyols. *ACS Sustain Chem Eng* 6(3):4390–4399. <https://doi.org/10.1021/acssuschemeng.8b00012>
- Li D et al (2020) Gold nanoclusters for NIR-II fluorescence imaging of bones. *Small* 16:2003851. <https://doi.org/10.1002/sml.202003851>
- Li Z et al (2021) A highly efficient three-liquid-phase-based enzymatic one-pot multistep reaction system with recoverable enzymes for the synthesis of biodiesel. *J Agric Food Chem* 69:5481–5490. <https://doi.org/10.1021/acs.jafc.0c07448>
- Li M et al (2022) Synthesis strategies of carbon nanotube supported and confined catalysts for thermal catalysis. *Chem Eng J* 431:133970. <https://doi.org/10.1016/j.cej.2021.133970>
- Liang W et al (2013) Microwave-assisted solvothermal synthesis and optical properties of tagged MIL-140A metal–organic frameworks. *Inorg Chem* 52:12878–12880
- Lim T-T et al (2011) TiO<sub>2</sub>/AC composites for synergistic adsorption-photocatalysis processes: present challenges and further developments for water treatment and reclamation. *Crit Rev Environ Sci Technol* 41:1173–1230. <https://doi.org/10.1080/10643380903488664>
- Lin Y et al (2019a) Boosted reactivity of ammonia borane dehydrogenation over Ni/Ni<sub>2</sub>P heterostructure. *J Phys Chem Lett* 10:1048–1054
- Lin C et al (2019b) Immobilization of amidase into a magnetic hierarchically porous metal–organic framework for efficient biocatalysis. *Chem Commun* 55:5697–5700
- Lincho J et al (2021) TiO<sub>2</sub> nanotube catalysts for parabens mixture degradation by photocatalysis and ozone-based technologies. *Proc Safe Environ Protect* 152:601–613. <https://doi.org/10.1016/j.psep.2021.06.044>
- Ling Z et al (2015) Freeze-drying for sustainable synthesis of nitrogen doped porous carbon cryogel with enhanced supercapacitor and lithium ion storage performance. *Nanotechnology* 26:374003. <https://doi.org/10.1088/0957-4484/26/37/374003>
- Ling J et al (2021) Preparation of Mn–Fe oxide by a hydrolysis-driven redox method and its application in formaldehyde oxidation. *ACS Omega* 6:23274–23280. <https://doi.org/10.1021/acscomega.1c02994>
- Liu G et al (2011) Crystal facet engineering of semiconductor photocatalysts: motivations, advances and unique properties. *Chem Commun* 47:6763–6783
- Liu W et al (2013a) Ag<sub>3</sub>PO<sub>4</sub>/ZnO: an efficient visible-light-sensitized composite with its application in photocatalytic degradation of Rhodamine B. *Mater Res Bull* 48:106–113. <https://doi.org/10.1016/j.materresbull.2012.10.015>
- Liu X et al (2013b) Visible light photocatalytic degradation of methylene blue by SnO<sub>2</sub> quantum dots prepared via microwave-assisted method. *Catal Sci Technol* 3:1805–1809. <https://doi.org/10.1039/C3CY00013C>
- Liu J et al (2014) Applications of metal–organic frameworks in heterogeneous supramolecular catalysis. *Chem Soc Rev* 43:6011–6061
- Liu Q et al (2014) Basicities and transesterification activities of Zn–Al hydrotalcites-derived solid bases. *Green Chem* 16(5):2604–2613. <https://doi.org/10.1039/c3gc42648c>
- Liu S et al (2015) Ceria-based catalysts for soot oxidation: a review. *J Rare Earth* 33:567–590. [https://doi.org/10.1016/S1002-0721\(14\)60457-9](https://doi.org/10.1016/S1002-0721(14)60457-9)
- Liu S et al (2017) Improved degradation of the aqueous flutriafol using a nanostructure macroporous PbO<sub>2</sub> as reactive electrochemical membrane. *Electrochim Acta* 253:357–367. <https://doi.org/10.1016/j.electacta.2017.09.055>
- Liu Y et al (2019) Cascade utilization of lignocellulosic biomass to high-value products. *Green Chem* 21(13):3499–3535. <https://doi.org/10.1039/c9gc00473d>
- Liu C et al (2020) A general approach to direct growth of oriented metal–organic framework nanosheets on reduced graphene oxides. *Adv Sci* 7:1901480
- Liu X et al (2021a) A novel approach to efficient degradation of indole using co-immobilized horseradish peroxidase-syringaldehyde as biocatalyst. *Chemosphere* 262:128411. <https://doi.org/10.1016/j.chemosphere.2020.128411>
- Liu S et al (2021b) Fundamentals and recent applications of catalyst synthesis using flame aerosol technology. *Chem Eng J* 405:126958. <https://doi.org/10.1016/j.cej.2020.126958>
- Liu Y et al (2021c) A review of water pollution arising from agriculture and mining activities in Central Asia: facts, causes and effects. *Environ Pollut* 291:118209. <https://doi.org/10.1016/j.envpol.2021.118209>
- Liu Z et al (2021d) Alleviating the burden of ion exchange brine in water treatment: from operational strategies to brine management. *Water Res* 205:117728. <https://doi.org/10.1016/j.watres.2021.117728>
- Lohrasbi S et al (2019) Green synthesis of iron nanoparticles using Plantago major leaf extract and their application as a catalyst for the decolorization of azo dye. *BioNanoScience* 9:317–322
- Long J-J et al (2011) Ultrasound-assisted extraction of flaxseed oil using immobilized enzymes. *Biores Technol* 102:9991–9996

- Long LY et al (2018) Cellulose aerogels: synthesis, applications, and prospects. *Polymers* 10(6):623. <https://doi.org/10.3390/polym10060623>
- Luo J et al (2019) A critical review on energy conversion and environmental remediation of photocatalysts with remodeling crystal lattice, surface, and interface. *ACS Nano* 13:9811–9840
- Luo Q et al (2020) Global review of phthalates in edible oil: an emerging and nonnegligible exposure source to human. *Sci Total Environ* 704:135369
- Luo H et al (2021) Facile synthesis of PVDF photocatalytic membrane based on NCQDs/BiOBr/TiO<sub>2</sub> heterojunction for effective removal of tetracycline. *Mater Sci Eng B Solid State Mater Adv Technol* 265:114996. <https://doi.org/10.1016/j.mseb.2020.114996>
- Lyulyukin M et al (2018) Hygienic aspects of TiO<sub>2</sub>-mediated photocatalytic oxidation of volatile organic compounds: air purification analysis using a total hazard index. *Appl Catal B* 220:386–396
- Ma H-F et al (2018) Chitosan crosslinked with genipin as supporting matrix for biodegradation of synthetic dyes: laccase immobilization and characterization. *Chem Eng Res Des* 132:664–676. <https://doi.org/10.1016/j.cherd.2018.02.008>
- Ma Z et al (2021) g-C<sub>3</sub>N<sub>4</sub> nanosheets exfoliated by green wet ball milling process for photodegradation of organic pollutants. *Chem Phys Lett* 766:138335. <https://doi.org/10.1016/j.cplett.2021.138335>
- Maalej-Achouri I et al (2009) Production of xylo-oligosaccharides from agro-industrial residues using immobilized *Talaromyces thermophilus* xylanase. *J Mol Catal B Enzym* 59:145–152. <https://doi.org/10.1016/j.molcatb.2009.02.003>
- Madduluri VR et al (2020) Rice husk-derived carbon-silica supported Ni catalysts for selective hydrogenation of biomass-derived furfural and levulinic acid. *Fuel* 261:116339. <https://doi.org/10.1016/j.fuel.2019.116339>
- Madhavan A et al (2021) Design of novel enzyme biocatalysts for industrial bioprocess: harnessing the power of protein engineering, high throughput screening and synthetic biology. *Biores Technol* 325:124617
- Mafakher L et al (2010) Isolation of lipase and citric acid producing yeasts from agro-industrial wastewater. *New Biotechnol* 27:337–340
- Magdalane CM et al (2019) Self-cleaning mechanism of synthesized SnO<sub>2</sub>/TiO<sub>2</sub> nanostructure for photocatalytic activity application for waste water treatment. *Surf Interface* 17:100346. <https://doi.org/10.1016/j.surfin.2019.100346>
- Mahanthappa M et al (2019) Enhanced photocatalytic degradation of methylene blue dye using CuS–CdS nanocomposite under visible light irradiation. *Appl Surf Sci* 475:828–838. <https://doi.org/10.1016/j.apsusc.2018.12.178>
- Mahdi MA et al (2022) Improved pechini sol-gel fabrication of Li<sub>2</sub>B<sub>4</sub>O<sub>7</sub>/NiO/Ni<sub>3</sub>BO<sub>3</sub> nanocomposites to advanced photocatalytic performance. *Arab J Chem* 15:103768. <https://doi.org/10.1016/j.arabjc.2022.103768>
- Mahmoodi NM, Saffar-Dastgerdi MH (2020) Clean Laccase immobilized nanobiocatalysts (graphene oxide-zeolite nanocomposites): from production to detailed biocatalytic degradation of organic pollutant. *Appl Catal B Environ* 268:118443. <https://doi.org/10.1016/j.apcatb.2019.118443>
- Mahy JG et al (2018) Acid acting as redispersing agent to form stable colloids from photoactive crystalline aqueous sol-gel TiO<sub>2</sub> powder. *J Sol-Gel Sci Technol* 87:568–583. <https://doi.org/10.1007/s10971-018-4751-6>
- Mahy JG et al (2021) Eco-friendly colloidal aqueous sol-gel process for TiO<sub>2</sub> synthesis: the peptization method to obtain crystalline and photoactive materials at low temperature. *Catal* 11:768
- Makropoulou T et al (2020) Photocatalytic facile ZnO nanostructures for the elimination of the antibiotic sulfamethoxazole in water. *J Water Process Eng* 36:101299. <https://doi.org/10.1016/j.jwpe.2020.101299>
- Mamaghani AH et al (2019) Hydrothermal/solvothermal synthesis and treatment of TiO<sub>2</sub> for photocatalytic degradation of air pollutants: preparation, characterization, properties, and performance. *Chemosphere* 219:804–825. <https://doi.org/10.1016/j.chemosphere.2018.12.029>
- Mandić M et al (2017) Effects of catalyst activity, particle size and shape, and process conditions on catalyst effectiveness and methane selectivity for Fischer–Tropsch reaction: a modeling study. *Ind Eng Chem Res* 56:2733–2745
- Manenti DR et al (2015) Insights into solar photo-Fenton process using iron(III)-organic ligand complexes applied to real textile wastewater treatment. *Chem Eng J* 266:203–212. <https://doi.org/10.1016/j.cej.2014.12.077>
- Manique MC et al (2017) Biodiesel production using coal fly ash-derived sodalite as a heterogeneous catalyst. *Fuel* 190:268–273. <https://doi.org/10.1016/j.fuel.2016.11.016>
- Mardiana S et al (2022) Hierarchical zeolite for biomass conversion to biofuel: a review. *Fuel* 309:122119. <https://doi.org/10.1016/j.fuel.2021.122119>
- Margesin R et al (2000) Monitoring of bioremediation by soil biological activities. *Chemosphere* 40:339–346. [https://doi.org/10.1016/S0045-6535\(99\)00218-0](https://doi.org/10.1016/S0045-6535(99)00218-0)
- Mariscal R et al (2016) Furfural: a renewable and versatile platform molecule for the synthesis of chemicals and fuels. *Energy Environ Sci* 9(4):1144–1189. <https://doi.org/10.1039/c5ee02666k>
- Martínez F et al (2018) Sustainable Fe-BTC catalyst for efficient removal of methylene blue by advanced fenton oxidation. *Catal Today* 313:6–11
- Martín-Hernández M et al (2012) Catalytic wet air oxidation of a high strength p-nitrophenol wastewater over Ru and Pt catalysts: Influence of the reaction conditions on biodegradability enhancement. *Appl Catal B Environ* 123–124:141–150. <https://doi.org/10.1016/j.apcatb.2012.04.001>
- Maruthai J et al (2018) Optical, biological and catalytic properties of ZnO/MgO nanocomposites derived via *Musa paradisiaca* bract extract. *Ceram Int* 44:13152–13160
- Matharu AS et al (2016) Opportunity for high value-added chemicals from food supply chain wastes. *Biores Technol* 215:123–130. <https://doi.org/10.1016/j.biortech.2016.03.039>
- Mathew GM et al (2021) Recent advances in biodiesel production: challenges and solutions. *Sci Total Environ* 794:148751. <https://doi.org/10.1016/j.scitotenv.2021.148751>
- Matsuyama K et al (2016) Catalytically active Pt nanoparticles immobilized inside the pores of metal organic framework using supercritical CO<sub>2</sub> solutions. *Microporous Mesoporous Mater* 225:26–32
- Mehandia S et al (2020) Immobilization of laccase on chitosan-clay composite beads to improve its catalytic efficiency to degrade industrial dyes. *Mater. Today Commun* 25:101513. <https://doi.org/10.1016/j.mtcomm.2020.101513>
- Meng Y et al (2017) Enhancing anaerobic digestion performance of crude lipid in food waste by enzymatic pretreatment. *Biores Technol* 224:48–55. <https://doi.org/10.1016/j.biortech.2016.10.052>
- Mikaeli F et al (2018) Flame-sprayed pure and ce-doped TiO<sub>2</sub> photocatalysts. *Catal* 8:342
- Miklos DB et al (2018) Evaluation of advanced oxidation processes for water and wastewater treatment—a critical review. *Water Res* 139:118–131. <https://doi.org/10.1016/j.watres.2018.03.042>
- Mirpoor SF et al (2021) Biorefining of seed oil cakes as industrial co-streams for production of innovative bioplastics. A review. *Trends Food Sci Technol* 109:259–270. <https://doi.org/10.1016/j.tifs.2021.01.014>



- Moftah OA et al (2013) Lipase production by *Yarrowia lipolytica* using olive oil processing wastes as substrates. *J Serb Chem Soc* 78:781–794
- Mohamed MM et al (2014) Unprecedented high photocatalytic activity of nanocrystalline  $\text{WO}_3/\text{NiWO}_4$  hetero-junction towards dye degradation: effect of template and synthesis conditions. *Appl Catal B Environ* 150–151:63–73. <https://doi.org/10.1016/j.apcatb.2013.12.001>
- Mohammadinezhad A, Akhlaghinia B (2017)  $\text{Fe}_3\text{O}_4@$  Boehmite-NH<sub>2</sub>-Co II NPs: an inexpensive and highly efficient heterogeneous magnetic nanocatalyst for the Suzuki–Miyaura and Heck–Mizoroki cross-coupling reactions. *Green Chem* 19:5625–5641
- Mondal T et al (2015) Catalytic oxidative steam reforming of bio-ethanol for hydrogen production over Rh promoted Ni/CeO<sub>2</sub>-ZrO<sub>2</sub> catalyst. *Int J Hydrog Energy* 40(6):2529–2544. <https://doi.org/10.1016/j.ijhydene.2014.12.070>
- Mondal M et al (2020) Enhanced photocatalysis performance of mechano-synthesized  $\text{V}_2\text{O}_5\text{-TiO}_2$  nanocomposite for wastewater treatment: correlation of structure with photocatalytic performance. *Mater Chem Phys* 248:122947. <https://doi.org/10.1016/j.matchemphys.2020.122947>
- Moon SY et al (2016) Detoxification of chemical warfare agents using a Zr6-based metal–organic framework/polymer mixture. *Chem A Eur J* 22:14864–14868
- Moretti E et al (2015) Ceria-zirconia based catalysts for ethanol steam reforming. *Fuel* 153:166–175. <https://doi.org/10.1016/j.fuel.2015.02.077>
- Morosuk T, Tsatsaronis G (2019) Advanced exergy-based methods used to understand and improve energy-conversion systems. *Energy* 169:238–246. <https://doi.org/10.1016/j.energy.2018.11.123>
- Morrison B, Golden JS (2015) An empirical analysis of the industrial bioeconomy: implications for renewable resources and the environment. *BioResources* 10:4411–4440. <https://doi.org/10.15376/biores.10.3.4411-4440>
- Mottillo C et al (2013) Mineral neogenesis as an inspiration for mild, solvent-free synthesis of bulk microporous metal–organic frameworks from metal (Zn, Co) oxides. *Green Chem* 15:2121–2131
- Mousset E et al (2021) Electrochemical technologies coupled with biological treatments. *Curr Opin Electrochem* 26:100668
- Munnik P et al (2015) Recent developments in the synthesis of supported catalysts. *Chem Rev* 115:6687–6718. <https://doi.org/10.1021/cr500486u>
- Muñoz-Batista MJ et al (2018) Mechanochemistry: toward sustainable design of advanced nanomaterials for electrochemical energy storage and catalytic applications. *ACS Sustain Chem Eng* 6:9530–9544. <https://doi.org/10.1021/acssuschemeng.8b01716>
- Munshi AM et al (2017) Magnetically recoverable  $\text{Fe}_3\text{O}_4@$ Au-coated nanoscale catalysts for the A3-coupling reaction. *Dalton Trans.* <https://doi.org/10.1039/c7dt00058h>
- Muradov NZ, Veziroğlu TN (2008) “Green” path from fossil-based to hydrogen economy: an overview of carbon-neutral technologies. *Int J Hydrog Energy* 33:6804–6839
- Murphy CJ (2008) Sustainability as an emerging design criterion in nanoparticle synthesis and applications. *J Mater Chem* 18:2173–2176
- Musa A et al (2017) Preparation, characterization and catalytic activity of biomaterial-supported copper nanoparticles. *Res Chem Intermed* 43:801–815
- Muthukumar H et al (2017) Biogenic synthesis of nano-biomaterial for toxic naphthalene photocatalytic degradation optimization and kinetics studies. *Int Biodet Biodegrad* 119:587–594
- Naikoo GA et al (2021) thermocatalytic hydrogen production through decomposition of methane—a review. *Front Chem* 9:34. <https://doi.org/10.3389/fchem.2021.736801>
- Najeeb J et al (2021) Nanobiocatalysts for biodiesel synthesis through transesterification—a review. *Catalysts* 11(2):171. <https://doi.org/10.3390/catal11020171>
- Narkhede N, Patel A (2013) Biodiesel production by esterification of oleic acid and transesterification of soybean oil using a new solid acid catalyst comprising 12-tungstosilicic acid and zeolite h $\beta$ . *Ind Eng Chem Res* 52(38):13637–13644. <https://doi.org/10.1021/ie402230v>
- Narowska B et al (2019) Use of activated carbons as catalyst supports for biodiesel production. *Renew Energy* 135:176–185. <https://doi.org/10.1016/j.renene.2018.11.006>
- Nasrollahzadeh M et al (2016) Waste chicken eggshell as a natural valuable resource and environmentally benign support for biosynthesis of catalytically active Cu/eggshell,  $\text{Fe}_3\text{O}_4$ /eggshell and Cu/ $\text{Fe}_3\text{O}_4$ /eggshell nanocomposites. *Appl Catal B* 191:209–227
- Navajas A et al (2018) Outstanding performance of rehydrated Mg–Al hydrotalcites as heterogeneous methanolysis catalysts for the synthesis of biodiesel. *Fuel* 211:173–181. <https://doi.org/10.1016/j.fuel.2017.09.061>
- Nazor J et al (2021) Enzyme evolution for industrial biocatalytic cascades. *Curr Opin Biotechnol* 69:182–190
- Ni J et al (2021) Oxygen vacancy-mediated sandwich-structural  $\text{TiO}_2\text{-x}$  /ultrathin  $\text{g-C}_3\text{N}_4/\text{TiO}_2\text{-x}$  direct Z-scheme heterojunction visible-light-driven photocatalyst for efficient removal of high toxic tetracycline antibiotics. *J Hazard Mater* 408:124432. <https://doi.org/10.1016/j.jhazmat.2020.124432>
- Nidheesh PV et al (2018) An overview on the removal of synthetic dyes from water by electrochemical advanced oxidation processes. *Chemosphere* 197:210–227. <https://doi.org/10.1016/j.chemosphere.2017.12.195>
- Nilsson A et al (1973) Anodic oxidation of phenolic compounds. Part III. Anodic hydroxylation of phenols. A simple general synthesis of 4-alkyl-4-hydroxycyclo-hexa-2,5-dienones from 4-alkylphenols. *J Chem Soc Perkin Trans 1*:2337–2345. <https://doi.org/10.1039/P19730002337>
- Nisar A et al (2022) Synthesis and characterization of ZnO decorated reduced graphene oxide (ZnO-rGO) and evaluation of its photocatalytic activity toward photodegradation of methylene blue. *Environ Sci Pollut Res* 29:345. <https://doi.org/10.1007/s11356-021-13520-6>
- Nunes YL et al (2021) Chemical and physical Chitosan modification for designing enzymatic industrial biocatalysts: How to choose the best strategy? *Int J Biol Macromol* 181:1124–1170. <https://doi.org/10.1016/j.ijbiomac.2021.04.004>
- Nuri A et al (2020) Synthesis and characterization of palladium supported amino functionalized magnetic-MOF-MIL-101 as an efficient and recoverable catalyst for Mizoroki–Heck cross-coupling. *Catal Lett* 150:2617–2629
- Ochando-Pulido JM et al (2017) A focus on advanced physico-chemical processes for olive mill wastewater treatment. *Sep Purif Technol.* <https://doi.org/10.1016/j.seppur.2017.02.004>
- Ogel E et al (2019) Impact of preparation method and hydrothermal aging on particle size distribution of Pt/ $\gamma\text{-Al}_2\text{O}_3$  and its performance in CO and NO oxidation. *J Phys Chem C* 123:5433–5446. <https://doi.org/10.1021/acs.jpcc.8b11065>
- Ohtani B (2013) Titania photocatalysis beyond recombination: a critical review. *Catalysts*. <https://doi.org/10.3390/catal3040942>
- Omer AM et al (2021) Facile fabrication of novel magnetic ZIF-67 MOF@ aminated chitosan composite beads for the adsorptive removal of Cr (VI) from aqueous solutions. *Carbohydr Polym* 265:118084
- Orooji Y et al (2021) Heterogeneous UV-Switchable Au nanoparticles decorated tungstophosphoric acid/TiO<sub>2</sub> for efficient photocatalytic degradation process. *Chemosphere* 281:130795. <https://doi.org/10.1016/j.chemosphere.2021.130795>

- Osman AI et al (2020a) Exploring the photocatalytic hydrogen production potential of titania doped with alumina derived from foil waste. *Int J Hydrog Energy* 45:34494–34502. <https://doi.org/10.1016/j.ijhydene.2020.02.065>
- Osman AI et al (2020b) Physicochemical characterization and kinetic modeling concerning combustion of waste berry pomace. *ACS Sustain Chem Eng* 8:17573–17586. <https://doi.org/10.1021/acssu.schemeng.0c07390>
- Osman AI et al (2021a) Bioethanol and biodiesel: Bibliometric mapping, policies and future needs. *Renew Sustain Energy Rev* 152:111677. <https://doi.org/10.1016/j.rser.2021.111677>
- Osman AI et al (2021b) Conversion of biomass to biofuels and life cycle assessment: a review. *Environ Chem Lett* 19:4075–4118. <https://doi.org/10.1007/s10311-021-01273-0>
- Osman AI et al (2022a) Biochar for agronomy, animal farming, anaerobic digestion, composting, water treatment, soil remediation, construction, energy storage, and carbon sequestration: a review. *Environ Chem Lett* 20(4):2385–2485. <https://doi.org/10.1007/s10311-022-01424-x>
- Osman AI et al (2022b) Cost, environmental impact, and resilience of renewable energy under a changing climate: a review. *Environ Chem Lett* 1–24. <https://doi.org/10.1007/s10311-022-01532-8>
- Ottone C et al (2021) Enzyme biocatalysis and sustainability. In: Nanostructured catalysts for environmental applications. Springer, pp 383–413
- Padmanabhan NT et al (2022) Antibacterial self-cleaning binary and ternary hybrid photocatalysts of titanium dioxide with silver and graphene. *J Environ Chem Eng* 10:107275. <https://doi.org/10.1016/j.jece.2022.107275>
- Palanisamy B et al (2013) Sol–gel synthesis of mesoporous mixed  $\text{Fe}_2\text{O}_3/\text{TiO}_2$  photocatalyst: application for degradation of 4-chlorophenol. *J Hazard Mater* 252:233–242
- Palomo JM (2021) Artificial enzymes with multiple active sites. *Current Opin Green Sustain Chem* 29:100452. <https://doi.org/10.1016/j.cogsc.2021.100452>
- Panahian Y, Arsalani N (2017) Synthesis of hedgehoglike F-TiO<sub>2</sub>(B)/CNT nanocomposites for sonophotocatalytic and photocatalytic degradation of malachite green (MG) under visible light: kinetic study. *J Phys Chem A* 121:5614–5624. <https://doi.org/10.1021/acs.jpca.7b02580>
- Panda J et al (2019) Adsorptive behavior of zeolitic imidazolate framework-8 towards anionic dye in aqueous media: combined experimental and molecular docking study. *J Mol Liq* 278:536–545
- Pandey VP et al (2017) Chitosan immobilized novel peroxidase from *Azadirachta indica*: characterization and application. *Int J Biol Macromol* 104:1713–1720. <https://doi.org/10.1016/j.ijbiomac.2017.02.047>
- Panwar N et al (2011) Role of renewable energy sources in environmental protection: a review. *Renew Sustain Energy Rev* 15:1513–1524
- Papailias I et al (2020) Novel torus shaped g-C<sub>3</sub>N<sub>4</sub> photocatalysts. *Appl Catal B Environ* 268:118733. <https://doi.org/10.1016/j.apcatb.2020.118733>
- Park J et al (2016) Coating Pt–Ni octahedra with ultrathin Pt shells to enhance the durability without compromising the activity toward oxygen reduction. *Chemosuschem* 9:2209–2215
- Park HS et al (2019) RuO<sub>2</sub> nanocluster as a 4-in-1 electrocatalyst for hydrogen and oxygen electrochemistry. *Nano Energy* 55:49–58. <https://doi.org/10.1016/j.nanoen.2018.10.017>
- Park JH et al (2022) Review of recent technologies for transforming carbon dioxide to carbon materials. *Chem Eng J* 427:130980. <https://doi.org/10.1016/j.cej.2021.130980>
- Pascanu V et al (2013) Sustainable catalysis: rational Pd loading on MIL-101Cr-NH<sub>2</sub> for more efficient and recyclable Suzuki–Miyaura reactions. *Chem A Eur J* 19:17483–17493
- Paul DR, Robeson LM (2008) Polymer nanotechnology: nanocomposites. *Polymer* 49:3187–3204
- Paysepar H et al (2018) Zeolite catalysts screening for production of phenolic bio-oils with high contents of monomeric aromatics/phenolics from hydrolysis lignin via catalytic fast pyrolysis. *Fuel Process Technol*. <https://doi.org/10.1016/j.fuproc.2018.07.013>
- Paz-Cedeno FR et al (2021) Magnetic graphene oxide as a platform for the immobilization of cellulases and xylanases: Ultrastructural characterization and assessment of lignocellulosic biomass hydrolysis. *Renew Energy* 164:491–501
- Peng L et al (2014) Highly mesoporous metal–organic framework assembled in a switchable solvent. *Nat Commun* 5:1–7
- Peng X et al (2023) Recycling municipal, agricultural and industrial waste into energy, fertilizers, food and construction materials, and economic feasibility: a review. *Environ Chem Lett* 1–37. <https://doi.org/10.1007/s10311-022-01551-5>
- Perego C, Villa P (1997) Catalyst preparation methods. *Catal Today* 34:281–305. [https://doi.org/10.1016/S0920-5861\(96\)00055-7](https://doi.org/10.1016/S0920-5861(96)00055-7)
- Phongprueksathat N et al (2019) Steam reforming of acetic acid for hydrogen production: catalytic performances of Ni and Co supported on CeO<sub>2</sub>/ZrO<sub>2</sub> catalysts. *Int J Hydrog Energy* 44(18):9359–9367. <https://doi.org/10.1016/j.ijhydene.2019.02.085>
- Pieper DH et al (2004) Genomic and mechanistic insights into the biodegradation of organic pollutants. *Curr Opin Biotechnol* 15:215–224. <https://doi.org/10.1016/j.copbio.2004.03.008>
- Pillai VV et al (2020) Template-free, solid-state synthesis of hierarchically macroporous S-doped TiO<sub>2</sub> nano-photocatalysts for efficient water remediation. *ACS Omega* 5:7969–7978. <https://doi.org/10.1021/acsomega.9b04409>
- Pilusa TJ et al (2013) Thermo-chemical extraction of fuel oil from waste lubricating grease. *Waste Manag* 33:1509–1515
- Ping Y et al (2002) Titanium dioxide nanoparticles co-doped with Fe<sup>3+</sup> and Eu<sup>3+</sup> ions for photocatalysis. *Mater Lett* 57:794–801
- Pirzada BM et al (2015) Synthesis, characterization and optimization of photocatalytic activity of TiO<sub>2</sub>/ZrO<sub>2</sub> nanocomposite heterostructures. *Mater Sci Eng B* 193:137–145
- Pliexhov O et al (2018) The Co-MOF-74 modified with *N,N'*-Dihydroxypyromellitimide for selective, solvent free aerobic oxidation of toluene. *Catal Commun* 110:88–92
- Polshettiwar V et al (2009) Microwave-assisted chemistry: a rapid and sustainable route to synthesis of organics and nanomaterials. *Aust J Chem* 62:16–26. <https://doi.org/10.1071/CH08404>
- Polychronopoulou K et al (2017) Rapid microwave assisted sol-gel synthesis of CeO<sub>2</sub> and CexSm1-xO<sub>2</sub> nanoparticle catalysts for CO oxidation. *Mol Catal* 428:41–55. <https://doi.org/10.1016/j.molcata.2016.11.039>
- Pongthawornsakun B et al (2018) Variability of particle configurations achievable by 2-nozzle flame syntheses of the Au–Pd–TiO<sub>2</sub> system and their catalytic behaviors in the selective hydrogenation of acetylene. *Appl Catal A Gen* 549:1–7. <https://doi.org/10.1016/j.apcata.2017.09.014>
- Popovski O (2004) Electrocatalysts in the last 30 years—from precious metals to cheaper but sophisticated complex systems. *Bull Chem Technol Maced* 23:101–112
- Prakash Tripathy S et al (2022) Hydrolytically stable citrate capped Fe<sub>3</sub>O<sub>4</sub>@UiO-66-NH<sub>2</sub> MOF: a hetero-structure composite with enhanced activity towards Cr (VI) adsorption and photocatalytic H<sub>2</sub> evolution. *J Colloid Interface Sci* 606:353–366. <https://doi.org/10.1016/j.jcis.2021.08.031>
- Pratsinis SE (1998) Flame aerosol synthesis of ceramic powders. *Prog Energy Combust Sci* 24:197–219. [https://doi.org/10.1016/S0360-1285\(97\)00028-2](https://doi.org/10.1016/S0360-1285(97)00028-2)
- Pudukudy M, Yaakob Z (2015) Methane decomposition over Ni, Co and Fe based monometallic catalysts supported on sol gel derived

- SiO<sub>2</sub> microflakes. *Chem Eng J* 262:1009–1021. <https://doi.org/10.1016/j.cej.2014.10.077>
- Pudukudy M et al (2015) Direct decomposition of methane over SBA-15 supported Ni, Co and Fe based bimetallic catalysts. *Appl Surf Sci* 330:418–430. <https://doi.org/10.1016/j.apsusc.2015.01.032>
- Pudukudy M et al (2017) One-pot sol–gel synthesis of Ni/TiO<sub>2</sub> catalysts for methane decomposition into CO<sub>x</sub> free hydrogen and multiwalled carbon nanotubes. *Int J Hydrog Energy* 42:16495–16513. <https://doi.org/10.1016/j.ijhydene.2017.04.223>
- Qian W et al (2021) Differences and Similarities of photocatalysis and electrocatalysis in two-dimensional nanomaterials: strategies, traps Applications and Challenges. *Nano-Micro Lett* 13:1–38. <https://doi.org/10.1007/s40820-021-00681-9>
- Quan F et al (2018) Biomass as a template leads to CdS@Carbon aerogels for efficient photocatalytic hydrogen evolution and stable photoelectrochemical cells. *ACS Sustain Chem Eng* 6:14911–14918. <https://doi.org/10.1021/acssuschemeng.8b03415>
- Queirós S et al (2015) Heterogeneous Fenton's oxidation using Fe/ZSM-5 as catalyst in a continuous stirred tank reactor. *Sep Purif Technol* 141:235–245. <https://doi.org/10.1016/j.seppur.2014.11.046>
- Quiroz MA et al (2014) Degradation of 1-hydroxy-2,4-dinitrobenzene from aqueous solutions by electrochemical oxidation: Role of anodic material. *J Hazard Mater* 268:6–13. <https://doi.org/10.1016/j.jhazmat.2013.12.050>
- Quiton KGN et al (2021) Synthesis and catalytic utilization of bimetallic systems for wastewater remediation: a review. *Chemosphere* 262:128371. <https://doi.org/10.1016/j.chemosphere.2020.128371>
- Rahmani AR et al (2019) Integrated advanced oxidation process, sono-Fenton treatment, for mineralization and volume reduction of activated sludge. *Ecotoxicol Environ Saf* 168:120–126. <https://doi.org/10.1016/j.ecoenv.2018.10.069>
- Rajput RB et al (2022) A review on TiO<sub>2</sub>/SnO<sub>2</sub> heterostructures as a photocatalyst for the degradation of dyes and organic pollutants. *J Environ Manag* 307:114533. <https://doi.org/10.1016/j.jenvman.2022.114533>
- Ralphs K et al (2013) Application of heterogeneous catalysts prepared by mechanochemical synthesis. *Chem Soc Rev* 42:7701–7718. <https://doi.org/10.1039/C3CS60066A>
- Ramakrishnan P et al (2021) Ternary metal-based inverse spinel oxide NiCrFeO<sub>4</sub> nanoparticles as a highly efficient oxygen evolution catalyst. *Appl Surf Sci* 566:150653. <https://doi.org/10.1016/j.apsusc.2021.150653>
- Ramos-Delgado NA et al (2013) Synthesis by sol-gel of WO<sub>3</sub>/TiO<sub>2</sub> for solar photocatalytic degradation of malathion pesticide. *Catal Today* 209:35–40. <https://doi.org/10.1016/j.cattod.2012.11.011>
- Rashid T et al (2020) Formulation of zeolite supported nano-metallic catalyst and applications in textile effluent treatment. *J Environ Chem Eng* 8:104023
- Reddy LH et al (2012) A rapid microwave-assisted solution combustion synthesis of CuO promoted CeO<sub>2</sub>-MxO<sub>y</sub> (M=Zr, La, Pr and Sm) catalysts for CO oxidation. *Appl Catal A Gen* 445–446:297–305. <https://doi.org/10.1016/j.apcata.2012.08.024>
- Reddy IN et al (2019) Effect of ball milling on optical properties and visible photocatalytic activity of Fe doped ZnO nanoparticles. *Mater Sci Eng A* 240:33–40. <https://doi.org/10.1016/j.mseb.2019.01.002>
- Rehman HU et al (2020) Encapsulation of pectinase within polyacrylamide gel: characterization of its catalytic properties for continuous industrial uses. *Heliyon* 6:e04578
- Reis PM et al (2018) Integrating Fenton's process and ion exchange for olive mill wastewater treatment and iron recovery. *Environ Technol (United Kingdom)* 39(3):308–316. <https://doi.org/10.1080/09593330.2017.1299797>
- Ren J et al (2022) Characteristics of immobilized dye-decolorizing peroxidase from *Bacillus amyloliquefaciens* and application to the bioremediation of dyeing effluent. *Biochem Eng J* 182:108430. <https://doi.org/10.1016/j.bej.2022.108430>
- Ribeiro JP et al (2020) Fenton processes for AOX removal from a kraft pulp bleaching industrial wastewater: optimisation of operating conditions and cost assessment. *J Environ Chem Eng* 8(4):104032. <https://doi.org/10.1016/j.jece.2020.104032>
- Rodríguez B et al (2007) Solvent-free carbon-carbon bond formations in ball Mills. *Adv Synth Catal* 394:2213–2233
- Rodríguez-Padrón D et al (2019) Environmental catalysis: present and future. *ChemCatChem* 11:18–38. <https://doi.org/10.1002/cctc.201801248>
- Rosa DR et al (2009) Performance and molecular evaluation of an anaerobic system with suspended biomass for treating wastewater with high fat content after enzymatic hydrolysis. *Biores Technol* 100:6170–6176
- Russo D (2021) Kinetic modeling of advanced oxidation processes using microreactors: challenges and opportunities for scale-up. *Appl Sci* 11(3):1042. <https://doi.org/10.3390/app11031042>
- Sadhasivam T et al (2017) Dimensional effects of nanostructured Mg/MgH<sub>2</sub> for hydrogen storage applications: a review. *Renew Sustain Energy Rev* 72:523–534
- Samsudin MFR et al (2019) Photocatalytic degradation of phenol wastewater over Z-scheme g-C<sub>3</sub>N<sub>4</sub>/CNT/BiVO<sub>4</sub> heterostructure photocatalyst under solar light irradiation. *J Mol Catal B* 277:977–988. <https://doi.org/10.1016/j.molliq.2018.10.160>
- Santamaria L et al (2019) Stability of different Ni supported catalysts in the in-line steam reforming of biomass fast pyrolysis volatiles. *Appl Catal B Environ* 242:109–120. <https://doi.org/10.1016/j.apcatb.2018.09.081>
- Saravanan A et al (2021) A review on catalytic-enzyme degradation of toxic environmental pollutants: Microbial enzymes. *J Hazard Mater* 419:126451. <https://doi.org/10.1016/j.jhazmat.2021.126451>
- Satar R, Husain Q (2011) Catalyzed degradation of disperse dyes by calcium alginate-pectin entrapped bitter melon (*Momordica charantia*) peroxidase. *J Environ Sci* 23:1135–1142. [https://doi.org/10.1016/S1001-0742\(10\)60525-6](https://doi.org/10.1016/S1001-0742(10)60525-6)
- Schimmoeller B et al (2010) Structure of flame-made vanadia/silica and catalytic behavior in the oxidative dehydrogenation of propane. *J Catal* 274:64–75. <https://doi.org/10.1016/j.jcat.2010.06.005>
- Schimmoeller B et al (2011) Flame aerosol synthesis of metal oxide catalysts with unprecedented structural and catalytic properties. *ChemCatChem* 3:1234–1256. <https://doi.org/10.1002/cctc.20100425>
- Schlapbach L, Züttel A (2011) Hydrogen-storage materials for mobile applications. In: *Materials for sustainable energy: a collection of peer-reviewed research and review articles from nature publishing group*. World Scientific, pp 265–270
- Schoenecker PM et al (2012) Effect of water adsorption on retention of structure and surface area of metal-organic frameworks. *Ind Eng Chem Res* 51:6513–6519
- Schwarz JA et al (1995) Methods for preparation of catalytic materials. *Chem Rev* 95:477–485. <https://doi.org/10.1021/cr00035a002>
- Seh ZW et al (2017) Combining theory and experiment in electrocatalysis: Insights into materials design. *Science* 355:eaad4998
- Seibert D et al (2019) Two-stage integrated system photo-electro-Fenton and biological oxidation process assessment of sanitary landfill leachate treatment: An intermediate products study. *Chem Eng J* 372:471–482. <https://doi.org/10.1016/j.cej.2019.04.162>
- Sellami K et al (2022) Peroxidase enzymes as green catalysts for bioremediation and biotechnological applications: a review. *Sci Total Environ* 806:150500

- Sevimli MF et al (2014) A comparative study for treatment of white liquor by different applications of Fenton process. *Arab J Chem* 7(6):1116–1123. <https://doi.org/10.1016/j.arabjc.2012.12.015>
- Shaabani A et al (2014) Cobalt (II) supported on ethylenediamine-functionalized nanocellulose as an efficient catalyst for room temperature aerobic oxidation of alcohols. *J Chem Sci* 126:111–115
- Shanmugam S et al (2020) Optimal immobilization of *Trichoderma asperellum* laccase on polymer coated Fe<sub>3</sub>O<sub>4</sub>@SiO<sub>2</sub> nanoparticles for enhanced biohydrogen production from delignified lignocellulosic biomass. *Fuel* 273:117777
- Sheldon RA (2016) Green chemistry, catalysis and valorization of waste biomass. *J Mol Catal A Chem* 422:3–12. <https://doi.org/10.1016/j.molcata.2016.01.013>
- Sheng Y et al (2018) Emerging applications of nanocatalysts synthesized by flame aerosol processes. *Curr Opin Chem Biol* 20:39–49. <https://doi.org/10.1016/j.coche.2018.01.009>
- Sherwood J (2020) The significance of biomass in a circular economy. *Biores Technol* 300:122755
- Shi Y et al (2012) Novel  $\alpha$ -Fe<sub>2</sub>O<sub>3</sub>/CdS cornlike nanorods with enhanced photocatalytic performance. *ACS Appl Mater Interfaces* 4:4800–4806
- Shi L et al (2014) Removal of sulfonamide antibiotics by oriented immobilized laccase on Fe<sub>3</sub>O<sub>4</sub> nanoparticles with natural mediators. *J Hazard Mater* 279:203–211. <https://doi.org/10.1016/j.jhazmat.2014.06.070>
- Shiva et al (2022) High-solids loading processing for an integrated lignocellulosic biorefinery: effects of transport phenomena and rheology—a review. *Bioresour Technol* 351:127044. <https://doi.org/10.1016/j.biortech.2022.127044>
- Shubha JP et al (2022) ZnO/La<sub>2</sub>O<sub>3</sub>/NiO based ternary heterostructure nano-photocatalyst: preparation, characterization and its application for the degradation of methylene blue. *J King Saud Univ Sci* 34:101738. <https://doi.org/10.1016/j.jksus.2021.101738>
- Siddeeg SM et al (2020) Iron oxide/chitosan magnetic nanocomposite immobilized manganese peroxidase for decolorization of textile wastewater. *Processes* 8:5
- Simmance K et al (2019) Evaluation of perovskite catalysts prepared by flame spray pyrolysis for three-way catalyst activity under simulated gasoline exhaust feeds. *Catal Today* 320:40–50. <https://doi.org/10.1016/j.cattod.2017.12.035>
- Singh RK et al (2019) Progress in microwave-assisted synthesis of quantum dots (graphene/carbon/semiconducting) for bioapplications: a review. *Mater Today Chem* 12:282–314. <https://doi.org/10.1016/j.mtchem.2019.03.001>
- Singh H et al (2020) Environmental impacts of oil spills and their remediation by magnetic nanomaterials. *Environ Nanotechnol Monit Manag* 14:345. <https://doi.org/10.1016/j.enmm.2020.100305>
- Singh AK et al (2021) Bioremediation of lignin derivatives and phenolics in wastewater with lignin modifying enzymes: Status, opportunities and challenges. *Sci Total Environ* 777:145988
- Sinha T, Ahmaruzzaman M (2015) Biogenic synthesis of Cu nanoparticles and its degradation behavior for methyl red. *Mater Lett* 159:168–171
- Sirés I et al (2014) Electrochemical advanced oxidation processes: today and tomorrow. A review. *Environ Sci Pollut Res* 21:8336–8367
- Smirniotis PG et al (2018) Single-step rapid aerosol synthesis of N-doped TiO<sub>2</sub> for enhanced visible light photocatalytic activity. *Catal Commun* 113:1–5. <https://doi.org/10.1016/j.catcom.2018.04.019>
- Solís RR et al (2022) Highly stable UiO-66-NH<sub>2</sub> by the microwave-assisted synthesis for solar photocatalytic water treatment. *J Environ Chem Eng* 10:107122. <https://doi.org/10.1016/j.jece.2021.107122>
- Song S et al (2015) CeO<sub>2</sub>-encapsulated noble metal nanocatalysts: enhanced activity and stability for catalytic application. *NPG Asia Mater* 7:e179–e179
- Song JY et al (2016) UiO-66-type metal–organic framework with free carboxylic acid: versatile adsorbents via H-bond for both aqueous and nonaqueous phases. *ACS Appl Mater Interfaces* 8:27394–27402
- Song G et al (2022a) Tailoring biochar for persulfate-based environmental catalysis: Impact of biomass feedstocks. *J Hazard Mater* 424:127663. <https://doi.org/10.1016/j.jhazmat.2021.127663>
- Song K et al (2022b) Tailoring the crystal forms of the Ni-MOF catalysts for enhanced photocatalytic CO<sub>2</sub>-to-CO performance. *Appl Catal B Environ* 309:121232. <https://doi.org/10.1016/j.apcatb.2022.121232>
- Sprenger P et al (2018) Structural evolution of highly active multicomponent catalysts for selective propylene oxidation. *Catal* 8:356
- Sreedhar B et al (2008) Synthesis and characterization of silica@ copper core–shell nanoparticles: application for conjugate addition reactions. *Chem Asian J* 3:1163–1169
- Sreeja PH, Sosamony KJ (2016) A comparative study of homogeneous and heterogeneous photo-fenton process for textile wastewater treatment. *Procedia Technol* 24:217–223. <https://doi.org/10.1016/j.protcy.2016.05.065>
- State RN et al (2019) A review of catalysts used in microwave assisted pyrolysis and gasification. *Bioresour Technol* 277:179–194. <https://doi.org/10.1016/j.biortech.2019.01.036>
- Stolar T, Užarević K (2020) Mechanochemistry: an efficient and versatile toolbox for synthesis, transformation, and functionalization of porous metal–organic frameworks. *CrystEngComm* 22:4511–4525. <https://doi.org/10.1039/D0CE00091D>
- Su J et al (2011) Macroporous V<sub>2</sub>O<sub>5</sub>–BiVO<sub>4</sub> composites: effect of heterojunction on the behavior of photogenerated charges. *J Phys Chem C* 115:8064–8071
- Subair R et al (2016) Polydopamine modified membranes with in situ synthesized gold nanoparticles for catalytic and environmental applications. *Chem Eng J* 295:358–369
- Subramonian W et al (2017) Using one-step facile and solvent-free mechanochemical process to synthesize photoactive Fe<sub>2</sub>O<sub>3</sub>–TiO<sub>2</sub> for treating industrial wastewater. *J Alloys Compd* 695:496–507. <https://doi.org/10.1016/j.jallcom.2016.10.006>
- Suen NT et al (2017) Electrocatalysis for the oxygen evolution reaction: recent development and future perspectives. *Chem Soc Rev* 46(2):337–365. <https://doi.org/10.1039/c6cs00328a>
- Suhas et al (2016) Cellulose: a review as natural, modified and activated carbon adsorbent. *Bioresour Technol* 216:1066–1076. <https://doi.org/10.1016/j.biortech.2016.05.106>
- Sulaiman S, Ruslan NIF (2017) A heterogeneous catalyst from a mixture of coconut waste and eggshells for biodiesel production. *Energy Sour Part A Recov Utiliz Environ Effects* 39:345. <https://doi.org/10.1080/15567036.2016.1205683>
- Sun XF et al (2013) Hemicellulose-based pH-sensitive and biodegradable hydrogel for controlled drug delivery. *Carbohydr Polym* 92(2):1357–1366. <https://doi.org/10.1016/j.carbpol.2012.10.032>
- Sun H et al (2017) Improved biodegradation of synthetic azo dye by horseradish peroxidase cross-linked on nano-composite support. *Int J Biol Macromol* 95:1049–1055. <https://doi.org/10.1016/j.ijbiomac.2016.10.093>
- Sun Y et al (2018) Bifunctional hybrid Ni/Ni<sub>2</sub>P nanoparticles encapsulated by graphitic carbon supported with N, S modified 3D carbon framework for highly efficient overall water splitting. *Adv Mater Interfaces* 5(15):1800473. <https://doi.org/10.1002/admi.201800473>
- Sutherland T et al (2004) Enzymatic bioremediation: from enzyme discovery to applications. *Clin Exp Pharmacol Physiol* 31:817–821. <https://doi.org/10.1111/j.1440-1681.2004.04088.x>

- Swann AL et al (2016) Plant responses to increasing CO<sub>2</sub> reduce estimates of climate impacts on drought severity. *Proc Natl Acad Sci* 113:10019–10024
- Szczęśniak B et al (2020) Mechanochemical synthesis of highly porous materials. *Mater Horizon* 7:1457–1473. <https://doi.org/10.1039/D0MH00081G>
- Tan K et al (2015) Water interactions in metal organic frameworks. *CrystEngComm* 17:247–260
- Tan YL et al (2018) Catalytic fast pyrolysis of durian rind using silica-alumina catalyst: effects of pyrolysis parameters. *Bioresour Technol* 264:198–205. <https://doi.org/10.1016/j.biortech.2018.05.058>
- Tang J et al (2019) Biomass-derived hierarchical honeycomb-like porous carbon tube catalyst for the metal-free oxygen reduction reaction. *J Electroanal Chem* 847:113230. <https://doi.org/10.1016/j.jelechem.2019.113230>
- Teerapatsakul C et al (2017) Repeated batch for dye degradation in an airlift bioreactor by laccase entrapped in copper alginate. *Int Biodeterior Biodegrad* 120:52–57. <https://doi.org/10.1016/j.ibiod.2017.02.001>
- Teoh WY et al (2010) Flame spray pyrolysis: an enabling technology for nanoparticles design and fabrication. *Nanoscale* 2:1324–1347. <https://doi.org/10.1039/C0NR00017E>
- Thangavel P et al (2020) Graphene-nanoplatelets-supported NiFe-MOF: high-efficiency and ultra-stable oxygen electrodes for sustained alkaline anion exchange membrane water electrolysis. *Energy Environ Sci* 13:3447–3458
- Theerachai M et al (2017) The culture or co-culture of *Candida rugosa* and *Yarrowia lipolytica* strain rM-4A, or incubation with their crude extracellular lipase and laccase preparations, for the biodegradation of palm oil mill wastewater. *Int Biodeterior Biodegrad* 121:11–18
- Thomas N et al (2021) Heterogeneous fenton catalysts: a review of recent advances. *J Hazard Mater* 404:124082. <https://doi.org/10.1016/j.jhazmat.2020.124082>
- Tian J et al (2019) Microwave solvothermal carboxymethyl chitosan templated synthesis of TiO<sub>2</sub>/ZrO<sub>2</sub> composites toward enhanced photocatalytic degradation of Rhodamine B. *J Colloid Interface Sci* 541:18–29
- Trapido M et al (2017) Bio-recalcitrant pollutants removal from wastewater with combination of the Fenton treatment and biological oxidation. *J Water Process Eng* 16:277–282. <https://doi.org/10.1016/j.jwpe.2017.02.007>
- Trinh MM, Chang MB (2021) Catalytic pyrolysis: new approach for destruction of POPs in MWIs fly ash. *Chem Eng J* 4:05. <https://doi.org/10.1016/j.cej.2020.126718>
- Tsai C-T, Meyer AS (2014) Enzymatic cellulose hydrolysis: enzyme reusability and visualization of β-glucosidase immobilized in calcium alginate. *Molecules* 19:19390–19406
- Tuna Ö et al (2022) Deposition of CaFe<sub>2</sub>O<sub>4</sub> and LaFeO<sub>3</sub> perovskites on polyurethane filter: a new photocatalytic support for flowthrough degradation of tetracycline antibiotic. *Environ Res* 205:112389. <https://doi.org/10.1016/j.envres.2021.112389>
- Ubeyitogullari A, Ciftci ON (2016) Formation of nanoporous aerogels from wheat starch. *Carbohydr Polym* 147:125–132. <https://doi.org/10.1016/j.carbpol.2016.03.086>
- Ullah R et al (2016) Comparison of the reactive adsorption desulfurization performance of Ni/ZnO–Al<sub>2</sub>O<sub>3</sub> adsorbents prepared by different methods. *Energy Fuels* 30:2874–2881. <https://doi.org/10.1021/acs.energyfuels.6b00232>
- Ulu A et al (2018) Chitosan/polyvinylpyrrolidone/MCM-41 composite hydrogel films: structural, thermal, surface, and antibacterial properties. *Starch-Stärke* 70:1700303
- Užarević K et al (2016) Mechanochemical and solvent-free assembly of zirconium-based metal–organic frameworks. *Chem Commun* 52:2133–2136
- Uzun BB et al (2012) Biodiesel production from waste frying oils: Optimization of reaction parameters and determination of fuel properties. *Energy* 44(1):347–351. <https://doi.org/10.1016/j.energy.2012.06.024>
- Vasanthakumar P et al (2020) Iron and chromium MOFs as sustainable catalysts for transfer hydrogenation of carbonyl compounds and biomass conversions. *New J Chem* 44:8223–8231
- Vasić K et al (2020) Biodiesel production using solid acid catalysts based on metal oxides. *Catalyst* 10:237. <https://doi.org/10.3390/catal10020237>
- Vilardi G et al (2018) Fenton oxidation and chromium recovery from tannery wastewater by means of iron-based coated biomass as heterogeneous catalyst in fixed-bed columns. *Chem Eng J* 351:1–11. <https://doi.org/10.1016/j.cej.2018.06.095>
- Vorontsov AV (2019) Advancing Fenton and photo-Fenton water treatment through the catalyst design. *J Hazard Mater* 372:103–112. <https://doi.org/10.1016/j.jhazmat.2018.04.033>
- Wan L, Wang H (2021) Control of urban river water pollution is studied based on SMS. *Environ Technol Innov* 22:101468. <https://doi.org/10.1016/j.eti.2021.101468>
- Wang D, Astruc D (2017) The recent development of efficient earth-abundant transition-metal nanocatalysts. *Chem Soc Rev* 46:816–854
- Wang Z, Chen Q (2016) Conversion of 5-hydroxymethylfurfural into 5-ethoxymethylfurfural and ethyl levulinate catalyzed by MOF-based heteropolyacid materials. *Green Chem* 18:5884–5889
- Wang J, Zhuang R (2020) Degradation of antibiotics by advanced oxidation processes: an overview. *Sci Total Environ* 701:135023. <https://doi.org/10.1016/j.scitotenv.2019.135023>
- Wang LK et al (2005) Chemical precipitation physicochem. *Treat Process* 3:141–197. <https://doi.org/10.1385/1-59259-820-x:141>
- Wang F et al (2012a) Rational band gap engineering of WO<sub>3</sub> photocatalyst for visible light water splitting. *ChemCatChem* 4:476–478
- Wang X et al (2012b) Photocatalytic overall water splitting promoted by an α–β phase junction on Ga<sub>2</sub>O<sub>3</sub>. *Angew Chem* 124:13266–13269
- Wang W et al (2013) Synthesis of Bi<sub>2</sub>O<sub>2</sub>CO<sub>3</sub>/Bi<sub>2</sub>S<sub>3</sub> hierarchical microspheres with heterojunctions and their enhanced visible light-driven photocatalytic degradation of dye pollutants. *J Colloid Interface Sci* 402:34–39. <https://doi.org/10.1016/j.jcis.2013.03.054>
- Wang S et al (2014) Synthesis and characterization of g-C<sub>3</sub>N<sub>4</sub>/Ag<sub>3</sub>VO<sub>4</sub> composites with significantly enhanced visible-light photocatalytic activity for triphenylmethane dye degradation. *Appl Catal B Environ* 56:19–24. <https://doi.org/10.1016/j.apcatb.2013.08.008>
- Wang Y et al (2016) Nanoparticle-stacked porous nickel-iron nitride nanosheet: a highly efficient bifunctional electrocatalyst for overall water splitting. *ACS Appl Mater Interfaces* 8(29):18652–18657. <https://doi.org/10.1021/acsami.6b05811>
- Wang Q et al (2016a) Effect of CeO<sub>2</sub>-ZrO<sub>2</sub> on Pt/C electrocatalysts for alcohols oxidation. *J Rare Earth* 34:276–282. [https://doi.org/10.1016/S1002-0721\(16\)60025-X](https://doi.org/10.1016/S1002-0721(16)60025-X)
- Wang Y et al (2016b) The electrochemical degradation of ciprofloxacin using a SnO<sub>2</sub>-Sb/Ti anode: influencing factors, reaction pathways and energy demand. *Chem Eng J* 296:79–89. <https://doi.org/10.1016/j.cej.2016.03.093>
- Wang L et al (2017) Plating precious metals on nonprecious metal nanoparticles for sustainable electrocatalysts. *Nano Lett* 17:3391–3395
- Wang S et al (2017) Lignocellulosic biomass pyrolysis mechanism: a state-of-the-art review. *Prog Energy Combust Sci* 62:33–86. <https://doi.org/10.1016/j.pecs.2017.05.004>
- Wang L et al (2019a) Recyclable β-glucosidase by one-pot encapsulation with Cu-MOFs for enhanced hydrolysis of cellulose to glucose. *ACS Sustain Chem Eng* 7:3339–3348. <https://doi.org/10.1021/acssuschemeng.8b05489>

- Wang N et al (2019b) Facile synthesis of copper ions chelated sand via dopamine chemistry for recyclable and sustainable catalysis. *Chem Eng Sci* 203:312–320
- Wang Z et al (2019c) Recent developments in heterogeneous photocatalysts for solar-driven overall water splitting. *Chem Soc Rev* 48:2109–2125
- Wang Y-J et al (2020) Flame-spray-pyrolysis amorphous alumina-silica for tailoring the product distribution of Fischer–Tropsch synthesis. *Catal Today* 339:40–47. <https://doi.org/10.1016/j.cattod.2019.01.048>
- Wang S et al (2021a) Hydrogen production from water electrolysis: role of catalysts. *Nano Converg* 8:1–23. <https://doi.org/10.1186/s40580-021-00254-x>
- Wang Y et al (2021a) Biomass-derived carbon materials: controllable preparation and versatile applications. *Small* 17:2008079. <https://doi.org/10.1002/sml.202008079>
- Wang Z et al (2021b) Ultrasonic-assisted hydrothermal synthesis of cobalt oxide/nitrogen-doped graphene oxide hybrid as oxygen reduction reaction catalyst for Al-air battery. *Ultrason Sonochem* 72:105457. <https://doi.org/10.1016/j.ultsonch.2020.105457>
- Wang Y et al (2021b) Non-noble metal-based catalysts applied to hydrogen evolution from hydrolysis of boron hydrides. *Small Struct* 2:2000135
- Wang Y et al (2021c) Co-precipitation synthesis of reusable ZnAl-CLDH/ZIF-8 heterojunction for enhanced photodegradation of organic dye. *J Mater Sci Mater Electron* 32:28051–28064. <https://doi.org/10.1007/s10854-021-07118-4>
- Wang G et al (2022) Mesoporous carbon framework supported Cu-Fe oxides as efficient peroxymonosulfate catalyst for sustained water remediation. *Chem Eng J* 430:133060. <https://doi.org/10.1016/j.cej.2021.133060>
- Wang S et al (2022) Microwave-assisted hydrothermal synthesis of NiMoO<sub>4</sub> nanorods for high-performance urea electrooxidation. *Chin Chem Lett* 33:1105–1109. <https://doi.org/10.1016/j.ccl.2021.08.042>
- Wee LH et al (2014) Cr-MIL-101 encapsulated Keggin phosphotungstic acid as active nanomaterial for catalysing the alcoholysis of styrene oxide. *Green Chem* 16:1351–1357
- Wegner K et al (2018) Tailoring catalytic properties of copper manganese oxide nanoparticles (hopcalites-2G) via flame spray pyrolysis. *ChemCatChem* 10:3914–3922. <https://doi.org/10.1002/cctc.201800639>
- Wegner K et al (2019) Molecular precursors for tailoring humidity tolerance of nanoscale hopcalite catalysts via flame spray pyrolysis. *ChemCatChem* 11:4593–4603. <https://doi.org/10.1002/cctc.201900990>
- Wei L et al (2011) Hydrogen production by methane cracking over different coal chars. *Fuel* 90(11):3473–3479. <https://doi.org/10.1016/j.fuel.2011.06.053>
- Wei K et al (2021a) Strategies for improving perovskite photocatalysts reactivity for organic pollutants degradation: a review on recent progress. *Chem Eng J* 414:128783
- Wei X et al (2021b) Facile ball-milling synthesis of CeO<sub>2</sub>/g-C<sub>3</sub>N<sub>4</sub> Z-scheme heterojunction for synergistic adsorption and photodegradation of methylene blue: Characteristics, kinetics, models, and mechanisms. *Chem Eng J* 420:127719. <https://doi.org/10.1016/j.cej.2020.127719>
- Wen X et al (2019) Immobilized laccase on bentonite-derived mesoporous materials for removal of tetracycline. *Chemosphere* 222:865–871
- Widayatno WB et al (2016) Upgrading of bio-oil from biomass pyrolysis over Cu-modified  $\beta$ -zeolite catalyst with high selectivity and stability. *Appl Catal B Environ* 186:166–172. <https://doi.org/10.1016/j.apcatb.2016.01.006>
- Wong JKH et al (2019) Potential and challenges of enzyme incorporated nanotechnology in dye wastewater treatment: a review. *J Environ Chem Eng* 7:103261. <https://doi.org/10.1016/j.jece.2019.103261>
- Wu S, Hu YH (2021) A comprehensive review on catalysts for electrocatalytic and photoelectrocatalytic degradation of antibiotics. *Chem Eng J* 409:127739
- Wu Y, Zhang F (2020) Exploiting molecular probes to perform near-infrared fluorescence-guided surgery. *View* 1:20200068. <https://doi.org/10.1002/VIW.20200068>
- Wu H et al (2013) Transesterification of soybean oil to biodiesel using zeolite supported CaO as strong base catalysts. *Fuel Process Technol* 109:13–18. <https://doi.org/10.1016/j.fuproc.2012.09.032>
- Wu X et al (2015) Polydopamine tethered enzyme/metal-organic framework composites with high stability and reusability. *Nanoscale* 7:18883–18886
- Wu Z et al (2018) Radially aligned hierarchical nickel/nickel-iron (oxy) hydroxide nanotubes for efficient electrocatalytic water splitting. *ACS Appl Mater Interfaces* 10(10):8585–8593. <https://doi.org/10.1021/acsami.7b16953>
- Wu D et al (2019a) Photocatalytic improvement of Y<sup>3+</sup> modified TiO<sub>2</sub> prepared by a ball milling method and application in shrimp wastewater treatment. *RSC Adv* 9:14609–14620. <https://doi.org/10.1039/C9RA02307K>
- Wu J et al (2019b) Nickel nanoparticles encapsulated in microporous graphenelike carbon (Ni@MGC) as catalysts for CO<sub>2</sub> methanation. *Ind Eng Chem Res* 58:20536–20542. <https://doi.org/10.1021/acs.iecr.9b03789>
- Xia Y et al (2012) Biotemplated fabrication of hierarchically porous NiO/C composite from lotus pollen grains for lithium-ion batteries. *J Mater Chem* 22:9209–9215. <https://doi.org/10.1039/C2JM16935E>
- Xiang Z et al (2022) Fabrications and applications of hemicellulose-based bio-adsorbents. *Carbohydr Polym* 278:118945. <https://doi.org/10.1016/j.carbpol.2021.118945>
- Xiao J et al (2022) Dimensionality, function and performance of carbon materials in energy storage devices. *Adv Energy Mater* 12:2100775. <https://doi.org/10.1002/aenm.202100775>
- Xie H et al (2015) Hydrogen production from steam reforming of simulated bio-oil over Ce–Ni/Co catalyst with in continuous CO<sub>2</sub> capture. *Int J Hydrog Energy* 40(3):1420–1428. <https://doi.org/10.1016/j.ijhydene.2014.11.137>
- Xie Y et al (2016) Oxidation of AOX and organic compounds in pharmaceutical wastewater in RSM-optimized-Fenton system. *Chemosphere* 155:217–224. <https://doi.org/10.1016/j.chemosphere.2016.04.057>
- Xie L et al (2018) Sustainable and scalable synthesis of monodisperse carbon nanospheres and their derived superstructures. *Green Chem* 20:4596–4601. <https://doi.org/10.1039/C8GC02196A>
- Xing X et al (2018) Maximization of current efficiency for organic pollutants oxidation at BDD, Ti/SnO<sub>2</sub>-Sb/PbO<sub>2</sub>, and Ti/SnO<sub>2</sub>-Sb anodes. *Chemosphere* 205:361–368. <https://doi.org/10.1016/j.chemosphere.2018.04.090>
- Xiong P et al (2019) Interface modulation of two-dimensional superlattices for efficient overall water splitting. *Nano Lett* 19(7):4518–4526. <https://doi.org/10.1021/acs.nanolett.9b01329>
- Xu J et al (2009) A novel Ce, C-codoped TiO<sub>2</sub> nanoparticles and its photocatalytic activity under visible light. *Appl Surf Sci* 256:884–888. <https://doi.org/10.1016/j.apsusc.2009.08.079>
- Xu C et al (2015a) Mechanochemical synthesis of advanced nanomaterials for catalytic applications. *Chem Commun* 51:6698–6713. <https://doi.org/10.1039/C4CC09876E>
- Xu Y et al (2015b) Recent advances in noble metal based composite nanocatalysts: colloidal synthesis, properties, and catalytic applications. *Nanoscale* 7:10559–10583


- Xu C-Z et al (2016) CeO<sub>x</sub> doping on a TiO<sub>2</sub>-SiO<sub>2</sub> supporter enhances Ag based adsorptive desulfurization for diesel. *J Fuel Chem Technol* 44:943–953. [https://doi.org/10.1016/S1872-5813\(16\)30042-1](https://doi.org/10.1016/S1872-5813(16)30042-1)
- Xu J et al (2019) Porous nitrogen-doped carbons as effective catalysts for oxygen reduction reaction synthesized from cellulose and polyamide. *ChemElectroChem* 6:5735–5743. <https://doi.org/10.1002/celec.201901763>
- Xu J et al (2020) Synthesis of direct Z-Scheme Bi<sub>3</sub>TaO<sub>7</sub>/CdS composite photocatalysts with enhanced photocatalytic performance for ciprofloxacin degradation under visible light irradiation. *J Alloys Compd* 834:155061. <https://doi.org/10.1016/j.jallcom.2020.155061>
- Xu C et al (2021) N-doped honeycomb-like porous carbon derived from biomass as an efficient carbocatalyst for H<sub>2</sub>S selective oxidation. *J Hazard Mater* 403:123806. <https://doi.org/10.1016/j.jhazmat.2020.123806>
- Xu Z et al (2022) Recent progress in single-atom alloys: Synthesis, properties, and applications in environmental catalysis. *J Hazard Mater* 424:127427. <https://doi.org/10.1016/j.jhazmat.2021.127427>
- Yadav S et al (2019) A review on the sustainable routes for the synthesis and applications of cuprous oxide nanoparticles and their nanocomposites. *Green Chem* 21:937–955
- Yan M et al (2016) Synthesis and characterization of novel BiVO<sub>4</sub>/Ag<sub>3</sub>VO<sub>4</sub> heterojunction with enhanced visible-light-driven photocatalytic degradation of dyes. *ACS Sustain Chem Eng*. <https://doi.org/10.1021/acssuschemeng.5b00690>
- Yan J et al (2018a) Engineering *Yarrowia lipolytica* to simultaneously produce lipase and single cell protein from agro-industrial wastes for feed. *Sci Rep* 8:1–10
- Yan R et al (2018b) Ultrasmall Au nanoparticles embedded in 2D mixed-ligand metal-organic framework nanosheets exhibiting highly efficient and size-selective catalysis. *Adv Func Mater* 28:1802021
- Yang M et al (2011) Carrier transport in dye-sensitized solar cells using single crystalline TiO<sub>2</sub> nanorods grown by a microwave-assisted hydrothermal reaction. *J Phys Chem C* 115:14534–14541. <https://doi.org/10.1021/jp2025126>
- Yang Q et al (2013) Metal oxide and hydroxide nanoarrays: Hydrothermal synthesis and applications as supercapacitors and nanocatalysts. *Prog Nat. Sci. Mater. Int.* 23:351–366. <https://doi.org/10.1016/j.pnsc.2013.06.015>
- Yang Y et al (2014) Microwave-assisted fabrication of nanoparticulate TiO<sub>2</sub> microspheres for synergistic photocatalytic removal of Cr(VI) and methyl orange. *ACS Appl Mater Interfaces* 6:3008–3015. <https://doi.org/10.1021/am405607h>
- Yang J et al (2016a) A novel Cu x O nanoparticles@ ZIF-8 composite derived from core-shell metal-organic frameworks for highly selective electrochemical sensing of hydrogen peroxide. *ACS Appl Mater Interfaces* 8:20407–20414
- Yang X et al (2016b) Conversion of dihydroxyacetone to methyl lactate catalyzed by highly active hierarchical Sn-USY at room temperature. *Catal Sci Technol* 6(6):1757–1763. <https://doi.org/10.1039/c5cy01037c>
- Yang F et al (2018a) Simultaneous control over lattice doping and nanocluster modification of a hybrid CuO<sub>x</sub>/TiO<sub>2</sub> photocatalyst during flame synthesis for enhancing hydrogen evolution. *Solar RRL* 2:1800215. <https://doi.org/10.1002/solr.201800215>
- Yang J et al (2018b) Ru coated Co nanoparticles decorated on cotton derived carbon fibers as a highly efficient and magnetically recyclable catalyst for hydrogen generation from ammonia borane. *Int J Hydrog Energy* 43:1355–1364. <https://doi.org/10.1016/j.ijhydene.2017.11.061>
- Yao D et al (2018) Co-precipitation, impregnation and so-gel preparation of Ni catalysts for pyrolysis-catalytic steam reforming of waste plastics. *Appl Catal B Environ* 239:565–577. <https://doi.org/10.1016/j.apcatb.2018.07.075>
- Yao M et al (2019) Self-supportive mesoporous Ni/Co/Fe phosphosulfide nanorods derived from novel hydrothermal electrodeposition as a highly efficient electrocatalyst for overall water splitting. *Small* 15(50):1905201. <https://doi.org/10.1002/sml.201905201>
- Yap PS, Lim TT (2011) Effect of aqueous matrix species on synergistic removal of bisphenol-A under solar irradiation using nitrogen-doped TiO<sub>2</sub>/AC composite. *Appl Catal B Environ* 101:709–717. <https://doi.org/10.1016/j.apcatb.2010.11.013>
- Yap PS, Lim TT (2012) Solar regeneration of powdered activated carbon impregnated with visible-light responsive photocatalyst: factors affecting performances and predictive model. *Water Res* 46:3054–3064. <https://doi.org/10.1016/j.watres.2012.03.008>
- Yi D et al (2021) Recent trends in biocatalysis. *Chem Soc Rev* 50:8003–8049
- Yin H et al (2020) Construction of carbon bridged TiO<sub>2</sub>/CdS tandem Z-scheme heterojunctions toward efficient photocatalytic antibiotic degradation and Cr(VI) reduction. *J Alloys Compd* 824:153915. <https://doi.org/10.1016/j.jallcom.2020.153915>
- Yin Z et al (2022) Mechanochemical synthesis of catalysts and reagents for water decontamination: Recent advances and perspective. *Sci Total Environ* 825:153992. <https://doi.org/10.1016/j.scitotenv.2022.153992>
- Yu L et al (2006) Polymer blends and composites from renewable resources. *Prog Polym Sci* 31:576–602
- Yu W et al (2017) Direct Z-scheme g-C<sub>3</sub>N<sub>4</sub>/WO<sub>3</sub> photocatalyst with atomically defined junction for H<sub>2</sub> production. *Appl Catal B* 219:693–704
- Yu F et al (2021a) ZnO/biochar nanocomposites via solvent free ball milling for enhanced adsorption and photocatalytic degradation of methylene blue. *J Hazard Mater* 415:125511. <https://doi.org/10.1016/j.jhazmat.2021.125511>
- Yu J et al (2021b) A review of the effects of alkali and alkaline earth metal species on biomass gasification. *Fuel Process Technol* 214:234. <https://doi.org/10.1016/j.fuproc.2021.106723>
- Yuan B et al (2016) Enhanced hydrothermal stability and catalytic performance of HKUST-1 by incorporating carboxyl-functionalized attapulgite. *ACS Appl Mater Interfaces* 8:16457–16464
- Yuan Y-J et al (2019) The role of bandgap and interface in enhancing photocatalytic H<sub>2</sub> generation activity of 2D–2D black phosphorus/MoS<sub>2</sub> photocatalyst. *Appl Catal B* 242:1–8
- Zahirinejad S et al (2021) Nano-organic supports for enzyme immobilization: scopes and perspectives. *Colloids Surf B Biointerfaces* 204:111774. <https://doi.org/10.1016/j.colsurfb.2021.111774>
- Zhang Y (2020) Preparation of heterogeneous catalysts based on CWAO technology. *J Phys Conf Ser* 1549:032052. <https://doi.org/10.1088/1742-6596/1549/3/032052>
- Zhang J et al (2011) Visible light photocatalytic H<sub>2</sub>-production activity of CuS/ZnS porous nanosheets based on photoinduced interfacial charge transfer. *Nano Lett* 11:4774–4779
- Zhang W et al (2014) A family of metal-organic frameworks exhibiting size-selective catalysis with encapsulated noble-metal nanoparticles. *Adv Mater* 26:4056–4060
- Zhang Y et al (2015) Enhanced activity of immobilized or chemically modified enzymes. *ACS Catal* 5:4503–4513. <https://doi.org/10.1021/acscatal.5b00996>
- Zhang H et al (2018) Magnetic biochar catalyst derived from biological sludge and ferric sludge using hydrothermal carbonization: preparation, characterization and its circulation in Fenton process for dyeing wastewater treatment. *Chemosphere* 191:64–71. <https://doi.org/10.1016/j.chemosphere.2017.10.026>
- Zhang Z et al (2018) Preparation, modification and development of Ni-based catalysts for catalytic reforming of tar produced from biomass gasification. *Renew Sustain Energy Rev* 94:1086–1109. <https://doi.org/10.1016/j.rser.2018.07.010>

- Zhang MH et al (2019) A review on Fenton process for organic wastewater treatment based on optimization perspective. *Sci Total Environ* 670:110–121. <https://doi.org/10.1016/j.scitotenv.2019.03.180>
- Zhang L et al (2019a) Characterization of semiconductor photocatalysts. *Chem Soc Rev* 48:5184–5206. <https://doi.org/10.1039/C9CS00172G>
- Zhang Y et al (2019b) Advanced multifunctional electrocatalysts for energy conversion. *ACS Energy Lett* 4:1672–1680. <https://doi.org/10.1021/acscenergylett.9b01045>
- Zhang W et al (2020) Z-Scheme photocatalytic systems for carbon dioxide reduction: where are we now? *Angew Chem Int Ed* 59:22894–22915
- Zhang H et al (2021a) An insight to pretreatment, enzyme adsorption and enzymatic hydrolysis of lignocellulosic biomass: Experimental and modeling studies. *Renew Sustain Energy Rev* 140:110758
- Zhang X et al (2021b) Interfacial characteristics in membrane filtration for oil-in-water treatment processes. *J Memb Sci* 623:119092. <https://doi.org/10.1016/j.memsci.2021.119092>
- Zhao H et al (2015) Introduction of a Fe<sub>3</sub>O<sub>4</sub> core enhances the photocatalytic activity of MIL-100 (Fe) with tunable shell thickness in the presence of H<sub>2</sub>O<sub>2</sub>. *ChemCatChem* 7:4148–4155
- Zhao X et al (2018) Engineering TiO<sub>2</sub> supported Pt sub-nanoclusters via introducing variable valence Co ion in high-temperature flame for CO oxidation. *Nanoscale* 10:13384–13392. <https://doi.org/10.1039/C7NR08717A>
- Zhao F et al (2019a) Synergetic effect over flame-made manganese doped CuO–CeO<sub>2</sub> nanocatalyst for enhanced CO oxidation performance. *RSC Adv* 9:2343–2352. <https://doi.org/10.1039/C8RA09626K>
- Zhao F et al (2019b) Catalytic behaviour of flame-made CuO–CeO<sub>2</sub> nanocatalysts in efficient CO oxidation. *Catal* 9:256
- Zheng Y et al (2012) Graphitic carbon nitride materials: controllable synthesis and applications in fuel cells and photocatalysis. *Energy Environ Sci* 5:6717–6731
- Zheng P et al (2013) Immobilized  $\beta$ -glucosidase on magnetic chitosan microspheres for hydrolysis of straw cellulose. *Process Biochem* 48:683–687. <https://doi.org/10.1016/j.procbio.2013.02.027>
- Zhong L et al (2021) Immobilization of polyphenol oxidase on chitosan/organic rectorite composites for phenolic compounds removal. *Water Sci Technol* 83:906–921
- Zhou J et al (2015) Photocatalytic enhancement of hybrid C<sub>3</sub>N<sub>4</sub>/TiO<sub>2</sub> prepared via ball milling method. *Phys Chem Chem Phys* 17:3647–3652. <https://doi.org/10.1039/C4CP05173D>
- Zhou C et al (2022) One-pot synthesis, characterization and ammonia-selective catalytic reduction performance of MnSAPO-18 molecular sieves. *J Clean Product* 336:130163. <https://doi.org/10.1016/j.jclepro.2021.130163>
- Zhu JY, Zhuang XS (2012) Conceptual net energy output for biofuel production from lignocellulosic biomass through biorefining. *Prog Energy Combust Sci* 38(4):583–598. <https://doi.org/10.1016/j.peccs.2012.03.007>
- Zhu Y et al (2018) Scale-up biomass pathway to cobalt single-site catalysts anchored on N-doped porous carbon nanobelt with ultrahigh surface area. *Adv Funct Mater* 28:1802167. <https://doi.org/10.1002/adfm.201802167>
- Zhu C et al (2019) Construction of CDs/CdS photocatalysts for stable and efficient hydrogen production in water and seawater. *Appl Catal B* 242:178–185
- Zhu Z et al (2020) Green preparation of palm powder-derived carbon dots co-doped with sulfur/chlorine and their application in visible-light photocatalysis. *Spectrochim Acta Part A Mol Biomol Spectrosc* 227:117659. <https://doi.org/10.1016/j.saa.2019.117659>

**Publisher's Note** Springer Nature remains neutral with regard to jurisdictional claims in published maps and institutional affiliations.



## Authors and Affiliations

Ahmed I. Osman<sup>1</sup>  · Ahmed M. Elgarahy<sup>2,3</sup> · Abdelazeem S. Eltaweil<sup>4</sup> · Eman M. Abd El-Monaem<sup>4</sup> · Hisham G. El-Aqapa<sup>4</sup> · Yuri Park<sup>5</sup> · Yuhoon Hwang<sup>5</sup> · Ali Ayati<sup>6,7</sup> · Mohamed Farghali<sup>8,9</sup> · Ikko Ihara<sup>8</sup> · Ala'a H. Al-Muhtaseb<sup>10</sup> · David W. Rooney<sup>1</sup> · Pow-Seng Yap<sup>11</sup> · Mika Sillanpää<sup>12,13,14,15</sup>

Mohamed Farghali  
mohamed.farghali@aun.edu.eg

<sup>1</sup> School of Chemistry and Chemical Engineering, Queen's University Belfast, Belfast BT9 5AG, Northern Ireland, UK

<sup>2</sup> Environmental Science Department, Faculty of Science, Port Said University, Port Said, Egypt

<sup>3</sup> Egyptian Propylene and Polypropylene Company (EPPC), Port-Said, Egypt

<sup>4</sup> Chemistry Department, Faculty of Science, Alexandria University, Alexandria, Egypt

<sup>5</sup> Department of Environmental Engineering, Seoul National University of Science and Technology, Seoul 01811, South Korea

<sup>6</sup> Department of Chemical Engineering, Quchan University of Technology, Quchan, Iran

<sup>7</sup> ChemBio Cluster, ITMO University, Lomonosova Street 9, Saint Petersburg, Russia 191002

<sup>8</sup> Department of Agricultural Engineering and Socio-Economics, Kobe University, Kobe 657-8501, Japan

<sup>9</sup> Department of Animal and Poultry Hygiene and Environmental Sanitation, Faculty of Veterinary Medicine, Assiut University, Assiut 71526, Egypt

<sup>10</sup> Department of Petroleum and Chemical Engineering, College of Engineering, Sultan Qaboos University, Muscat, Oman

<sup>11</sup> Department of Civil Engineering, Xi'an Jiaotong-Liverpool University, Suzhou 215123, China

<sup>12</sup> Department of Chemical Engineering, School of Mining, Metallurgy and Chemical Engineering, University of Johannesburg, P. O. Box 17011, Doornfontein 2028, South Africa

<sup>13</sup> Department of Applied Physics, Faculty of Science and Technology, Universiti Kebangsaan Malaysia, 43600 Bangi, Selangor, Malaysia

<sup>14</sup> Zhejiang Rongsheng Environmental Protection Paper Co. Ltd, No. 588 East Zhennan Road, Pinghu Economic Development Zone, Zhejiang 314213, People's Republic of China

<sup>15</sup> Department of Civil Engineering, University Centre for Research and Development, Chandigarh University, Gharuan, Mohali, Punjab, India